A mineralogical and geochemical investigation of sulfide mineralization in the McConnell Ni-Cu-PGE occurrence, McConnell Offset Dyke, Garson Mine area, Sudbury, Ontario, Canada

By
Brandon Michael Boucher

Thesis submitted to
Saint Mary's University, Halifax, Nova Scotia
in partial fulfillment of the requirements for
the Degree of Master in Applied Science

June, 2015, Halifax, Nova Scotia

Approved: Dr. Jacob Hanley
Supervisor
Department of Geology
Saint Mary's University

Approved: Dr. Doreen Ames
Supervisory Committee
Geological Survey of Canada

Approved: Dr. Victor Owen
Supervisory Committee
Department of Geology
Saint Mary's University

Approved: Dr. Jason Clyburne
Supervisory Committee
Dept. of Chemistry
Saint Mary's University

Approved: Dr. Stephen Barnes
External examiner
Lead Research Scientist
CSIRO, Perth, Australia

Date: June 2, 2015

Abstract

A mineralogical and geochemical investigation of sulfide mineralization in the McConnell Ni-Cu-PGE occurrence, McConnell Offset Dyke, Garson Mine area, Sudbury, Ontario, Canada

By Brandon Michael Boucher

The Sudbury mining camp hosts the largest and only known impact-related metallogenic system in the world, containing significant resources of Cu-Ni-platinum group element-rich sulfide mineralization. The undeveloped, Vale-owned McConnell concentric offset dyke hosts low Ni grade magmatic Ni-Cu sulfide mineralization with unusually high PGE tenor, showing marked differences in mineralogy and geochemistry compared to other South Range offset-type deposits. This study shows that: (i) the low As, Ni, and high PGE in bulk assays and Co and Pd-rich pentlandite in the ores reflects an unusual evolution of the McConnell sulfide melt explained by three possible models, or a combination of models (“uncontaminated”, “locally enriched”, and “late-stage” sulfide melts); (ii) a post-crystallization hydrothermal fluid passed through the system, remobilizing Ni and Pb within the deposit and altering primary ore mineralogy forming pyrite and marcasite; and (iii) the McConnell ores crystallized from an O-rich Ni-poor sulfide melt, as reflected by magnetite geochemistry.

June 02, 2015.

Acknowledgments

I would like to thank Dr. Jacob Hanley for the opportunity to undertake this project, as well as the continued assistance and support over the course of the project as primary supervisor. I would also like to thank my supervisory committee members for their time and input into this thesis. The additional work they have voluntarily undertaken by sitting on the committee and reviewing the document and defence is greatly appreciated. Their comments and insights have added to the quality of this project. Dr. Doreen Ames (Geological Survey of Canada) has assisted greatly in the collection and interpretation of laser ablation data and lead isotope analyses, and I am very grateful for all her help. This project was made possible by funding from Vale, and the assistance and support of many members from their Sudbury operation. Of special note are Clarence Pickett and Sherri Digout who made sample collection possible, and John Townend, Chris Davis, and Chris Gauld. I would like to thank the members, both past and current, of the Hanley lab group MEOFL, for creating a professional work environment and an unprofessional pub environment. Mitch, I'm glad your computer problems were always worse than anything else ever, it made the days better. Craig, Gladney, Darren, Erin, and any of the hundred names I've missed, thanks for everything over the years. Of course, a big thank you to my parents Tom and Mary for all the free food and lodging over my lifetime, my twin sister Megan and my rock hound brother Vincent.

Table of Contents

List of Figures

In Chapter 2

In Chapter 3

List of Tables

Chapter 1: Introduction

1.0 Structure of Thesis

This document contains 4 chapters. Following an introduction chapter serving as an outline of the thesis, chapters 2 and 3 describe studies of sulfide mineralogy and geochemistry of samples from the offset-style McConnell mineralization. Chapter 2 describes a bulk rock and in-situ geochemical, petrographic, and mass balance study of sulfides from the McConnell offset. Techniques were used to characterize the economic and deleterious element distribution within the ore body, as well as characterize aspects of mineralogy relevant to beneficiation and smelting efficiency. Chapter 3 focuses on accessory magnetite geochemistry, allowing the timing and chemical characteristics of associated sulfides to be determined. Both chapters 2 and 3 are structured as stand-alone manuscripts for publication. Chapter 4 contains brief concluding statements and a short review of all major findings.

1.1 Primary objectives and study area

The McConnell Ni-Cu-PGE occurrence is a concentric offset-type deposit that occurs along the South Range of the Sudbury Igneous Complex, in the Garson mine area. The offset dike, comprised of inclusion-free and inclusion-rich quartz diorite, is only 1 km along its strike and ~ 60 meters wide, and is characterized by massive to disseminated sulfide mineralization hosted partially within quartz diorite and also along the contact between quartz diorite and host rocks of the Huronian Supergroup. These host rocks range from metasediments to metabasalts, with the contact between the two lithologies running approximately along the length of the McConnell ore body. As no detailed mineralogical analysis has been performed on the ores of the McConnell deposit, the

primary objective of this study was to provide Vale with a comprehensive characterization of the Ni-Cu-platinum group element (PGE) sulfide minerals, and their association with host rock types. This focused on identifying the mineralogical controls and spatial distribution of precious and deleterious metals, with the aim of providing a comprehensive mineralogical model to aid Vale in future exploration and development of the mineralization into an ore body.

To achieve these goals, a large sample set was obtained from drill core provided by Vale (Ontario operations) from 4 holes drilled through the McConnell offset (1985-1990). These drill holes intersect a representative cross section of sulfide mineralization and host lithologies from the McConnell offset. Petrographic reports, LA-ICP-MS (Laser Ablation Inductively Coupled Plasma Mass Spectrometry) and SEM (Scanning Electron Microscope) data were used to provide comprehensive reports on the mineralogical and geochemical aspects of McConnell ores.

Chapter 2: Mineralogical and geochemical investigation of Ni-Cu-Platinum Group Element mineralization within the McConnell Offset Occurrence, Garson Mine area, South Range, Sudbury Igneous Complex, Ontario, Canada

Abstract

The concentric McConnell offset (Garson mine area, Sudbury Igneous Complex, Ontario; Figure 2.1) hosts mineralization that shows depletion in As and Ni compared to other South Range offset and contact-type Ni-Cu-PGE sulfide deposits, despite having very similar mineralogy. Evidence is presented that shows that a Co-enriched, Ni-depleted sulfide melt was responsible for the formation of the ore body, and that an absence of As within the melt resulted in pentlandite scavenging more Co and Pb, and crystallizing at a higher temperature than is typical for Sudbury offset dyke deposits. The resulting magmatic ores were sourced from a sulfide melt without economic Ni tenors or significant As contamination achieved through possible models: (i) an oxygen-rich sulfide liquid accumulated in the silicate melt sheet and significantly altered the partitioning of Ni and As between the silicate reservoir and the sulfide liquid; (ii) zones of local vs regional contamination dictated by the digestion of As- or metal-bearing host rocks, where sulfide liquids are more highly influenced by the size and composition of the local silicate reservoir (R factor); or (iii) a sulfide liquid that remained in equilibrium with, or was sourced from, an evolved silicate reservoir which lost significant metal concentrations to previously emplaced sulfide liquids, indicating that the McConnell system was emplaced after other larger South Range offsets. Elevated platinum-group element (PGE) concentrations within the McConnell mineralization (as Pd-Bi-tellurides or pentlandite) indicate that the process responsible for PGE enrichment in the

McConnell system was not affected by the factors that limited or depleted the As and Ni concentrations within the initial sulfide melt. Platinum-group elements (PGEs) were unable to partition into early forming arsenide melts and solid solutions. Intense hydrothermal alteration of Cu-Ni-PGE ores at McConnell created zones of marcasite-pyrite along the stratigraphically lower margin of the ore body. Hydrothermal fluids of unknown origin altered primary pentlandite (to smythite and pyrrhotite), which was originally highly unstable in the presence of fluids owing to its unusually Co- and Pb-enriched nature. Lead isotope analyses from unaltered pentlandite show that high Pb concentrations are related to initial crystallization at the time of the formation of the SIC. This study incorporates LA-ICP-MS, SEM, Pb isotope, and bulk rock data to develop a preliminary mineralogical and genetic model of the offset mineralization.

2.0 Introduction

Radial and concentric quartz diorite offset dykes, a component of the Sudbury Igneous Complex (SIC), are considered to result from the injection of an early undifferentiated impact melt (shortly after the Sudbury impact event) into pre and syn–impact faults within the country rocks (Morrison et al., 1994; Grieve, 1994; Rickard and Watkinson, 2001; Farrow and Watkinson, 1996; Lightfoot et al., 1997a; Wood and Spray, 1998; Patterson, 2001; Murphy and Spray, 2002; Lightfoot and Farrow, 2002; Keays and Lightfoot, 2004; Barnes and Lightfoot, 2005; Lightfoot, 2007; Ames and Farrow, 2007; Ames et al., 2008). Offset dykes formed from multiple injections of melt through the cooling history of the melt sheet, resulting in both barren (QD) and inclusion-bearing (IQD) quartz dioritic lithologies being present within single dykes (Morris, 1982; Lightfoot et al., 1997; Wood and Spray, 1998; Rickard and Watkinson, 2001; Tuchscherer and Spray, 2002; Murphy and Spray, 2002). The offset dyke systems vary in size, and may host Ni-Cu-platinum-group element (PGE) sulfide deposits which account for a large percentage of the overall Sudbury ore metal inventory. Inclusion-bearing quartz diorite is the lithology associated with economic Ni-Cu-PGE mineralization and often contains disseminated to massive sulfides. Inclusion-bearing quartz diorite was emplaced into the cores of offset dyke systems after inclusion-free QD and synchronous with sulfide emplacement, producing zonation in the dykes with respect to lithology and mineralization (Lightfoot et al., 1997; Wood and Spray, 1998; Rickard and Watkinson, 2001; Farrow and Lightfoot, 2002). Sulfides are closely spatially associated with inclusions. Inclusions within the quartz diorite dykes range from locally-derived host rock clasts, to clasts of early QD, to exotic xenolithic mafic and ultramafic lithologies of

ambiguous origin (Scribbins et al., 1984; Lightfoot et al., 1997; Rickard and Watkinson, 2001).

Large mineralized offset systems have received a disproportionate amount of attention in research owing to their longevity of mining in Sudbury and contained world-class Ni-Cu-PGE deposits (e.g., the radial Copper Cliff and Worthington offsets; Cochrane, 1984; Stewart et al., 1999; Szentpéteri, 1999; Magyarosi et al., 1999; Rickard, 2000; Carter, 2000; Carter et al., 2001; Rickard and Watkinson, 2001; Lightfoot and Farrow, 2002; Szentpéteri et al., 2002; Magyarosi et al., 2002; Stewart, 2002; Huminicki, 2003; Huminicki et al., 2005). Many studies have characterized the mineralogy and geochemistry of barren and mineralized offset systems. These studies have broadened our understanding of offset emplacement and ore genesis and have benefited from continuing advances in analytical techniques. Due to the suspected poor economic potential of some smaller offset dyke systems (e.g. McConnell) and corresponding limited exploration undertaken, they are poorly characterized, leaving many questions unanswered about these systems. There are, however, larger offset systems that do not contain significant sulfide mineralization (Foy), indicating that size alone does not dictate economic metal potential of offsets.

Although base metal sulfide assemblages are similar in mineralized offsets at all scales, the abundance and composition of major and accessory ore phases varies significantly from one offset to another, as have the effects of contamination and hydrothermal alteration. It remains unclear whether the differences in ore composition in different offset dyke systems are due to only localized secondary processes (contamination, alteration), or if these differences are the consequence of primary

magmatic variables associated with the evolution of silicate and sulfide melts of the SIC prior to, and during, offset dyke emplacement. In addition to providing the first mineralogical and geochemical characterization of the McConnell offset, this study will: (i) address the potential causes for variable metal tenors in different offset dykes; (ii) compare these rocks to nearby and related deposits; and (iii) provide evidence for the alteration and modification of ores and possible redistribution of ore and ore metals.

2.1 Regional Geology

The 1850 Ma (Krogh et al., 1984) Sudbury structure cuts the boundary between the Grenville, Southern, and Superior provinces of the Canadian Shield, and forms an elliptical structure that stretches 60 x ~27km (Dietz, 1964; Grieve, 1994; Szabó and Halls, 2006). This astrobleme is believed to have been much larger than it is today, with the original diameter estimated between 190 and 260 km, and a much less deformed shape; it has been widely accepted as a large impact structure (Dietz, 1964; Peredery and Morrison, 1984; Dressler, 1984; Grieve et al., 1991; Ames et al., 2008; Hanley et al., 2011). The impact occurred in a shallow marine basin in the foreland of the Penokean Orogen, and caused nearly instantaneous melting of the rocks below the impact site. A large melt sheet formed at the base of the impact structure (e.g. Grieve, 1994; Ames, 1999; Mungall et al. 2004). The impact produced a large multi-ring basin occupied by an andesitic impact melt that crystallized to form the Sudbury Igneous Complex (SIC) (Card, 1978; Peredery and Morrison, 1984; Fleet et al., 1987; Stöffler et al., 1994; Deutsch et al., 1995; Ivanov and Deutsch, 1999; Mungall et al, 2004). The ejecta that formed during impact created a large plume above the crater that settled onto the melt sheet creating the Onaping Formation, a unit made up of discontinuous mass flow

deposits, fall-back breccias, and plume collapse units (French, 1972; Peredery, 1972; Stevenson, 1972; Rousell, 1984; Ames, 1999; Ames et al., 2002). Evidence for a bolide impact forming the Sudbury structure and associated melt sheet is provided by the occurrence of shatter cones, impact diamonds, shock-related rock types (i.e. pseudotachylites) and their distribution around the SIC, and Ir anomalies in the fallback breccias (Guy-Bray, 1966; French, 1972; Rousell, 1981; Morrison, 1984; Stöffler et al., 1994; Thompson and Spray, 1996; Spray, 1998; Mungall et al., 2004).

The host rocks which surround the SIC comprise the north, south, and east ranges. The Sudbury structure consists of the Sudbury basin (filled by the Whitewater Group), the brecciated Archean (north, east) and Proterozoic (south) footwall rocks of the SIC, and the main mass of the SIC. The footwall rocks comprise Archean gneisses, metavolcanic-metasedimentary rocks, migmatites, and felsic and mafic plutonic rocks, which are unconformably overlain by metavolcanic and metasedimentary rocks of the Early Proterozoic Huronian Supergroup (Dressler, 1984). This group forms an assemblage of volcanic and sedimentary rocks that makes up part of the Penokean Fold Belt in the Southern Province, and is believed to have been created during an intra-continental rifting event associated with a mantle plume that was located under the Sudbury impact target area (Dressler, 1984; Heaman, 1997; Card and Poulsen, 2000; Ernst and Buchan, 2001; Young et al., 2001; James et al., 2002). Emplacement of the Huronian flood basalts was associated with large-scale magmatic activity during rifting between 2.48–2.45 Ga, and also accounted for the emplacement of the Matachewan and Hearst dike swarms (Heaman, 1997). James et al (2002) describe a suite of plutonic igneous rocks associated with this rifting event (the “rifting suite”) comprised of two separate pulses of

magmatism: a mafic pulse at roughly 2475 Ma, forming the East Bull Lake intrusive suite, and a felsic pulse at roughly 2450 Ma, forming the volcanic rocks of the Elliot Lake Group. Subsequent sedimentation, emplacement of Nipissing gabbro (~ 2.2 Ga; Nobel and Lightfoot, 1992), and regional and shock/contact metamorphism of Huronian volcanic rocks by the Penokean Orogeny and Sudbury events occurred, respectively, with the peak of Penokean metamorphism occurring around 1835 Ma (Holm et al., 2001). The Huronian sequence is characterized by cycles of conglomerate, mudstone, wacke, and quartz-feldspar arenite, and has been divided into 4 groups: the Elliot Lake Group, the Hough Lake Group, the Quirke Lake Group, and the Cobalt Group, with volcanic rocks occurring only in the Elliot Lake Group (Dressler, 1984).

Archean gabbroic, dioritic, tonalitic, and granitic gneisses form the SIC footwall prominently in the North Range where they occur as the “Levack Gneiss Complex” (Langford, 1960; Dressler, 1984; Card, 1994; Ames et al., 2008). The gneisses experienced localized shock and contact metamorphism associated with impact and SIC heating, and earlier, pervasive granulite to amphibolite facies regional metamorphism pre-SIC, but were largely unaffected by syn to post–SIC orogenic events (Dressler, 1984). According to Dressler (1984), the Levack Gneiss Complex rocks are supracrustal, sedimentary-volcanic in origin, so compositional variations in the gneisses represented alternating sequences of metamorphosed clastic sediments interbedded with mafic-ultramafic volcanic rocks and possible felsic volcanic units. The Sudbury breccia is an important host rock unit to the footwall sulfide deposits that occur in the country rock surrounding the SIC, and displays textures indicative of recrystallization, partial melting, and in situ shock brecciation (Dressler, 1984). Rousell et al. (2003) classify Sudbury

breccia into the following types: (i) “clastic” types, occurring dominantly in the Huronian supergroup and Nipissing gabbros as rounded clasts in a cataclastic matrix; (ii) fine-grained pseudotachylites occurring most commonly in Archean North Range rocks and igneous plutons in the South Range; and (iii) coarse-textured, microcrystalline types occurring very close to, or along the contact of, the SIC, having experienced contact metamorphism and partial recrystallization. Footwall breccia (Greenman, 1970; Dressler, 1984) locally underlies the contact sublayer. It too can host significant economic mineralization (contact-style sulfide deposits), and shows evidence of partial melting, shock brecciation, and contact metamorphism. However, unlike Sudbury breccia, it has been suggested that footwall breccia represents the partially melted crater floor beneath the melt sheet, accounting for the residual xenolithic fragments of country rock that occur in this unit (Lakomy, 1990).

The main mass of the SIC consists of granophyric residue overlying quartz gabbro and norites commonly in contact with a basal or contact “sublayer” unit (Naldrett and Hewins, 1984; Lightfoot et al., 1997; Ames et al., 2008). A widely recognized model for the formation of the SIC involves in situ differentiation of the melt sheet during the ongoing assimilation of some local country rocks (i.e. Naldrett, 1984; Lightfoot et al., 1997). The SIC differs from most other layered igneous intrusions as it has no fine or cyclic igneous layering, and relatively high SiO_2 contents (dioritic bulk composition; Naldrett and Hewins, 1984).

The contact sublayer occurs discontinuously around the outer margin (base) of the SIC. It consists of two different lithologies: (i) a fine- to medium-grained, inclusion-bearing noritic rock containing hypersthene, augite, and plagioclase as its primary

minerals; this unit contains some of the economic mineralization zones associated with SIC (e.g. Creighton, Frood); and (ii) inclusion-bearing and inclusion-free quartz diorite hosted within radial and concentric offset dyke systems (Naldrett et al., 1984; Morrison, 1984; Lightfoot et al., 1997), with radial dykes still physically connected to the base of the SIC through "embayment" structures (e.g. Copper Cliff). Notably, the quartz diorite offset dykes are host to many of the largest Ni-Cu-PGE magmatic sulfide deposits. The dykes formed by multiple injections of impact-related melt into structures in the surrounding country rock (Grant and Bite, 1984; Lightfoot et al., 1997; Farrow and Lightfoot, 2002; Lightfoot and Farrow, 2002).

The offset dykes comprise an envelope of early, inclusion-free sulfide-poor quartz diorite (QD) and a discontinuous core of inclusion-bearing, sulfide-mineralized quartz diorite (IQD). The QD was emplaced before differentiation and sulfide saturation of the overlying melt sheet occurred at temperatures of at least ~1180˚ C (Lightfoot et al., 1997; Farrow and Lightfoot, 2002; Keays and Lightfoot, 2004; Darling et al., 2010; Watts, MSc thesis 2014). The IQD formed by the injection of a later melt phase that had reached sulfide saturation. Numerous lithologies (e.g. Sudbury breccia, QD, country rocks, and exotic xenolithic fragments) are hosted in the IQD (Lightfoot et al., 1997, Farrow and Lightfoot, 2002). The melt that formed economic sulfide mineralization within IQD *may* have reached sulfide saturation or metal enrichment before other portions of the main melt sheet due to significant melting and incorporation of S and metal-bearing country rocks (e.g. Nipissing mafic rocks, mafic-ultramafic rocks of ambiguous origin) or contributions from regional contamination (e.g. Mungall et al., 2004) that locally enriched the lowermost mafic portion of the melt sheet in S, As, and base and precious

metals (e.g. Dickin et al., 1999; Darling et al., 2010; Darling et al., 2012); the pooling and accumulation of very early sulfide liquids from the superheated melt sheet into embayments before the injection of the IQD may have also promoted significant metal enrichment or contamination of radial offset systems. Although this theory is not widely accepted, it is clear that the assimilation of country rocks and exotic fragments significantly enriched the melt sheet in S, As, and economic metals (Ni, Cu) at a local and regional scale, and contributed to early sulfide segregation and ore formation through sulfur saturation that did not rely on significant cooling and fractional crystallization of the overlying melt (Naldrett et al., 1984; Lightfoot et al., 1997; Lightfoot and Farrow, 2002; Farrow and Lightfoot, 2002; Keays and Lightfoot, 2004; Darling et al., 2010; Darling et al., 2012).

Offset dyke systems are subdivided into 3 types based on their location and orientation with respect to the main mass of the SIC: (i) radial offset dikes (e.g. Copper Cliff and Worthington offset dykes), which originate at noritic/dioritic sublayer-filled embayments at the footwall contact and continue into surrounding country rock; (ii) parallel or concentric dykes (e.g. Manchester, McConnell, and Hess offset dykes), which lie parallel to the SIC lower contact hosted within massive Sudbury Breccia zones; and (iii) discontinuous quartz diorite occurrences, small bodies of quartz diorite within embayments that occur with other Sublayer rocks (Grant and Bite, 1984).

Three primary magmatic-hydrothermal Ni-Cu-PGE deposit styles are associated with the SIC: (i) offset-dyke deposits (as discussed above); (ii) contact-style deposits; and (iii) footwall-type deposits (Pye et al., 1984; Cochrane, 1984; Morrison, 1984; Morrison et al., 1994; Farrow and Lightfoot, 2002; Ames; 2008 and references therein). Contact and

offset-style mineralization consists primarily of pentlandite-pyrrhotite with minor chalcopyrite, whereas footwall deposits are richer in Cu and PGE (e.g. Naldrett, 1984; Farrow and Lightfoot, 2002 and references therein). Pentlandite occurs as cm-sized masses, thin rims around pyrrhotite, and fine-grained exsolution lamellae, whereas chalcopyrite forms xenomorphic masses, veins, and stockworks (Naldrett, 1984). In the South Range, PGE are often sequestered in discrete arsenide and sulfarsenide phases, as well as discrete bismuth-tellurides (Cabri and LaFlamme, 1976; Rickard and Watkinson, 2001; Magyarosi et al., 2002; Szentpéteri et al., 2002; Huminicki et al., 2005; Dare et al., 2010; Lefort 2012).

Contact-style deposits host pyrrhotite-dominant, Ni-rich PGE-poor mineralization that commonly occurs in embayments at the base of the contact sublayer and quartz diorite, and within footwall breccia (e.g. Naldrett, 1984; Farrow and Lightfoot, 2002; Dare et al., 2010). The sublayer and footwall breccia units that host most contact-style deposits occur discontinuously around the SIC, and have undergone modification ranging from hydrothermal alteration to localized metamorphism, partial melting, and recrystallization (Farrow and Lightfoot, 2002).

Footwall-style deposits have been classified into two physically and chemically distinct sub-types: (i) “high-sulfide” mineralization comprised of sheet-like massive chalcopyrite +/- millerite + cubanite veins and vein networks formed by emplacement of a fractionated primary sulfide liquid followed by modification (remobilization and redistribution of ore metals) by volatile phases, and (ii) “low-sulfide” mineralization and consisting of blebby to disseminated chalcopyrite-bornite-millerite assemblages with PGE/S ratios an order of magnitude higher than in high-sulfide mineralization (Farrow

and Watkinson, 1992; Li et al., 1992; Li and Naldrett, 1994; Morrison et al., 1994; Molnár et al., 2001; Farrow and Lightfoot, 2002; Hanley et al., 2004, 2005, 2011; Farrow et al., 2005; Péntek et al., 2008; Tuba et al., 2010). It has been suggested that the low-sulfide ores may have a predominant hydrothermal origin and may pre-date the emplacement of the high-sulfide ores (Farrow et al., 2005; Hanley et al., 2005; Hanley and Bray, 2009). A saline magmatic-hydrothermal fluid may have leached Cu and precious metals from contact deposits and redistributed them into the footwall forming low-sulfide deposits (Farrow and Watkinson, 1992; Farrow, 1994; Farrow et al., 1994; Everest, 1999; Molnàr et al., 1997, 1999, 2001; Pèntek et al., 2006, 2008, 2009, 2012; Tuba et al., 2010, 2012, 2013). These fluids may have been mixtures of saline groundwater and magmatic hydrothermal fluids sourced from the mineralized contact region or main mass of the SIC (Marshall et al., 1999; Hanley et al., 2005; Péntek et al., 2008; Tuba et al., 2010; Hanley et al., 2011).

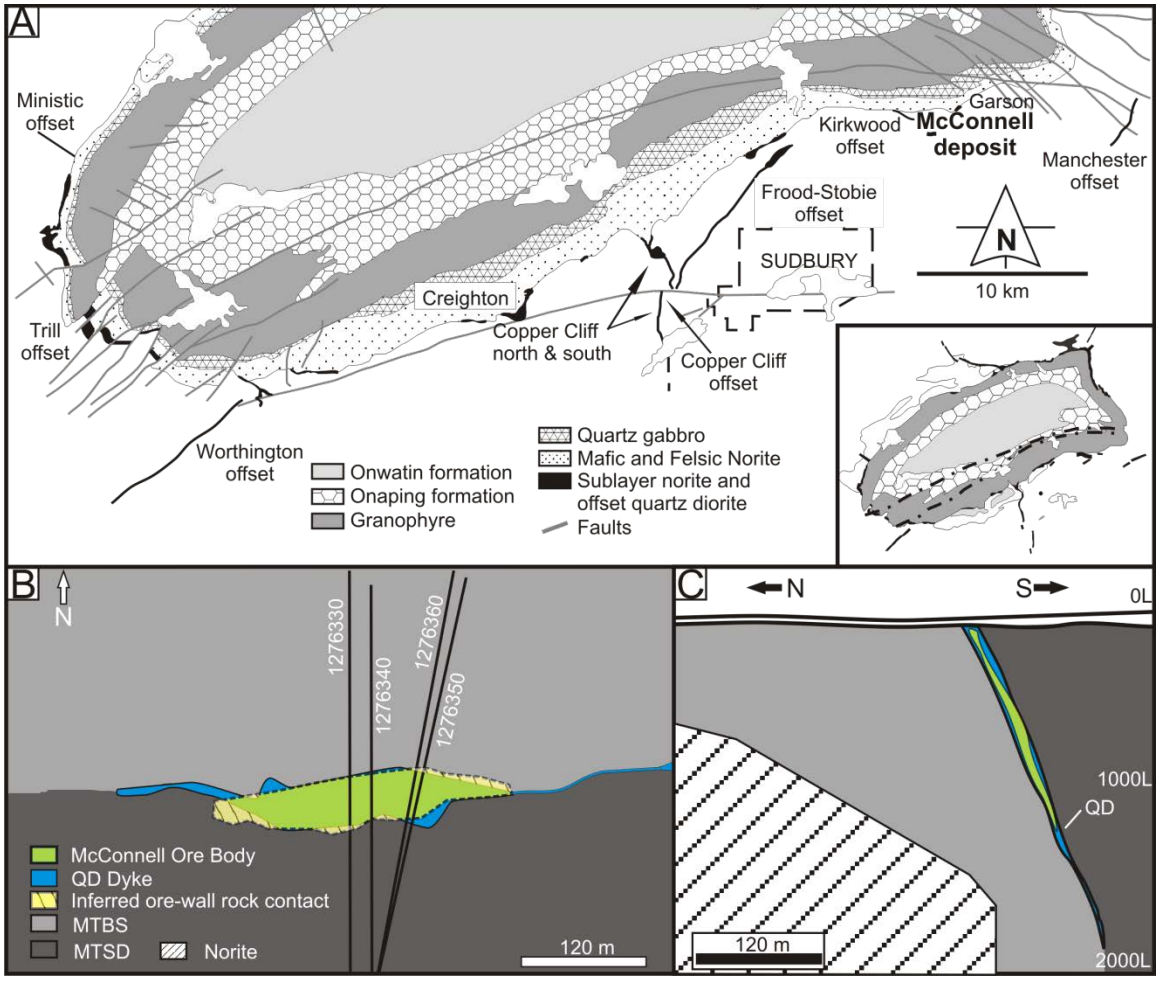

Figure 2.1 Location and orientation of the McConnell offset. (A) South range of the Sudbury structure showing offsets, contacts, faults, and a few mine locations. (B) Plan view of the McConnell deposit in the Kirkwood/Garson mine area, metasediments (MTSD) and metabasalts (MTBS) host the quartz diorite (QD) dyke in which the majority of the mineralization is confined. Dashed lines represent intermediate-disseminated sulfides and QD in contact with host rocks. Drilling information provided by Vale. (C) Cross section of the McConnell offset.

2.2 Sampling and analytical methods

2.2.1 Sample collection

A total of 125 samples, each approximately 12 cm in length, were selected from BQ drill core from Vale and Inco drilling programs, resulting in a large suite of representative host rocks and sulfide mineralization sections which pass through the McConnell deposit (Figure 2.1). Sections were chosen at intervals showing mineralogical and textural representivity and changes (e.g. the appearance of pyrite as an alteration phase). The sample set was logged and labelled with increasing depth to create general graphic drill logs columns of mineralogical observations, separating zones of massive sulfide (MASU), inclusion-rich massive sulfide (INMS), disseminated sulfide (DISS), and host rock (metasediments, metabasalts, quartz diorite). This method was used when sampling from all 4 drill holes that intersected the McConnell deposit (DDH-1276330, 1276340, 1276350, 1276360, Figure 2.1B). Samples were cut into blocks for creation of polished thick and thin sections, and prepared into 100 g batches for bulk rock assays (ALS Minerals, Sudbury, Ontario).

2.2.2 Optical and scanning electron microscopy

Petrographic observations were collected using a Nikon Eclipse H550L microscope with reflected and transmitted light capabilities. These observations were augmented by scanning electron microscopy using a LEO 1450 VP Scanning Electron Microscope (Saint Mary's University) with a maximum resolution up to 3.5 nm at 30 kV. Analyses were performed at 25 kV accelerating voltage and 5 nA beam current. The SEM was used to quantify mineral composition and identify discrete trace and accessory phases. The SEM uses INCA™ software to quantify X-ray spectra using a standard-enhanced semi quantitative routine, and to create element distribution maps which were made for

selected pentlandite and pyrite grains to better understand Ni, Fe, Co, and S distribution in altered samples. To discriminate between monoclinic and hexagonal pyrrhotite, a magnetic colloid (powdered magnetite-hematite blend mixed into a solution with methanol) was applied to 10 representative polished thin sections of MASU and INMS. The magnetic colloid is strongly attracted to monoclinic pyrrhotite and magnetite grains (though the two are easily distinguishable from each other by optical properties), and is not attracted to hexagonal pyrrhotite, pentlandite, pyrite, or chalcopyrite.

2.2.3 Laser ablation inductively-coupled plasma mass spectrometry

LA-ICP-MS data were obtained at the Geological Survey of Canada (Ottawa, Ontario) using an Agilent 7700 quadrupole inductively-coupled plasma mass spectrometer coupled to a 193 nm Ar-F Excimer laser for sample aerosol introduction. Ablation was performed at a 43 micron spot size (ablation pit diameter) and at a 10 Hz repetition (pulse) rate at 40% of 5 mJ (attenuated) output energy (Table 2.1). A 40 second gas blank was collected before each mineral analysis, followed by 65 seconds of mineral ablation (Figure 2.2). Standard reference materials were used to calibrate analyte sensitivities to account for instrument drift and for quality control, analyzed before and after blocks of 11 mineral analyses. Standards utilized at the GSC were synthetic pyrrhotite (Po726 from Memorial University, Saint Johns, Newfoundland and Labrador) for Au and PGE, a granitic glass (GSE-1G from USGS) for base metals and S, and a pressed sulfide pellet (MASS-1 from USGS). Ablation sites were selected in the centers of large grains, avoiding any cracks or grain boundaries (mixed matrices) with adjacent minerals. Collected spectra were observed in real time to note the presence of mineral inclusions in larger analyzed grains or inhomogeneous grains, allowing for scrutiny of raw data prior

Table 2.1: LA-ICP-MS operating and data reduction parameters

LA	
Model	Photon Machines Analyte.193
Wavelength	193 nm
Pulse duration (FWHM)	4 ns
Repetition rate	10 Hz
Spot diameter	32-86 µm
Energy density	ca. 4 J/cm^2
Primary (calibration) standards	**Po726** (synthetic, PGE and Au doped pyrrhotite, Sylvester et al., 2005; reference values from certificate) **MASS-1**(synthetic, doped, precipitated sulfide; reference values from Wilson et al., 2002, except Te from Dare et al., 2010b, and Ni (98 ppm) and Pb (73 ppm) determined in house)
Secondary (QC) standard	**GSE-1** (synthetic silicate glass; provided by GSC) **JB Sulfide** (synthetic sulfide [University of Toronto] reference values from Mungall and Brenan, 2014)
ICP-MS	
Model	Agilent 7700x with additional interface rotary pump which approximately doubles instrument sensitivity
Forward power	1550 kW
Shield torch	Used
Sampling depth	7 mm
Gas flows (He carrier mixed downstreamn from cell with Ar make up):	
Carrier (He)	0.6 L/min
Make up (Ar)	1.08 L/min
ThO^+/Th^+	<0.3%
U^+/Th^+ (NIST 612)	ca. 1.05
Data acquisition parameters	
Data acquisition protocol	Time Resolved Analysis
Scanning mode	Peak hopping, 1 point per blank
Dwell time per isotope	10 ms for all masses (earlier analyses) or as indicated below
Detector mode	Pulse counting except analogue for isotopes in italics below
Isotopes determined (dwell time ms)	^{34}S(5), ^{51}V(10), ^{53}Cr(10), ^{57}Fe(5), ^{59}Co(10), ^{60}Ni(5), ^{61}Ni(10), ^{65}Cu(10), ^{65}Cu(10),^{66}Zn(10), ^{75}As(10), ^{77}Se(10), ^{88}Sr(5), ^{89}Y(5), ^{90}Zr(5), ^{99}Ru(15),^{101}Ru(15), ^{102}Ru(15), ^{103}Rh(15), ^{105}Pd(15), ^{106}Pd(15), ^{107}Ag(15), ^{108}Pd(15), ^{109}Ag(15), ^{111}Cd(10), ^{118}Sn(15), ^{121}Sb(10), ^{125}Te(10), ^{181}Ta(5), ^{193}Ir(15), ^{195}Pt(15), ^{197}Au(15),^{205}Tl(10), ^{206}Pb(10), ^{208}Pb(10),^{209}Bi(10)
Quadrupole settling time	1-5 ms depending upon mass jump
Analysis time	100 s: ~40 s gas blank, up to ~60 s of ablation

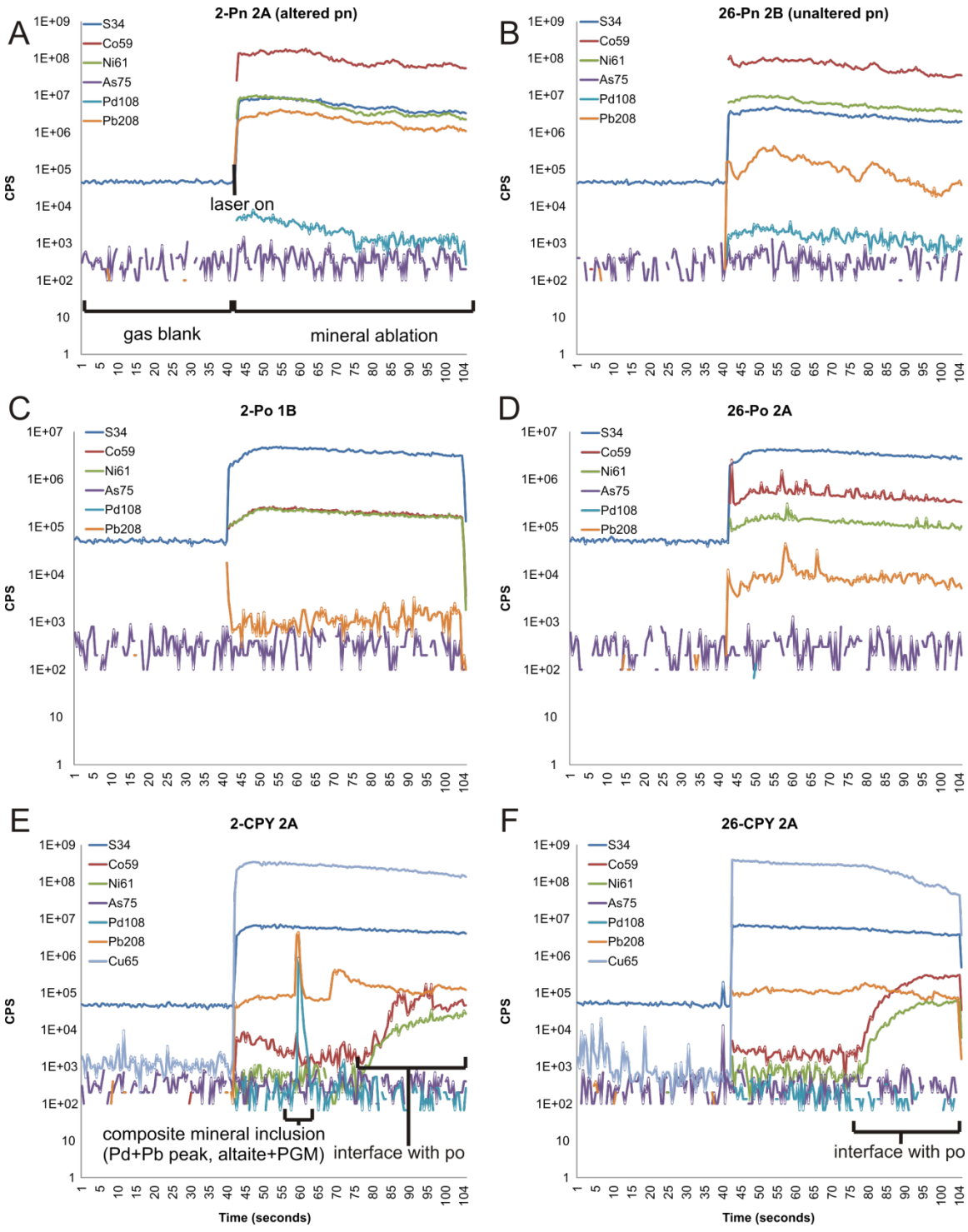

Figure 2.2 Time resolved LA-ICPMS signals (counts per second) during 60 second mineral ablations of base metal sulfides pentlandite (Pn), pyrrhotite (Po) and chalcopyrite (cpy). A 40 second gas blank was collected before each ablation. (A-D) Nearly-homogenous grains showing plateaus of element concentrations. (E) An inclusion (galena and Pd-telluride) occurs within chalcopyrite at ~60 seconds, while intersection of a pyrrhotite grain begins at ~80 seconds. (F) A homogenous grain of chalcopyrite occurs on top of a grain of pyrrhotite, intersected at ~80 seconds.

to data reduction. Figure 2.2 (time-resolved signals) demonstrates distribution of Pb and Co through base metal sulfide grains during ablation. Isotopes measured were ^{34}S, ^{51}V, ^{53}Cr, ^{57}Fe, ^{59}Co, ^{60}Ni, ^{61}Ni, ^{65}Cu, ^{66}Zn, ^{75}As, ^{77}Se, ^{99}Ru, ^{101}Ru, ^{102}Ru, ^{103}Rh, ^{105}Pd, ^{106}Pd, ^{107}Ag, ^{108}Pd, ^{111}Cd, ^{118}Sn, ^{121}Sb, ^{125}Te, ^{181}Ta, ^{193}Ir, ^{195}Pt, ^{197}Au, ^{205}Tl, ^{206}Pb, ^{208}Pb, and ^{209}Bi (Table 2).

2.2.4 Mass balance calculations

Mass balance calculations were determined by combining SEM and optical petrographic modal abundance determinations, LA-ICP-MS data for dissolved metals, and bulk rock analyses. Phases that contributed a negligible control on bulk element abundance (<0.5 wt%) were not included in the diagrams. For major phases, by reconciling combined laser ablation modal mass % data with bulk assay data, the contribution of each phase to the overall metal budget of the ore samples was determined. For discrete phases that were not analyzed by LA-ICP-MS (hessite, galena, altaite, sulfarsenides, sperrylite, michenerite-merenskyite) ideal formula compositions or SEM-EDS analyses were used in the mass balances. Metal contribution estimations for discrete accessory phases were made based on the grain size and vol% abundance (by grain area point counting), coupled with bulk mineral densities for ideal end-member compositions.

2.3 Results

The Appendices contain full data tables for sample depth (along diamond drill core, Table A1), bulk rock assays (Table A2), and LA-ICP-MS mineral compositional analyses (Table A3).

2.3.1 Petrography and metal grade characteristics of the ores

Each sample was classified based on sulfide abundance and texture similar to classification used by Vale for Sudbury South Range ore systems: i) massive sulfide

(MASU) samples composed primarily of pyrrhotite with sporadic chalcopyrite-rich intervals consist of more than 80% sulfide minerals and >30 wt% S; ii) inclusion-rich massive sulfide (INMS) samples have similar pyrrhotite dominant mineralogy to MASU but have higher proportions of silicate gangue inclusions (e.g. brecciated quartz veins, chloritized wall rock fragments), with bulk rock assays reporting between 20–30 wt% S and higher Cu/S ratios than MASU samples; iii) disseminated sulfide samples (DISS) contain variable chalcopyrite: pyrrhotite ratios, showing disseminated, net, and blebby textures with a gangue: sulfide ratio of >1 in hand sample, and with <20 wt% bulk rock S reported in assays. Characteristic textures and mineralogy in drill core are shown in photos and the graphic log (Figures 2.3 and 2.4), with average bulk rock analyses and metal grade in 100% sulfide for each sulfide texture listed in Table 2.2.

Massive pyrrhotite hosts coarse-grained (< 2 mm) pentlandite along inter-grain boundaries, and often contains >5 vol% magnetite (MASU, Figure 2.3A). Pentlandite "eyes" and mm-wide prismatic (elongated) flames are visible in hand sample (Figure 2.3). Although chalcopyrite was found only in trace amounts in the massive, pyrrhotite-rich sulfides, several depth intervals have high chalcopyrite abundances represented by veins (5-10 cm), xenomorphic masses, and complex intergrowths with pyrrhotite and gangue (Figure 3B,C,F,G). Rarely, massive chalcopyrite was observed (Figure 2.3D). MASU contains irregular, mm-to cm-sized inclusions of angular to rounded quartz diorite, metabasalt, metasediment, and other unidentified lithic fragments. Locally, inclusion volume can increase to 10-15%, and these increased abundances are often associated with an increase in chalcopyrite abundance. Commonly, small veinlets of quartz-carbonate and hydrous silicates (chlorite+epidote+quartz) cross cut MASU,

coating fracture surfaces. Contacts between MASU and other units are sharp, though locally MASU appears to grade into INMS. In thin section, samples of MASU typically contain primary pyrite. Some of these pyrite-bearing samples show cubic grains hosted within pyrrhotite, and lenses restricted to secondary (alteration) pentlandite textures and infilling fractures within pyrrhotite.

Samples of INMS contain at least 20 vol% host rock inclusions (quartz diorite, metasedimentary, metabasalt) and typically contain more chalcopyrite than the MASU (pyrrhotite-dominant, < 2 vol % cpy) samples (Figure 2.3E, Table 2.2). Samples of INMS commonly occur interstitially between MASU and DISS and are interpreted to be a transitional stage between them, but are also found enclosed within inclusion-bearing MASU intervals (Figure 2.4). Characterized by lower Ni:Cu ratios than MASU (Table 2.2, Figure 2.5) and higher inclusion volume %, INMS contains less pentlandite and more chalcopyrite than MASU, with variable magnetite (5–20%) and pyrite (<2%) abundances. As sulfide abundance decreases and INMS grades to DISS, pyrrhotite abundance decreases while chalcopyrite either increases slightly (<5 %) or remains the same. As pyrrhotite decreases in abundance and grain size, pentlandite grains become increasingly rare and much smaller. DISS most commonly marks the transition from MASU-INMS to barren intervals, but are also found less commonly where inclusions or silicates occur in higher proportions within MASU intervals. DISS (sulfides and silicate hosts) and inclusions within INMS that occur close to host rock contacts are slightly deformed and often display textural fabrics indicating deformation. Pyrite-marcasite-chalcopyrite vein networks occur in QD and metasediment host rocks, and often occur with, or are cross cut by, thin quartz-carbonate veins. Moderate to strong chlorite alteration is pervasive in

Table 2.2 Whole rock geochemical analyses of McConnell ore samples

	Ni	Cu	S	Co	Ag	Bi	Cd	As	Pb	Zn	Au	Pt	Pd
	wt %	wt %	wt %	wt %	ppm	ppm	ppm	ppm	ppm	ppm	ppm	ppm	ppm
MASU													
n	*35*	*35*	*35*	*35*	*35*	*31*	*19*	*2*	*35*	*30*	*35*	*35*	*35*
avg	1.32	0.96	34.6	0.10	7.19	12.6	4.99	6.00	38.77	163	0.156	1.16	3.12
stdev	0.13	0.90	2.65	0.02	6.17	7.32	6.72	1.00	55.47	335	0.360	1.54	3.30
max	1.50	2.87	39.7	0.12	25.8	35.0	28.6	7.00	274	1770	1.98	7.22	16.1
min	0.98	0.03	29.3	0.07	1.80	2.00	0.600	6.00	3.00	2.00	0.002	0.006	0.225
INMS													
n	*26*	*26*	*26*	*26*	*26*	*19*	*23*	*3*	*26*	*26*	*26*	*26*	*26*
avg	0.78	4.26	25.2	0.06	23.9	16.3	6.81	6.33	63.6	343	0.219	1.36	2.42
stdev	0.22	4.85	2.31	0.02	28.3	9.72	6.93	2.31	101	351	0.197	0.823	1.62
max	1.17	18.9	29.1	0.11	100	41.0	26.1	9.00	472	1460	0.725	3.53	6.78
min	0.29	0.39	20.6	0.02	2.10	3.00	0.60	5.00	5.00	41.0	0.024	0.053	0.512
DISS													
n	*17*	*17*	*17*	*17*	*16*	*13*	*17*	*2*	*17*	*17*	*17*	*17*	*17*
avg	0.40	3.13	14.0	0.03	22.3	12.5	6.67	5.00	60.0	443	0.945	1.57	2.88
stdev	0.25	3.58	5.81	0.02	26.7	9.06	6.91	n.a.	85.47	377	1.68	1.56	1.81
max	0.72	11.6	19.7	0.07	100	33.0	24.0	5.00	342	1200	7.22	6.34	5.46
min	0.02	0.02	2.41	0.01	2.60	1.00	0.500	5.00	5.00	65.0	0.002	0.159	0.015
normalized to 100% sulfide (all samples recalculated to ~ 38 wt % S)													
n	*78*	*78*	*78*	*78*	*77*	*63*	*59*	*7*	*78*	*73*	*78*	*78*	*78*
avg	1.30	4.69	38.8	0.11	30.1	20.4	12.8	8.54	97.1	634	0.689	2.11	4.62
stdev	0.35	7.06	0.92	0.03	48.3	14.3	18.9	1.33	174	1010	1.84	2.59	4.22
max	1.91	28.3	39.5	0.17	260	66.3	100	12.7	941	4830	15.1	16.1	19.8
min	0.33	0.03	35.8	0.03	1.99	2.12	0.639	5.00	3.23	2.58	0.002	0.006	0.243

Notes: n = number of samples with element above routine detection limits for that element
38 wt% S reported in assay for samples containing 95 - 100 % sulfide minerals

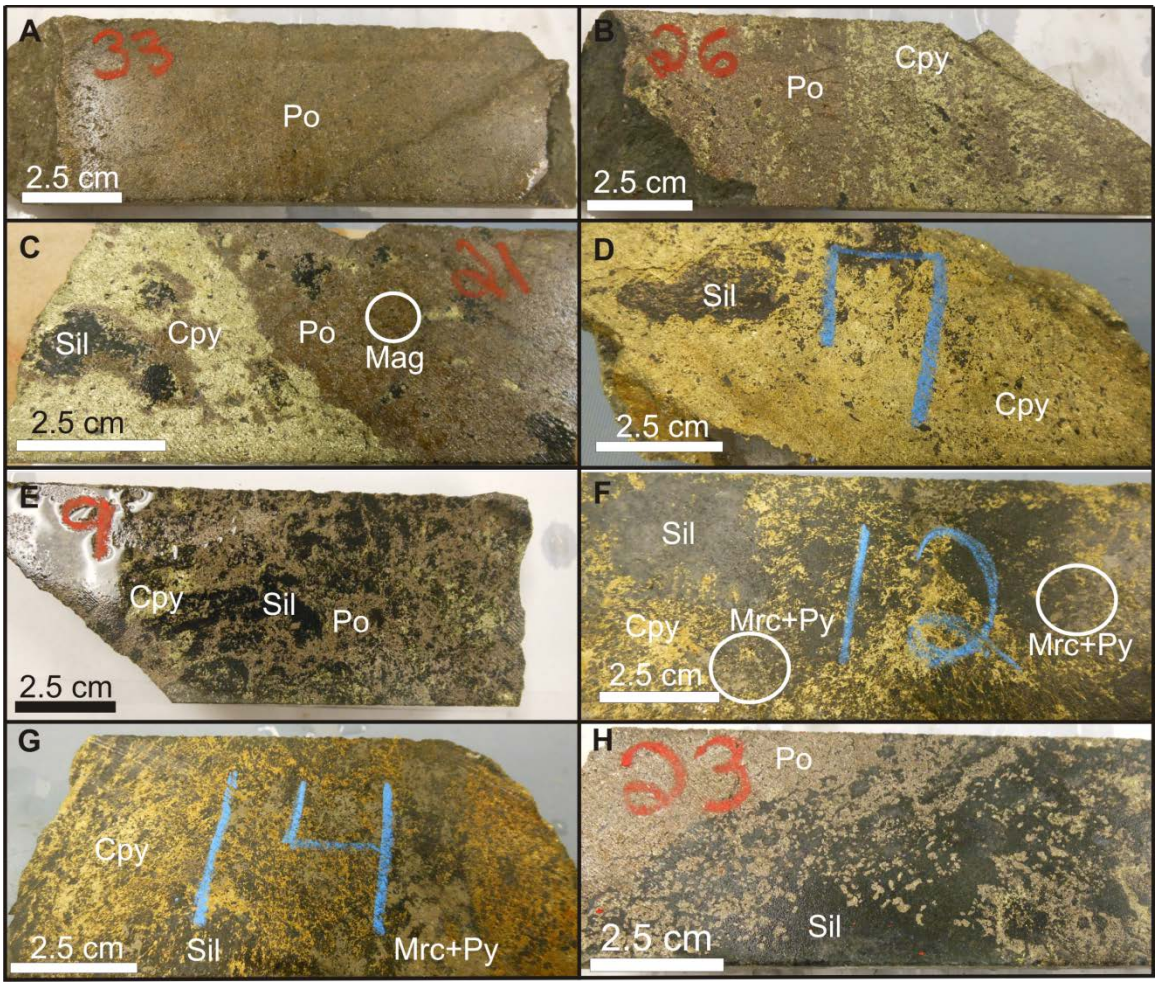

Figure 2.3 Representative McConnell mineralization samples of massive (MASU), inclusion-rich massive (INMS), and disseminated (DISS) sulfides. A. Typical sample of massive pyrrhotite (Po) hosting small pentlandite eyes and magnetite grains (not visible). B. Pyrrhotite-rich chalcopyrite-bearing (Cpy) massive sulfides typically occur as disseminated chalcopyrite within a matrix of small pyrrhotite grains. C. Contact between a chalcopyrite-rich and pyrrhotite-rich interval, silicate gangue inclusions (Sil) are commonly semi-rimmed by chalcopyrite, circled area shows very small magnetite grains. D. Copper-rich massive sulfide interval 330-7 occurs as one of the only samples to contain 80+ vol% chalcopyrite with only trace pyrrhotite. E. Typical intermediate-massive sulfide sample, gangue increases in abundance with chalcopyrite relative to pyrrhotite. F. Disseminated chalcopyrite occurs in gangue around inclusions of silicates with marcasite+pyrite (Mrc-Py) intergrowths which have completely replaced original pyrrhotite, circled areas show disseminated pyrite and marcasite. G. Intermediate-massive sample is dominated by disseminated chalcopyrite and semi-massive marcasite+pyrite. H. Massive sulfides transition quickly to disseminated pyrrhotite which is present in one of the few samples that exists as INMS-DISS in the absence of chalcopyrite.

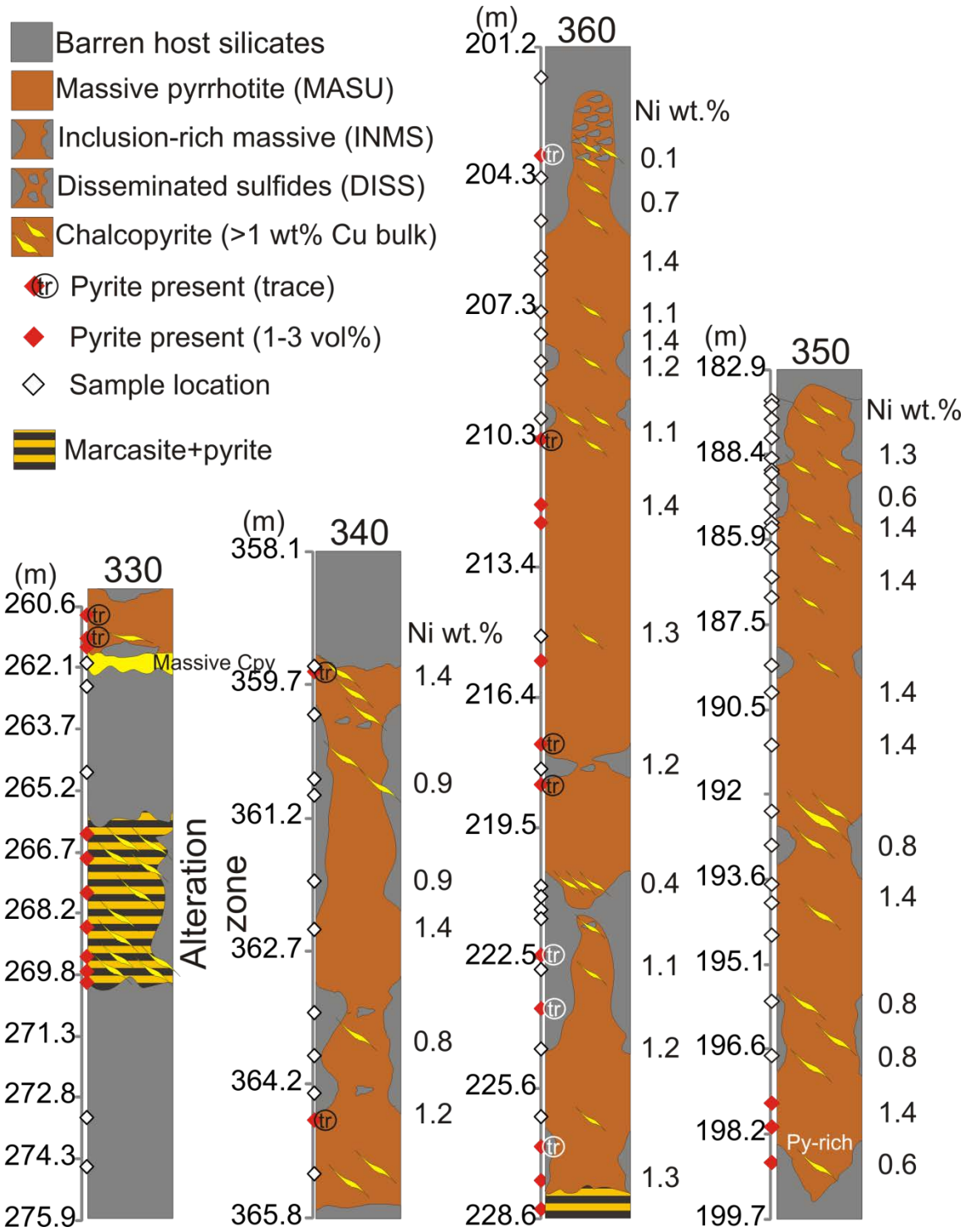

Figure 2.4 Graphical columns showing ore textures, ore types, accessory minerals and bulk rock Ni content through the 4 drill holes intersecting the McConnell ore body. Chalcopyrite distribution is shown by yellow lenses; the size and frequency of the symbol indicates higher proportions of chalcopyrite. Note: DDH indicated as last 3 digits of full hole number at top of each column drawing.

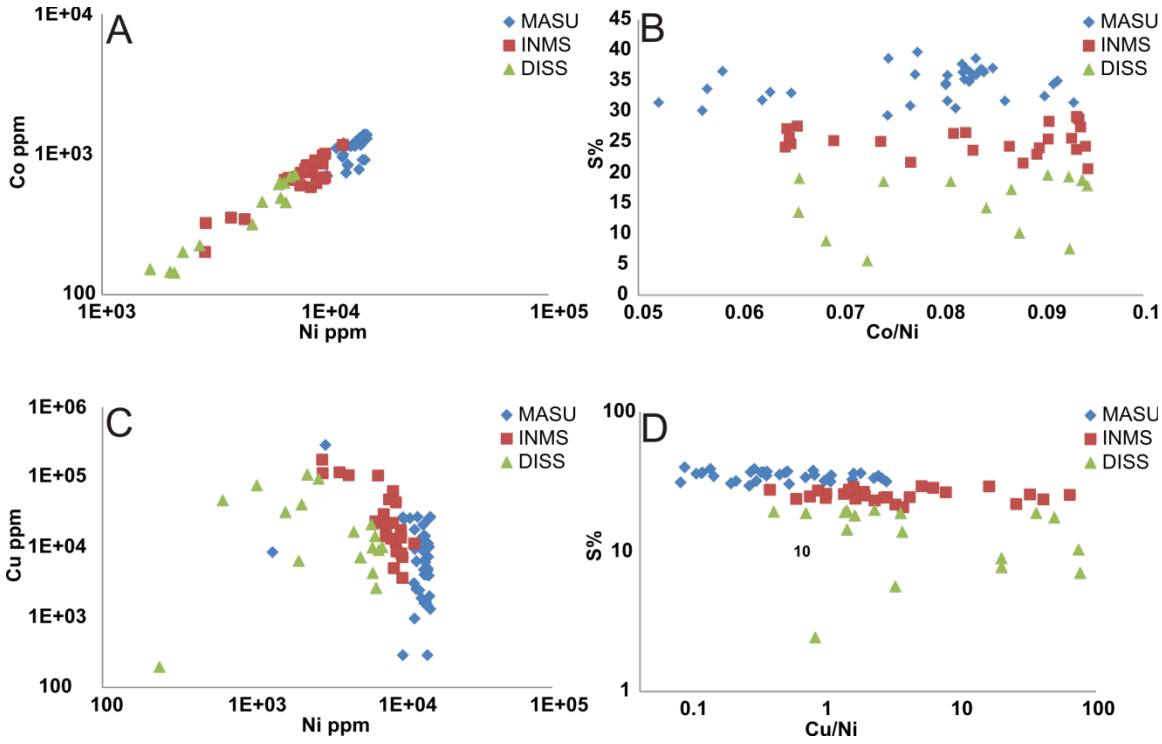

Figure 2.5 Relationships between Cu, Ni, and Co concentrations in bulk McConnell ores. A) Co and Ni show a direct correlation in all ore types, owing to cobalt abundance controlled by pentlandite. B) Wt% S and Co/Ni ratios in various ore textures; Ni concentrations rarely exceed 1.5 wt.%. C) Cu concentration in McConnell ores have some inverse relationship to Ni concentrations. D) Cu/Ni ratio typically increases with decreasing S as chalcopyrite is more abundant than pentlandite in INMS and DISS ore types.

these zones with fracture surfaces coated in hydrous silicates and thin sulfide layers. Sudbury breccia also occurs as clasts within quartz diorite near the host rock-QD contact, and their abundance marks the transition between quartz diorite and higher grade metamorphic rocks (quartzite, amphibolite). Foliation within local host lithologies increases with distance away from the margins of the ore body.

The degree of hydrothermal alteration within the McConnell deposit is based on mineral replacement reactions of pyrrhotite: (i) unaltered samples show no replacement textures of any kind, save for the distinctive pits within pentlandite grains (Figures 2.6D, E; 2.7A); (ii) low to moderately-altered samples show prismatic secondary pyrite (py II) radiating from cracks within pyrrhotite (Figure 2.6C, F), and; (iii) high or advanced alteration is distinguishable by the presence of marcasite intergrown with pyrite, replacing nearly 100% of primary pyrrhotite (Figures 2.6B; 2.7H, I). Advanced hydrothermal alteration of sulfide was observed within 2 drill holes in the McConnell deposit (Figures 2.4, 2.6), within the deepest 7 samples in drill hole 1276330 (~12 ft, 873.5 – 885.6 ft interval down hole) and the deepest sampled interval of hole 1276360 (at 749.3 ft down hole). Within these intervals pyrrhotite is altered to secondary pyrite and marcasite, occurring in association with chalcopyrite (Figures 2.6A,H; 2.7H,I). Unaltered grains of pyrrhotite and primary pyrite are often found enclosed within chalcopyrite. Nickel concentration is low (<0.5 wt% Ni) in altered samples due to pentlandite being nearly completely removed from the ores, with residual Ni remaining only in pyrite (~3-5 wt% Ni) and marcasite (0.5-3 wt% Ni). Hydrothermal alteration (chloritization) was also observed as pervasive within country rocks surrounding the ore body, especially near the zone of altered ore. Bulk rock assays are summarized in Table 2.2 by average and

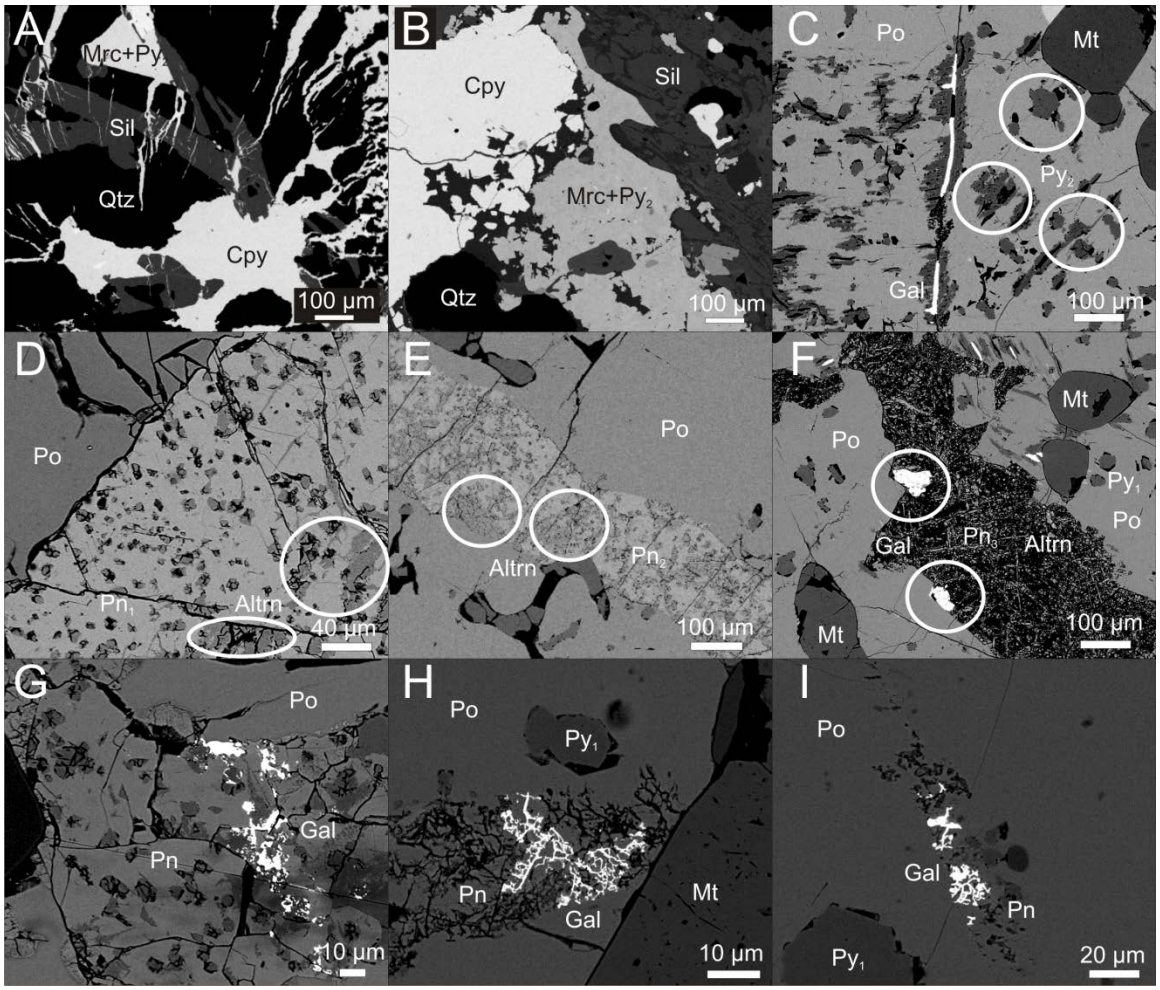

Figure 2.6 SEM images showing pentlandite and pyrrhotite alteration, and association of galena with altered pentlandite. A) Chalcopyrite (Cpy) occurs as veinlets through silicate gangue (Sil) and quartz (Qtz). B) Marcasite and secondary pyrite (Mrc+Py_2) completely replace pyrrhotite. Strong alteration does not appear to effect chalcopyrite (Cpy). C) Weak alteration of pyrrhotite (Po) to pyrite (Py_2) occurs along cracks and grain boundaries, cracks are often in-filled with galena (Gal). D,E) Pentlandite alteration (Altrn) initiated along cracks, with pentlandites always displaying a distinctive pitted surface at weak to moderate alteration intensity (Pn_1 - Pn_2). Pyrrhotite appears unaffected by this alteration, except for a slight increase in Ni content. F) Completely altered pentlandite (Pn_3) is in-filled with silicates and galena. Pyrite occurs as primary cubes (Py1) and secondary fracture-associated flames (Py_2). G) Galena is intergrown with weakly altered pentlandite, concentrating mainly near fractures and altered surfaces. H,I) Galena networks in strongly altered pentlandite. Silicate gangue in-fills pentlandite, galena forms complex networks along fractures within gangue. Primary and secondary pyrite (Py) are often abundant when these textures are encountered.

standard deviation per sulfide texture. An assay list is in Appendix Table A2.

The pyrrhotite-rich massive sulfides of all 4 drill holes typically show very low Ni:S and Cu:S ratios (0.03-0.04 and 0.02-0.36 respectively; Table 2.2, Figure 2.5), illustrating the low abundance of economic phases relative to total pyrrhotite host abundance. Ni:Cu ratios are generally 1–2 for all massive sulfide samples, with the exception of the massive chalcopyrite interval present within hole 1276330. Concentrations of Pt+Pd in massive sulfides are typically between 3–4 ppm, with Pd more abundant than Pt (Pd/Pt $\geq$1) in most samples. Contaminants such as Pb and Cd vary widely depending on alteration intensity and relative chalcopyrite and gangue abundances, but generally range from 12 – 50 ppm Pb (when pentlandite-pyrrhotite alteration intensity and gangue inclusion abundance is low) and <0.5 – 10 ppm Cd. Cadmium shows a general increase in concentration as Cu increases, but also appears to be much lower in holes 1276360 and 1276350 (<0.5 – 3 ppm) than in 1276340 and 1276330 (2 – 13 and 6 – 53 ppm Cd, respectively), even when Cu abundance is comparable. As MASU transitions texturally to INMS and DISS, gangue and chalcopyrite abundances increase relative to pyrrhotite, whereas Ni:S and Ni:Cu ratios decrease as pentlandite becomes less abundant. A decrease in cobalt abundance also occurs as textures transition from MASU to INMS to DISS (Figure 2.5). The INMS and DISS samples show higher concentrations of Cu than in massive ores (except sample 330-7, comprised of massive chalcopyrite) but show similar Pt+Pd concentrations and ratios. Pd increases as gangue becomes more abundant, while Zn and Cd abundances are associated with increased abundances of chalcopyrite. In comparing all samples, those from hole 1276330 have the highest proportions of Cu, Zn, Cd, Ag, and typically have higher than average abundances of Pb. The majority of these

samples have experiences a high degree of hydrothermal alteration, and completely lack pyrrhotite and pentlandite in samples that contain pyrite and marcasite. Although Ni concentrations are typically low in these samples, marcasite and pyrite retain some Ni content (1–5 wt% typically) as previously mentioned.

2.3.2 Mineralogical and trace element characteristics of major and minor sulfide phases

2.3.2.1 Pyrrhotite

Pyrrhotite is the most abundant sulfide mineral in the McConnell deposit and is the primary host for other major and minor sulfide and accessory phases (Figure 2.7A,D,E). Pyrrhotite occurs as both hexagonal grains hosting lamellae of monoclinic pyrrhotite, and as masses of monoclinic grains containing minor amounts of hexagonal pyrrhotite; these features were distinguishable using a magnetic colloidal solution. Monoclinic pyrrhotite is the more common polymorph in McConnell ores, approximately twice as abundant as hexagonal pyrrhotite (60-65% of pyrrhotite). Variations in pyrrhotite polymorph abundance do not correlate with any mineralogical or textural features. In massive sulfide samples, pyrrhotite forms large masses of mm-to cm-sized grains commonly hosting magnetite along inter grain boundaries (Figure 2.7D). Very rarely, pyrrhotite hosts lamellae of a second exsolved phase (troilite) along parallel planes (*c.f.* Voisey's Bay: Huminicki et al., 2012). The suspected exsolved troilite is non-magnetic and occurs most commonly within hexagonal pyrrhotite in massive sulfide samples containing larger grain sizes (0.1–0.5 mm). Pyrrhotite within the McConnell ores contains 0.6–1.4 wt% Ni, shows variable S:metal ratios (S between 38–43 wt%), and very low concentrations of dissolved deleterious metals (As <0.5 ppm, Pb <3 ppm; Table 3) compared to other deposits on the South Range.

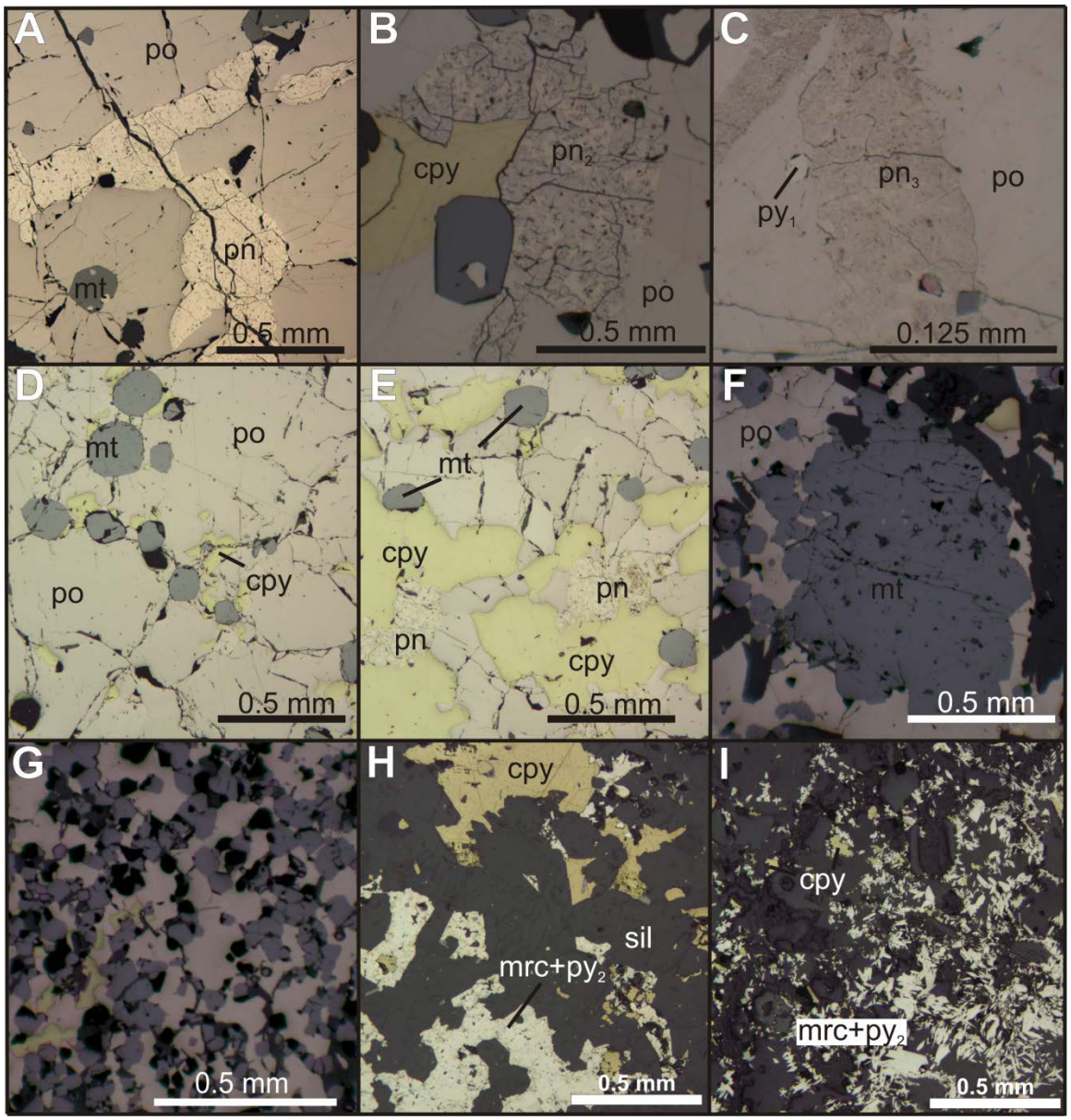

Figure 2.7 Textures and mineralogical association of McConnell ores. A. Coarse grains of pentlandite (pn_1) hosted along pyrrhotite-pyrrhotite (po) grain boundaries and triple junctions. B. Moderate to strongly altered pentlandite grain (pn_2) with chalcopyrite (cpy) and magnetite (mt) in massive pyrrhotite. C. Fully-altered pentlandite (pn_3) resembles little more than smudges along previous grain boundaries. Pyrite (py_1) occurs here. D. Typical assemblage in most McConnell ores, magnetite and chalcopyrite occur along and within grain boundaries of pyrrhotite. Pentlandite not shown. E. Samples which are more abundant in chalcopyrite often show a spatial relationship with creamy yellow pentlandite. F. Magnetite aggregate with silicate gangue and pyrrhotite. G. Magnetite-rich interval where hundreds of small euhedral-rounded grains occur along and within almost every pyrrhotite grain. H. Unaltered chalcopyrite with marcasite (mrc), secondary pyrite (py), and primary pyrite in a silicate gangue matrix. I. Disseminated marcasite and pyrite occur as blades within silicate minerals.

Table 2.3 LA-ICP-MS analyses (ppm) of pentlandite, pyrrhotite, chalcopyrite, and magnetite in the McConnell ores

	V	Cr	Co	Ni	Cu	Zn	As	Se	Ru[2]	Rh[3]	Ag	Pd	Cd
Pn_1 Unaltered-Light alteration													
n[1]	23	22	23	23	23	18	17	23		19	23	23	9
avg	12.3	25.7	$3.73x10^{4}$	$32.5x10^{4}$	540	33.2	0.282	50.7		0.017	26.0	3.79	0.809
stdev	8.36	35.9	$7.59x10^{3}$	$1.73x10^{4}$	859	65.7	0.111	6.79		0.019	14.5	2.75	1.46
max	31.6	115	$5.91x10^{4}$	$36.2x10^{4}$	$0.332x10^{4}$	244	0.590	69.7		0.072	66.9	8.66	4.64
min	3.28	0.540	$2.47x10^{4}$	$29.0x10^{4}$	16.6	0.610	0.152	42.9		0.003	10.6	0.799	0.048
Pn_2 Moderate alteration													
n	10	10	10	10	10	9	9	10		10	10	10	10
avg	28.1	22.4	$3.81x10^{4}$	$21.3x10^{4}$	441	6.63	0.222	53.4		0.017	55.5	3.14	0.117
stdev	30.6	38.8	$9.25x10^{3}$	$3.18x10^{4}$	517	10.1	0.073	10.2		0.011	31.8	2.36	0.073
max	111	135	$5.39x10^{4}$	$27.4x10^{4}$	$0.172x10^{4}$	32.5	0.340	69.9		0.043	120.8	7.95	0.300
min	4.85	0.930	$2.47x10^{4}$	$17.4x10^{4}$	6.12	0.530	0.129	38.5		0.007	16.2	0.828	0.037
Pn_3 Strong alteration													
n	6	5	6	6	6	5	6	6		6	6	6	6
avg	54.5	18.2	$2.76x10^{4}$	$10.8x10^{4}$	190	10.6	0.169	50.7		0.014	41.0	0.682	0.124
stdev	32.0	29.6	$7.24x10^{3}$	$2.52x10^{4}$	107	13.9	0.077	6.64		0.003	16.8	0.541	0.029
max	91.0	77.2	$4.14x10^{4}$	$15.9x10^{4}$	398	37.6	0.312	61.3		0.019	72.3	1.79	0.169
min	12.0	0.480	$1.86x10^{4}$	$7.68x10^{4}$	48.9	0.770	0.077	40.6		0.012	22.2	0.068	0.087
Pyrrhotite													
n	36	39	39	39	32	27	18	39	39	29	39	11	4
avg	4.37	11.8	157	$0.789x10^{4}$	173.857	13.797	0.201	52.502	0.060	0.021	0.354	0.006	0.048
stdev	7.16	28.1	46.6	$0.126x10^{4}$	293.899	25.131	0.108	5.310	0.036	0.049	0.189	0.004	0.014
max	33.8	163	255	$1.05x10^{4}$	$0.119x10^{4}$	120.250	0.536	63.730	0.146	0.249	0.883	0.017	0.069
min	0.014	0.420	75.0	$0.601x10^{4}$	0.471	0.450	0.105	45.430	0.008	0.002	0.084	0.001	0.029
Chalcopyrite													
n	35	34	39	39	39	39	12	39	39		39	24	39
avg	4.610	16.842	1.733	36.872	$31.993x10^{4}$	425.102	0.263	62.687	0.064		17.973	0.019	4.692
stdev	6.020	31.005	4.631	50.566	$0.774x10^{4}$	168.011	0.350	11.304	0.013		14.001	0.020	2.730
max	19.960	126.920	29.670	333.400	$33.664x10^{4}$	965.520	1.210	89.790	0.093		51.810	0.079	14.540
min	0.011	0.242	0.182	3.040	$30.371x10^{4}$	277.150	0.062	42.370	0.041		1.187	0.003	2.130
Magnetite													
n	36	36	36	35	30	36	35	24	13	7	27	25	8
avg	$0.124x10^{4}$	$0.448x10^{4}$	11.146	125.520	78.819	942.290	0.280	0.570	0.001	0.007	0.041	0.021	0.053
stdev	508.917	$0.576x10^{4}$	3.870	118.924	281.999	$0.172x10^{4}$	0.110	1.412	0.001	0.009	0.118	0.029	0.101
max	$0.212x10^{4}$	$2.454x10^{4}$	23.660	700.770	$0.121x10^{4}$	$0.709x10^{4}$	0.600	6.060	0.004	0.022	0.564	0.135	0.320
min	413.880	8.670	2.340	74.650	0.121	10.030	0.159	0.074	0.000	0.000	0.002	0.000	0.011

1 = number of analyses above detection limit
2 = NiAr interference prohibits accurate analyses of Ru in pentlandite
3 = CuAr interference prohibits accurate analyses of Rh in chalcopyrite

Table 2.3 Cont'd.

	Sn	Sb	Te	Ta	Re	Os	Ir	Pt	Au	Tl	Pb	Bi
Pn_1 Unaltered-Light alteration												
n	23	23	20	13	16	8	10		13	23	23	23
avg	0.883	0.261	0.499	0.007	0.010	0.017	0.019	bdl	0.029	3.493	90.414	1.542
stdev	0.628	0.229	0.474	0.011	0.004	0.005	0.035		0.048	4.462	49.319	1.235
max	2.710	0.807	2.000	0.036	0.021	0.026	0.110		0.185	22.070	224.750	4.610
min	0.132	0.038	0.122	0.000	0.006	0.007	0.001		0.007	0.640	25.880	0.058
Pn_2 Moderate alteration												
n	10	10	10	5	9	5	2		5	10	10	10
avg	1.464	0.398	0.679	0.003	0.008	0.015	0.002	bdl	0.016	20.746	392.656	2.681
stdev	1.056	0.586	0.526	0.003	0.005	0.009	0.000		0.010	18.682	252.835	2.670
max	4.020	2.135	1.470	0.008	0.019	0.032	0.002		0.035	51.010	735.170	9.270
min	0.316	0.089	0.126	0.001	0.005	0.008	0.002		0.005	2.120	85.830	0.630
Pn_3 Strong alteration												
n	6	6	6	5	5	3	1		6	6	6	6
avg	4.578	0.738	0.964	0.064	0.011	0.006	0.001	bdl	0.024	18.493	500.853	2.27
stdev	5.546	0.558	0.518	0.122	0.002	0.003	0.000		0.014	8.721	114.025	1.82
max	16.930	1.558	1.630	0.308	0.014	0.009	0.001		0.048	35.160	650.740	6.02
min	1.230	0.145	0.310	0.000	0.009	0.003	0.001		0.003	10.020	273.590	0.617
Pyrrhotite												
n	37	6	36	24	34	19	13	8	4	12	39	37
avg	0.115	0.028	0.159	0.006	0.032	0.011	0.041	0.009	0.003	0.019	1.606	0.101
stdev	0.067	0.016	0.062	0.016	0.134	0.005	0.080	0.008	0.000	0.015	1.284	0.111
max	0.390	0.063	0.362	0.073	0.802	0.020	0.260	0.022	0.004	0.044	5.040	0.660
min	0.053	0.015	0.047	0.000	0.001	0.003	0.000	0.001	0.002	0.002	0.177	0.004
Chalcopyrite												
n	39	28	39	20	13	6	15	5	19	33	39	39
avg	10.528	0.037	1.892	0.010	0.007	0.008	0.324	0.065	0.012	0.076	15.868	0.200
stdev	14.886	0.023	0.705	0.026	0.005	0.012	1.086	0.103	0.015	0.182	7.581	0.161
max	56.990	0.126	3.760	0.119	0.017	0.035	4.380	0.270	0.055	1.060	31.110	0.838
min	0.595	0.016	0.450	0.000	0.002	0.001	0.000	0.003	0.002	0.003	5.090	0.014
Magnetite												
n	36	36	11	32	21	6	9	9	6	18	36	32
avg	1.110	0.087	0.068	0.117	0.005	0.002	0.005	0.006	0.018	0.011	0.486	0.031
stdev	0.642	0.076	0.060	0.159	0.008	0.002	0.009	0.004	0.021	0.013	0.381	0.043
max	3.650	0.350	0.235	0.571	0.036	0.005	0.031	0.014	0.052	0.060	1.532	0.214
min	0.336	0.007	0.026	0.001	0.001	0.000	0.000	0.002	0.001	0.002	0.020	0.003

1 = number of analyses above detection limit
2 = NiAr interference prohibits accurate analyses of Ru in pentlandite
3 = CuAr interference prohibits accurate analyses of Rh in chalcopyrite

2.3.2.2 Chalcopyrite

Chalcopyrite occurs heterogeneously throughout the deposit as masses of interlocking xenomorphic grains within coarse-grained pyrrhotite cumulates, and often hosts subordinate pentlandite and magnetite within and along grain boundaries (Figure 2.7E). In chalcopyrite-rich intervals, monoclinic pyrrhotite is more common than hexagonal pyrrhotite, and pentlandite grains occur intergrown with, or as lamellae interstitial to, pyrrhotite and chalcopyrite. Intervals with po:cpy ratios > 1 show chalcopyrite occurring in veins and flame-like structures in massive pyrrhotite which are often associated with small abundances of pentlandite. Very rarely, chalcopyrite is associated with trace amounts of sphalerite that occur as irregular blebs within and along chalcopyrite grains. Chalcopyrite has very low concentrations of contaminant metals (As <1 ppm, Cd 2.5–7.0 ppm, Pb 8.5–26.0 ppm) and variable but appreciable amounts of Ag (up to 38 ppm Ag, Table 3). In areas where pyrrhotite has been completely replaced by marcasite and secondary pyrite, chalcopyrite shows no textural or chemical modification due to alteration (Figures 2.6, 2.7).

2.3.2.3 Pentlandite

Pentlandite grains are most commonly hosted between pyrrhotite grain boundaries as blocky, subhedral “eyes” (rarely > 1cm in diameter, Figure 2.7A), which contain octahedral pits filled by inclusions of pyrrhotite (Figure 2.6D). Grains of pentlandite hosted along pyrrhotite boundaries occur as elongated masses that rim smaller interstitial pyrrhotite grains. Coarse-grained pentlandite occurs as unaltered to strongly altered grains that show both textural and chemical differences with increasing degree of alteration (Figure 2.7B, C; Figure 2.6D-F; Table 2.3). The degrees of alteration is reflected in the physical attributes of pentlandite; (i) advanced alteration (pn_2) shows a

higher proportion of pyrrhotite inclusions and alteration patches than low alteration, losing its typical creamy-yellow coloration and appearing more like pyrrhotite (Figures 2.6D-F; 2.7A-C); (ii) increasing degrees of alteration ($pn_{2\text{-}3}$) show higher proportions of fractures and silicate networks within individual pentlandite grains (Figure 2.6F-I), though low to unaltered pentlandite also shows fractures and shrinkage cracks (Figure 2.7A), and (iii) oxidation occurs very rapidly in pentlandite which has suffered higher degrees of alteration, forming oxidation tarnish in as little as one week in thin section. Textural alteration ranges from optically homogenous, creamy-yellow pentlandite (pn_1, Figure 2.7A) to dull, "hazy" relics (pn_3, Figure 2.7C) which remain as patches that optically and compositionally resemble a Ni-rich pyrrhotite. Notably, the chemical composition of pentlandite shows a depletion of Ni, Co, As, and Pd with increasing degrees of alteration, while Ag, Sn, Sb, Te, Bi, and Pb increase (variably) with alteration (Table 2.3). The Ni content of pentlandite alteration products range from 32 wt% Ni (Ni:Co 9.02, $1\sigma = 1.76$ in least altered) to 10 wt% Ni (Ni:Co 4.13, $1\sigma = 0.24$) in most altered grains), with Co contents ranging from 2–6 wt% (Table 2.3). The Pb content of pentlandite and alteration products is also high, ranging from 65–663 ppm, with strongly altered grains containing higher concentrations (500 ppm, $1\sigma = 114$) than the values for unaltered samples (90 ppm, $1\sigma = 49.3$; Table 3.3). Pentlandite also contains appreciable amounts of Ag (17–85 ppm) and Pd (1–8 ppm; Table 2.3); Pd tends to decrease with alteration intensity while Ag increases with alteration intensity, the most Ag-rich grains occurring as moderately altered intergrowths of pentlandite and alteration products. In addition to the coarse-grained variety, pentlandite also occurs as exsolution (flame) lamellae within pyrrhotite grains and along pyrrhotite-pyrrhotite and pyrrhotite-

chalcopyrite grain boundaries. These lamellae are oriented parallel to basal parting planes (001) in individual pyrrhotite grains. In all samples, pentlandite is only a minor phase (up to 3 vol%; Figure 7). Pentlandite is most common in massive sulfide intervals with coarser pyrrhotite grains and subordinate chalcopyrite, and is absent where pyrrhotite is altered to marcasite except where completely encased (isolated) in chalcopyrite protected it from secondary alteration by hydrothermal solutions.

2.3.2.4 Magnetite

Magnetite occurs as euhedral to subhedral single grains (0.05–1 mm in diameter) and crystal aggregates of varying size (Figure 2.7F) in sulfide and gangue hosts in abundances ranging from 0–20 vol% (Figure 2.7G). The abundance of magnetite in samples does not appear to correlate to any other mineral abundances. Within pyrrhotite and chalcopyrite, magnetite occurs completely included along boundaries between sulfide grains, or partially included along sulfide-gangue boundaries (Figure 2.7D, E). Magnetite grains uncommonly contain small polyphase sulfide mineral assemblages included within them composed of pyrrhotite+chalcopyrite. Phase proportions in these sulfide inclusions are consistent from one inclusion to another, suggesting that they are recrystallized sulfide melt inclusions (see Discussion in Chapter 3). Magnetite distribution and chemistry are discussed in detail in Chapter 3.

2.3.2.5 Pyrite

Euhedral to subhedral cubic crystals of primary pyrite (py_1) rarely exceed 0.05 mm in size and occur in abundances < 5 vol%. Early pyrite is hosted within base metal sulfides and occasionally within gangue minerals, concentrated along grain boundaries between silicates and sulfides, and can occur with or without secondary pyrite in samples which contain altered pentlandite (Figure 2.7C). The overall distribution of pyrite is highly

sporadic. In samples showing hydrothermal alteration of sulfides, secondary pyrite (py_2) occurs as prismatic radiating crystals intergrown with pyrrhotite (Figure 2.6C). Secondary pyrite intergrowths are spatially hosted along small cracks in otherwise unaltered pyrrhotite. In intervals with intense alteration ("marcasite alteration zone", Figure 4), secondary pyrite is intergrown with marcasite and has completely replaced pyrrhotite (Figure 2.7H,I). In this zone primary pyrite occurs as rare, relict, partially altered grains or as unaltered inclusions encased within chalcopyrite. Primary and secondary pyrite contain small amounts of Ni, between 3–4.5 wt% (SEM analyses, Table A4), occurring in Ni-rich cores in primary pyrite and homogeneously distributed in secondary pyrite. The distribution of pyrite in the studied drill cores is shown in Figure 2.4.

2.3.2.6 Marcasite

Occurring only in heavily altered intervals, marcasite is intergrown with secondary pyrite and replaces pyrrhotite to create large masses of interlocking, small grains (Figure 2.7H) that mimic the original pyrrhotite grain boundaries and occur with chalcopyrite and gangue minerals, as well as some trace magnetite. Marcasite occurs only in the lower-most (deepest) sections of the ore body. Like pyrite, marcasite grains contain small amounts of Ni (up to 4.5 wt%; SEM analyses, appendix).

2.3.3 Discrete and precious metal phases

2.3.3.1 Sulfarsenide solid solution minerals (SSS)

Sulfarsenide solid solution is the principle carrier of As within McConnell but is uncommon within the deposit. Occurring as small (10–50 µm) euhedral rhombs (Figure 2.8 A-C) of distinct cross-sectional forms (4-sided or 6-sided), this phase ranges in crystal system and form in the ores (cobaltite: orthorhombic pyramidal, glaucodot: orthorhombic

dipyramidal, gersdorffite: isometric tetartoidal). These sulfarsenide minerals also show compositional ranges between the solid solution end members cobaltite-glaucodot-gersdorffite and are commonly zoned in their PGE content with some grains containing a tiny inclusion enriched in Ir (irarsite) or Rh (hollingworthite) at their cores (Figure 2.8 A,B). The SSS grains are hosted entirely within pyrrhotite or along pyrrhotite-gangue grain boundaries, and are rarely hosted entirely within gangue. When occurring along pyrrhotite-gangue grain boundaries, SSS grains are rarely intergrown with PGE minerals (Figure 2.8D,E; Table 2.4).

2.3.3.2 Galena and altaite

Small blebs of galena and rare grains of altaite (PbTe) rarely exceed 5 μm in size. Galena is dominantly hosted by gangue minerals (Figure 2.8I, J) or along pyrrhotite-gangue grain boundaries, whereas altaite is more commonly included within pyrrhotite (Table 2.4). Abundances of Pb-bearing discrete minerals are ubiquitously very low in the ores and rarely exceed ~0.001 vol% (100 * grain area and abundance divided by overall section area), though some samples do show slightly higher abundances of these phases locally within some intervals (up to 0.003 vol%). Larger grains (up to 50 μm) of galena occur within silicate gangue within Pb-rich intervals (Table 2.4; Figure 2.8H, I, J). In samples where secondary pyrite is present, galena occurs with silicate gangue and pyrite, infilling fractures in pyrrhotite (Figure 2.6C). Notably, altered pentlandite (pn_{2-3}) also hosts these galena-gangue fracture infillings (Figure 2.6G-I); the fracture infillings of galena in pentlandite are very fine grained, and increase in abundance as alteration intensity increases in the host pentlandite.

Table 2.4 Trace phases within McConnell ores

Sample	Phase	Size µm	Mode of occurrence	% occurrence	abundance (# of occurrences)	wt% S	Fe	Co	Ni	As	Rh	Pd	Ag	Te	Pt	Pb	Bi
330-04	galena	3x10 - 5x15	fracture-filling silicates	20	rare (2-3)												
	galena	2x2	inclusions in silicates	80	rare (5)												
	altaite	~11x14	inclusions in pyrrhotite	100	rare (2)												
330-12	hessite	30x60 - 10x15	sulfide/silicate boundary	100	rare (2)								63.23	36.77			
													62.28	37.72			
330-13	galena	3x5	inclusions in silicates	100	rare (5-10)	15.3										84.7	
	SSS	15x20	inclusion in marcasite	50	1												
	SSS	200x50	inclusion in marcasite	50	1	23.95	6.66	19.09	8.28	42.02							
	sperrylite	25x20	inclusion in py/mrc	100	1					45.2					54.8		
350-14	galena	15x30 - 9x14	inclusions in silicates	100	rare (5-10)	15.3										84.7	
	merenskyite	70x50	gangue-po boundary	5	rare (1)							27.18		34.64			38.18
	merenskyite	30 - 15x10	gangue-po boundary	95	common (20)							26.63		35.09			38.28
	hessite + merenskyite	10x20	gangue-po boundary	100	rare (1)							19.36	13.92	32.35			34.37
350-15	galena	3x5	inclusions within silicates	100	common (25-30)												
	sperrylite	5x8	inclusion in silicates	100	1					44.8					55.3		
350-21	galena	15x12	inclusion in silicate	100	1												
	merenskyite	7x14	inclusion in pyrrhotite	100	1							26.7		34.73			38.57
	SSS	20x40	inclusion in pyrrhotite	66	2	24.18	8.13	16.89	7.16	40.42	3.21						
						23.2	8.19	16.63	5.28	38.36	8.33						
	SSS	15x20	inclusion in pyrrhotite	33	1	23.97	6.87	18.63	6.15	39.74	4.64						
350-24	galena	5x7	inclusions in silicates	100	rare (5-10)												
	SSS	45x25 - 30x35	inclusions in pyrrhotite	100	moderate (10-15)												
	core					23.98	6.94	19.53	6.83	40.94		1.78					
	rim					23.48	7.36	17.14	7.38	40.98	3.67						
	core					24.66	6.49	21.84	5.21	39.83		1.98					
	rim					23.48	7.36	17.14	7.38	40.98	3.67						
	core					23.07	7.36	16.57	7.03	39.93	3.24	2.8					
	core					24.08	8.14	18.25	6.52	41.1	3.52	2.15					
	core					24.57	6.36	21.05	5.96	42.06							
	core					21.93	5.95	15.59	5.53	38.88	9.51	2.61					
	altaite + merenskyite	80x50	gangue/pyrrhotite boundary	100	1							18.63		50.5		19.1	11.79
	merenskyite	15x27	gangue/pyrrhotite boundary	100	rare (3-5)							26.75		33.96			39.29

Table 2.4 Cont'd.

Sample	Phase	Size µm	Mode of occurrence	% occurrence	abundance (# of occurrences)	wt% S	Fe	Co	Ni	As	Rh	Pd	Ag	Te	Pt	Pb	Bi
350-27	galena	100x100	pyrrhotite/silicate boundary	1	rare (1)												
	galena	30 - 50X30	pyrrhotite/silicate boundary	30	common (20-25)												
	galena	10x10	inclusions within silicates	69	abundant (50+)												
350-33	galena	5 - 10x20	infilling fractures	100	common (20-25)												
350-34	galena	25-50x60	grains within pentlandite	40	abundant (30-40)												
	galena	5-10x20	infilling fractures	60	abundant (40+)												
	sperrylite + SSS	20x30	inclusion in pyrrhotite	100	1												
350-35	galena	50x50 - 20x25	inclusions within silicates	40	abundant (35-50)												
	galena	5x10 - 3x3	blebs within silicates	60	abundant (50+)												
	sperrylite	70x50	inclusion in pyrrhotite	100	1					44.24					55		
360-06	galena	≤ 5	inclusion in silicate	100	rare (3-6)												
	merenskyite	10 - 15x20	inclusion in pyrrhotite	100	rare (1-4)							26.2		40.69			33.12
	SSS	15 - 23x35	inclusion in pyrrhotite	100	rare (5-8)												
	rim					22.28	7.28	17.57	4.99	39.45	5.43	2.99					
	core					23.01	7.24	16.89	5.11	39.29	8.46						
	core					22.87	7.03	16.6	5.1	38.87	9.53						
	rim					24.34	7.37	21.12	5.76	39.75		1.66					
	core					22.76	6.67	17.16	5.38	39.01	9.02						
	core					22.85	7.19	17.32	5.73	39.23	7.68						
	core					23.81	6.52	21.72	4.82	40.42	2.71						
	core					23.12	6.14	18.81	5.43	40.5	6						
360-19	galena	2 x 10 - 100	Fracture filling in pn	100	abundant (30-40)												
	Cored SSS	5 - 10x15	inclusions in pyrrhotite	50	rare (1)												
	rim					23.8	5.92	21.04	6.83	40.77		1.63					
	core					23.03	5.45	18	5.77	42.16	5.58						
	Un-cored SSS	5 - 10x15	inclusions in pyrrhotite	50	rare (1)	23.93	6.9	19.64	8.03	41.5							

Notes: All compositions given in wt%; CGSS are solid solution sulfarsenides
% occurrence = % of grains occurring in a specific textural association

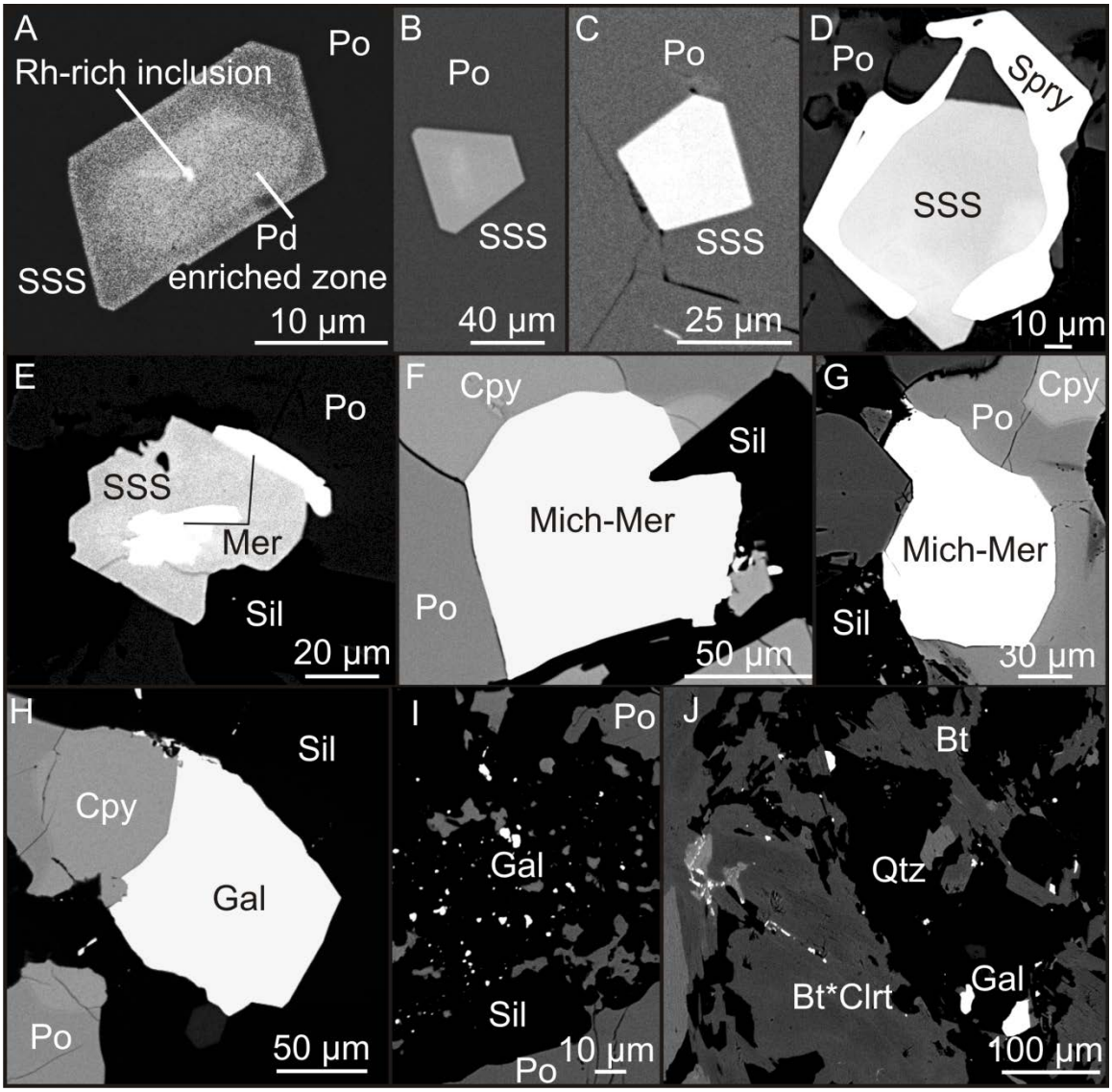

Figure 2.8 Backscatter electron images of discrete phases. A-C) Solid solution sulfarsenides (SSS) exist as euhedral inclusions within pyrrhotite (Po) and often contain some concentration of Pd rimming a core of either Rh bearing mineral (hollingworthite) or Ir bearing mineral (irarsite). D, E) Sulfarsenides (SSS) occurring along sulfide-silicate (Sil) boundaries are intergrown with sperrylite (Spry) and merenskyite (Mer). F, G) Michenerite-merenskyite (Mich-Mer) occurs along pyrrhotite-chalcopyrite-silicate (Po-Cpy-Sil) boundaries. H) A large grain of galena (Gal) occurs between sparse sulfides and silicates (Sil). I, J) Galena (Gal) most often occurs as small blebs within silicates (Sil), concentrating locally in samples.

2.3.3.3 Au, Ag, and platinum-group minerals (PGM)

Palladium is hosted in solid solution bismuth-tellurides ranging in composition from michenerite (PdBiTe) and merenskyite [$(Pd,Pt)(Te,Bi)_2$], as well as in rare grains of kotulskite Pd(Te,Bi) (Table 2.4). Almost exclusively hosted along grain boundaries of base metal sulfides and silicate gangue, Pd-Bi-tellurides are larger (up to 130 μm in diameter, Table 2.4) and more common than other PGM (sperrylite) or tellurides (hessite, altaite) combined. They commonly occur as unzoned xenomorphic crystals as isolated grains or intergrown with other accessory PGE-Au-Ag phases (Figure 2.8E-F). Silver and Pb tellurides are present as hessite (Ag_2Te), which forms rare, irregular grains (up to 60 μm in diameter) often intergrown with altaite (PbTe) and Pd-Bi-Te phases along silicate-sulfide boundaries. Platinum-bearing PGM are extremely uncommon and are represented only by sperrylite, which occur as inclusions (up to 70 μm) hosted entirely within pyrrhotite, inclusions hosted within alteration products of pyrrhotite (pyrite and marcasite), or as rare intergrowths of sperrylite and SSS along sulfide-silicate grain boundaries (Figure 2.8D; Table 2.4).

2.3.4 Mass balance calculations

The proportions of total assay carried by discrete minerals and dissolved metals in base metal sulfides are shown in Figure 2.9. Nickel and cobalt are controlled by pentlandite and pyrrhotite (Ni hosted in pyrrhotite (40-80%), Ni hosted in pentlandite (20-60%); Co hosted in pyrrhotite (15-25%), Co hosted in pentlandite (75-85%). The contribution of Ni and Co from solid solution sulfarsenides (SSS) is negligible (<0.5 %) in all samples. Arsenic is very low (< 5 ppm), and is controlled primarily by sperrylite and sulfarsenides, although pyrrhotite in bulk abundance can often contain >50% of the overall As budget of the ores. It should be noted that while magnetite can actually host a

substantial portion (3-5 wt%) of the bulk As due to its concentration within the ores, it was omitted for re-calculation to 100% sulfide. Platinum is controlled predominantly by sperrylite, but in intervals where sperrylite was not encountered, chalcopyrite was the only other Pt-bearing phase to host the bulk of the Pt, though Pt dissolved in solid solution in nearly all base metal sulfides studied was found to be negligible (via LA-ICP-MS, Table 2.3). Platinum may also be hosted within discrete Pd-Bi-Te minerals, though no laser ablation analyses were performed to confirm this due to the size of the grains. Palladium is distributed between base metal sulfides, SSS grains, and discrete Pd-Te phases, with the primary hosts being pentlandite and michenerite-merenskyite (Tables 2.3, 2.4). Lead distribution within McConnell ores is controlled primarily by base metal sulfides (pentlandite, pyrrhotite) rather than discrete Pb phases. Silver-bearing phases are hessite (Ag_2Te) and base metal sulfides (pentlandite, chalcopyrite, pyrrhotite), with pentlandite containing the highest concentration of Ag among the major sulfide phases.

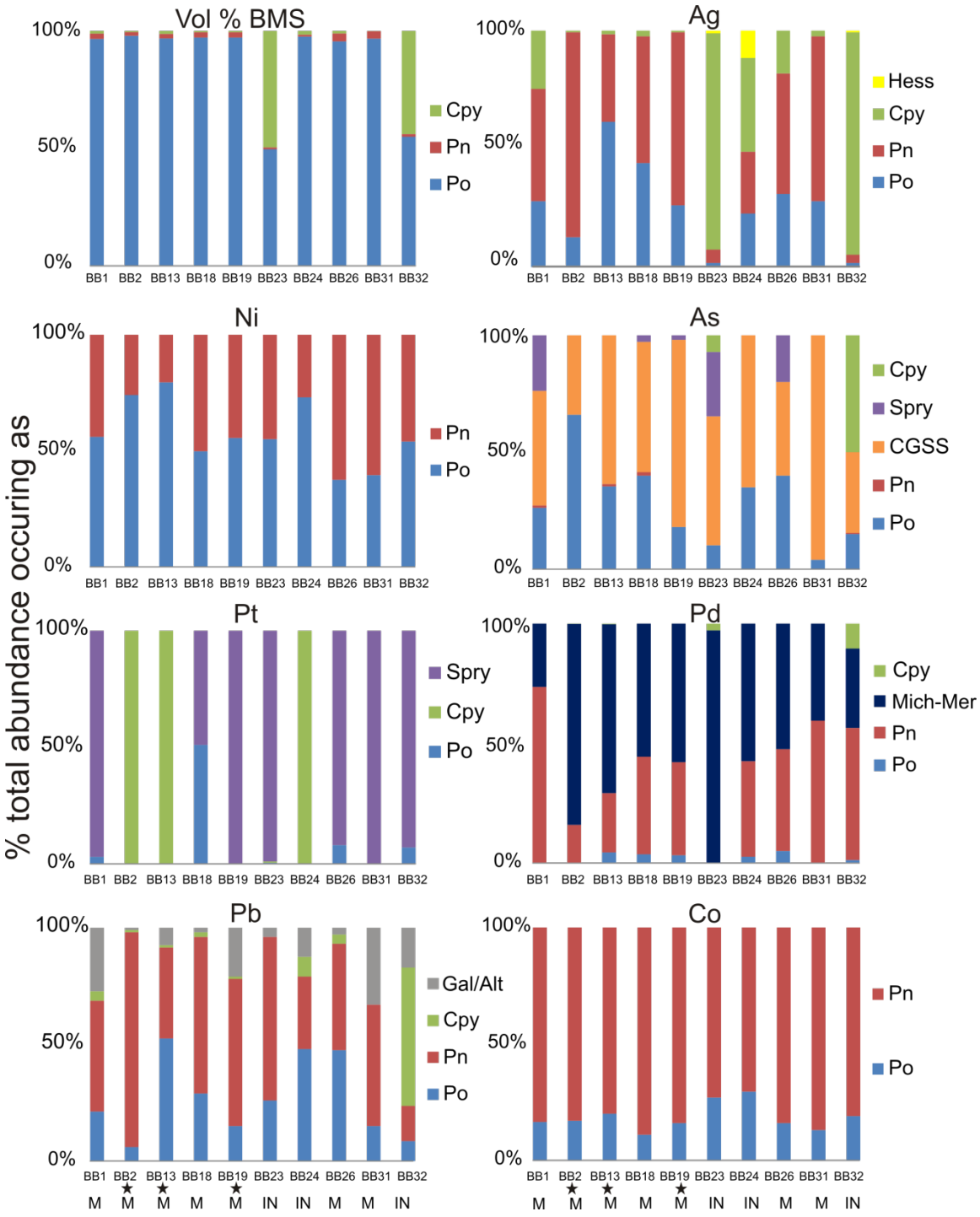

Figure 2.9 Element distribution among base metal sulfides and discrete phases from mass balance calculations. Samples analyzed are from hole 1276360. Pn – pentlandite, Po- pyrrhotite, Cpy – chalcopyrite, CGSS – solid solution sulfarsenides, Spry – sperrylite, Mich-mer – michenerite-merenskyite (solid solution palladio-tellurides), Gal/Alt – galena and altaite. X axis indicates sample number, y axis indicates the amount of each mineral that controls each element. Letters below sample number on bottom frame indicate MASU (M) or INMS (IN). Star symbols indicate samples with intense pentlandite alteration.

2.3.5 Distribution of trace elements in sulfides

Laser ablation maps (Figures 2.10 and 2.11) of element distribution in altered and unaltered pentlandite grains in typical sulfide-oxide assemblages show that, regardless of degree of alteration, pentlandite shows enrichment of Co, Ni, Pd, Ag, Pb, and Ru compared to associated pyrrhotite or chalcopyrite. Altered pentlandite (Figure 2.10) retains elevated (primary) Co, Ag, and Pd, though the texture and heterogeneity of grains suggests that this phase is not (or was not) stable at the conditions of pyrrhotite formation and during subsequent aging and hydrothermal alteration. Lead and Ag are enriched not only in the unstable altered phases, but also show elevated concentration between grain boundaries of primary unaltered minerals (i.e. pyrrhotite and magnetite). Cobalt shows a slight enrichment between grain boundaries, but is primarily localized to pentlandite. Cobalt, Ni, and Pd are distributed homogeneously in pentlandite (with the exception of the interstitial mineral filling the pitted grains), showing an enrichment in these elements compared to other phases. The distribution of Co, Pb, and Ag is similar (and homogenous) in pentlandite alteration products, with Ag and Pb showing fracture controlled behaviour which confirm that these elements were mobile during alteration (Figure 2.10). Pd distribution in alteration products is also homogenous. Pentlandite grains which show the least alteration contain less Pb than alteration products, but still occur as isolated Pb rich “hot spots” which is consistent with the onset of Pb mobilization and contamination. Silver also occurs as isolated “hot spots” very similar to Pb, while the distribution of Pd and Co is homogenous (Figure 2.11). In samples where altered/unstable pentlandite is found, very little pyrrhotite alteration and related enrichment or depletion of trace metals is encountered. Aside from textural differences and Pb enrichment with Ni

depletion, the presence of pyrite is also noted as distinguishing characteristics of unstable and stable pentlandite-bearing assemblages.

2.3.6 Range of Pb-isotope analyses

Pb-isotope ratios were collected from pyrrhotite and pentlandite at the GSC using the same laser ablation system as the previous LA-ICP-MS analyses. Full isotope ratios for pentlandite and pyrrhotite are listed in Table 2.5 Pyrrhotite errors are primarily due to variable Hg concentrations which, when analysed by LA-ICP-MS, cause interferences between ^{204}Hg and ^{204}Pb. Pentlandite shows variability between altered and unaltered grains, with fresh pentlandite Pb ratios of; $Pb^{206/204}$ 19.34-20.07; $Pb^{208/204}$ 39.54-40.63; and $Pb^{207/204}$ 15.81-16.08. Altered pentlandite grains show consistent but lower ratios; $Pb^{206/204}$ 17.86-18.55; $Pb^{208/204}$ 37.90-38.78; and $Pb^{207/204}$ 15.68-15.87. Table 2.5 and Figure 2.13 show detailed results of Pb isotope ratios. All values have been corrected for Pb/Hg interferences.

Table 2.5 Lead isotope ratios of unaltered and altered pentlandite grains from the McConnell ore deposit

	Background subtracted CPS data					204Hg interference and mass bias corrected Pb isotope ratios									
Sample Name	204	206	207	208	Pb/Hg	206/204	64SE	207/204	74SE	208/204	84SE	207/206	76SE	208/206	86SE
Unaltered pentlandite															
B350141	4338	85286	67947	173029	1220	20.07	0.09	15.83	0.08	40.32	0.16	0.791	0.004	2.004	0.007
B350142	3556	68621	56377	141763	1071	19.93	0.10	16.08	0.08	40.39	0.17	0.812	0.004	2.043	0.009
B350143	3306	64729	52365	132135	899	20.04	0.10	16.06	0.09	40.63	0.19	0.803	0.004	2.025	0.009
B350144	2930	57013	46292	117334	1053	19.69	0.13	16.17	0.12	40.32	0.25	0.827	0.007	2.060	0.014
B350145	4292	81264	68372	168901	1292	19.34	0.09	16.04	0.09	39.54	0.17	0.833	0.004	2.054	0.009
B350146	3191	61196	50044	127042	1061	19.60	0.11	15.81	0.09	39.82	0.21	0.808	0.005	2.047	0.012
B350147	4065	79186	64361	163550	1251	20.03	0.10	16.08	0.09	40.59	0.23	0.804	0.004	2.026	0.011
Altered pentlandite															
BB5Pn1	35248	638925	553580	1355951	2121	18.44	0.03	15.87	0.03	38.78	0.07	0.859	0.002	2.101	0.003
BB5Pn2	32740	590681	513683	1258245	3662	18.25	0.04	15.73	0.04	38.46	0.09	0.860	0.002	2.102	0.005
BB5Pn3	58042	1041831	908753	2224877	4435	18.22	0.03	15.78	0.03	38.50	0.07	0.866	0.002	2.110	0.004
BB5-Pn1	30911	561483	483013	1188703	7834	18.47	0.04	15.69	0.03	38.53	0.08	0.851	0.002	2.094	0.005
BB5-Pn2	21647	389299	338914	830645	8857	18.25	0.05	15.71	0.04	38.44	0.09	0.861	0.002	2.110	0.005
BB5-Pn3	42659	771861	665975	1644419	15639	18.38	0.04	15.70	0.04	38.59	0.08	0.853	0.002	2.104	0.005
bb5-Pn4	18078	327524	282612	695929	11230	18.37	0.06	15.74	0.05	38.46	0.12	0.855	0.003	2.097	0.006
bb5-Pn5	15223	277774	238061	587286	7555	18.55	0.06	15.71	0.05	38.58	0.12	0.847	0.003	2.081	0.007
bb5-Pn6	9553	172844	149337	367418	12187	18.45	0.07	15.73	0.07	38.44	0.15	0.853	0.003	2.091	0.008
bb5-Pn7	8720	157502	136097	335471	11465	18.34	0.07	15.71	0.07	38.56	0.14	0.856	0.004	2.099	0.008
bb5-Pn8	15155	273428	237230	580902	15817	18.39	0.06	15.74	0.05	38.45	0.12	0.855	0.003	2.091	0.006
bb5-Pn9	13799	247615	216046	528045	10708	18.26	0.06	15.80	0.05	38.37	0.11	0.866	0.003	2.104	0.006
bb5-Pn10	13662	249061	213298	525723	12747	18.53	0.06	15.70	0.05	38.56	0.12	0.847	0.003	2.086	0.006
bb5-Pn11	9235	165018	144071	352800	4852	17.86	0.12	15.68	0.10	37.90	0.21	0.871	0.006	2.112	0.012

SE = Standard error of isotope ratios (e.g. SE64 = $Pb^{206/204}$)

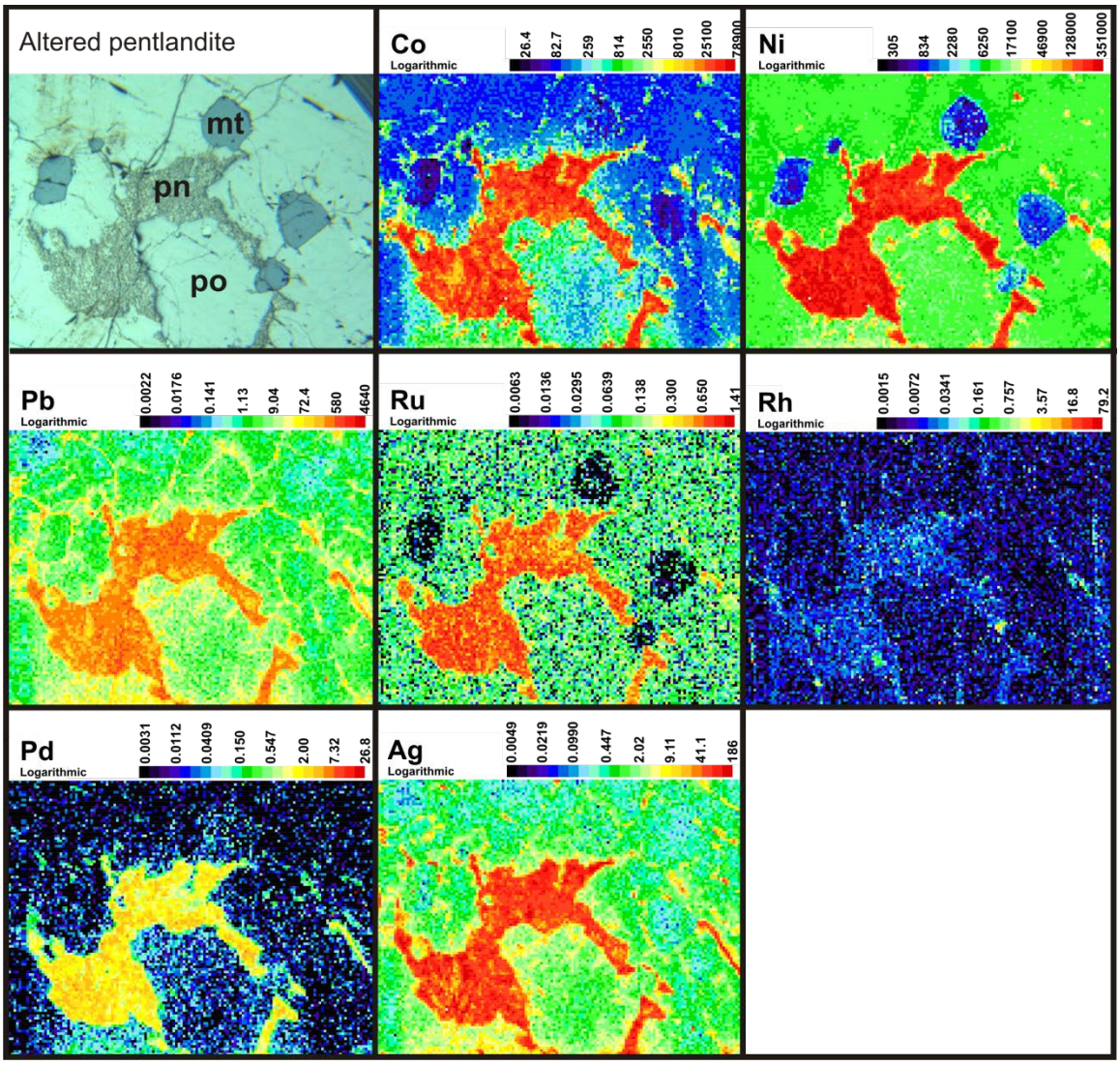

Figure 2.10 Distribution of elements within heavily altered pentlandite. Concentration is in logarithmic ppm scale. Unaltered pyrrhotite (po) and magnetite (mt) are also present.

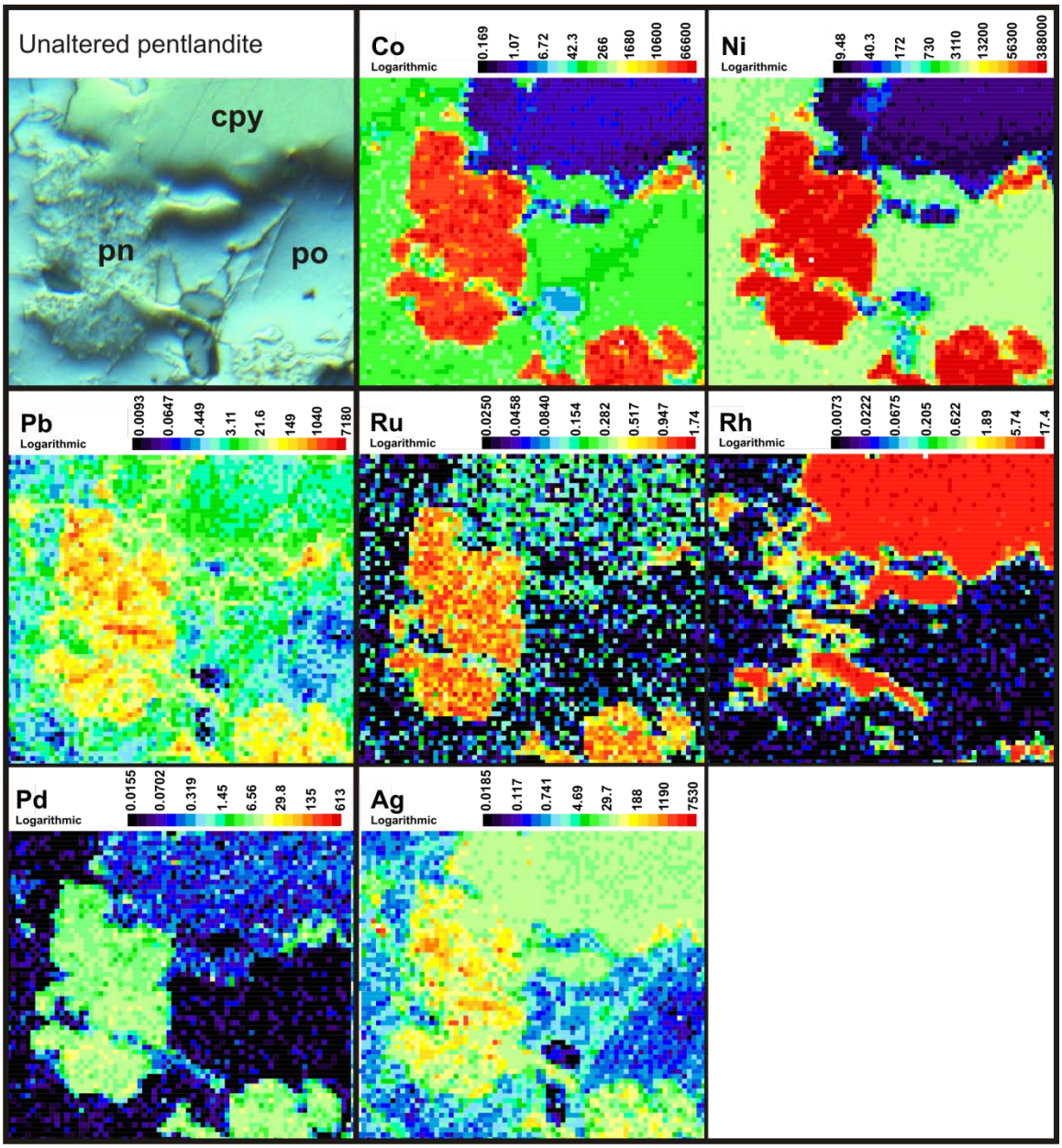

Figure 2.11 Distribution of elements within fresh unaltered pentlandite. Concentration is in logarithmic ppm scale. Pyrrhotite (po) and chalcopyrite (cpy) are also present. Rhodium concentration in chalcopyrite is a result of CuAr interferences.

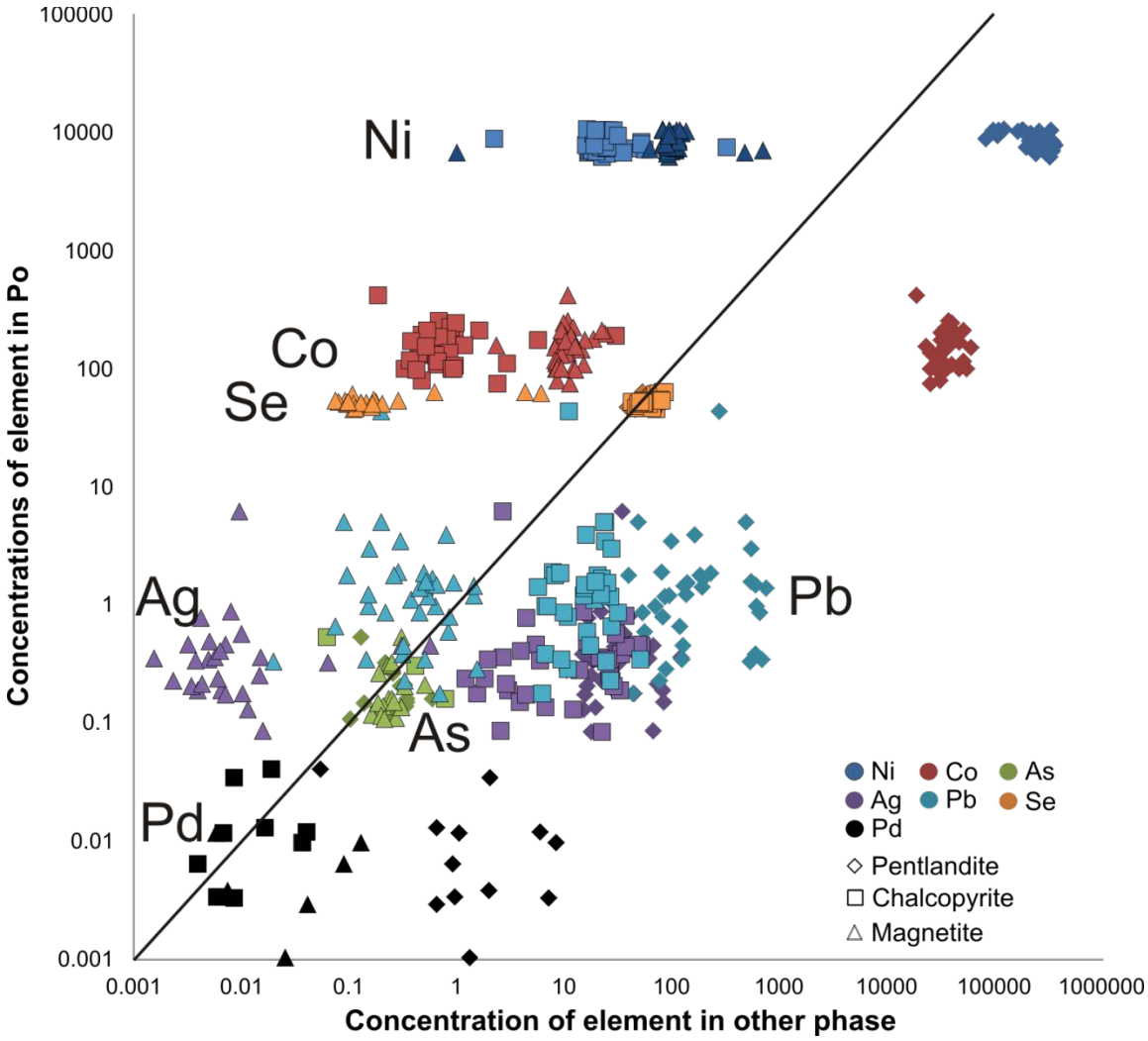

Figure 2.12 Element distribution between major phases in ppm in the McConnell deposit.

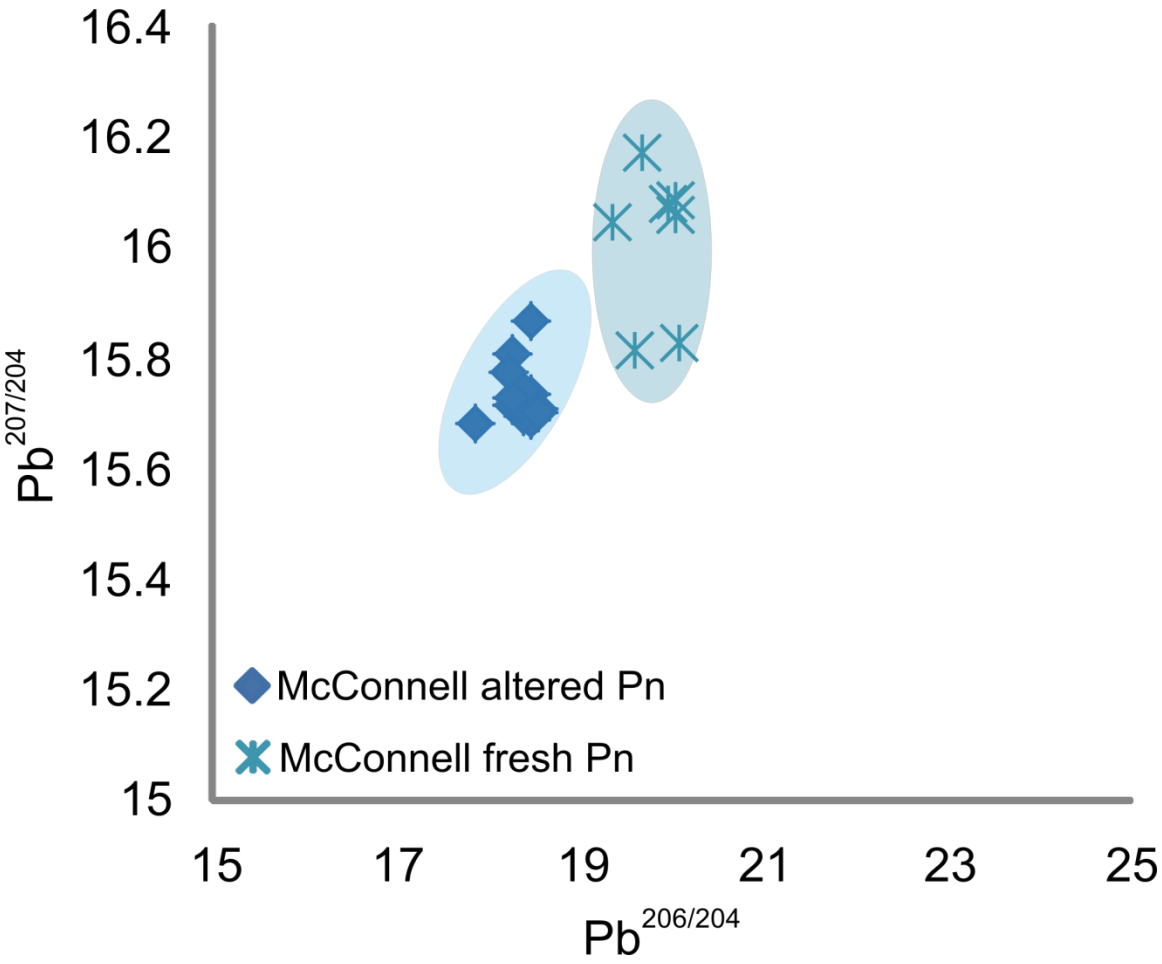

Figure 2.13 Lead isotope ratios of unaltered and altered pentlandite grains in the McConnell deposit.

2.4 Discussion

2.4.1 Offset formation at the SIC

Models for concentric and radial offset formation in the Sudbury Igneous Complex argue that quartz diorite offset dykes were sourced from the initial superheated melt sheet from which melt was injected into radial and concentric structures surrounding the original crater shortly after the time of impact (Grant and Bite, 1984; Lightfoot et al., 1997; Corfu and Lightfoot, 1997; Wood and Spray, 1998; Rickard and Watkinson, 2001; Lightfoot and Farrow, 2002; Murphy and Spray, 2002; Rousell et al., 2003;). The assimilation of country rocks introduced sufficient S, base metals, and As into the melt sheet to lead to the formation of large quantities of sulfide liquid (e.g. Naldrett, 1984; Golightly, 1994; Lightfoot et al., 2001; Ames et al., 2008; Dare et al., 2010; Lefort et al., 2014 in press). The extent of country rock-melt interaction is still under investigation today, with debate focusing on: i) the relative contributions of metals and S into the melt sheet from different crustal materials, and why these contributions differed in various parts of the SIC leading to variations in ore tenor and composition (Naldrett et al., 1982; Darling et al., 2010a,b, 2012); and ii) the impact event, target rocks, and evolution of the early impact melt sheet through processes such as vigorous convection and thermal erosion of country rocks (Grieve et al., 1991; Grieve, 1994; Dickin et al., 1996, 1999; Ivanov and Deutsch, 1999; Keays and Lightfoot, 1999).

Sulfides occur in a variety of lithologies within offset dyke environments, ranging from relatively barren QD that contains disseminated sulfides to semi-massive and massive sulfide lens, pods, and sheets (e.g. Rickard and Washington, 2001; Keays and Lightfoot, 2004; Naldrett, 2004; Huminicki et al., 2005; Ames et al, 2008;) hosted in inclusion-rich quartz diorite (IQD) dyke cores. In offsets where QD dykes crosscut and

interact extensively with wall rock lithologies (e.g. Worthington offset), sulfides are also hosted within brecciated metamorphic country rocks (metagabbro or amphibolite; e.g. Totten deposit). Silicate liquids injected into the dykes were sulfide-saturated before or synchronous to emplacement (Ebel and Naldrett, 1996; Rickard and Watkinson, 2001; Farrow and Lightfoot, 2002; Mungall, 2002; Naldrett, 2004; Naldrett, 2005; Mungall et al., 2005; Mungall, 2007). The metal tenor and volume of sulfide melt were influenced by a combination of initial silicate melt reservoir metal concentration and R-factor (e.g., Theriault et al., 1996; Barnes and Lightfoot, 2005), partition coefficients for base and precious metals between the silicate and sulfide liquids (e.g., MacLean and Shimazaki, 1976; Fleet et al., 1993; Peach et al., 1993; Peach et al., 1994; Fleet et al., 1996; Jana and Walker, 1997; Mungall, 2002), oxygen concentration and sulfur fugacities (e.g. Doyle and Naldrett, 1987; Ballhaus et al., 2001, Fonseca et al., 2008), and the assimilation of local country rocks as a potential S and metal (ore and accessory) sources (e.g., Naldrett et al., 1986; Lightfoot et al., 1997; Farrow and Lightfoot, 2002). As this sulfide liquid cooled, it crystallized monosulfide solid solution (MSS) to leave a residual Cu-rich sulfide liquid that either remained encapsulated (in equilibrium) within the cooling MSS cumulates and silicate host, or fractionated and was emplaced locally along sulfide-wall rock contacts and in structural zones within the host rocks (Naldrett and Kellerud, 1967; Li et al., 1992; Naldrett et al., 1994; Ballhaus et al., 2001; Mungall et al., 2005; Mungall, 2007). The partition coefficients for Ni between MSS and residual sulfide liquid is close to unity but varies considerably with the S content of the two phases (0.19 – 1.17, Li et al., 1993; Barnes et al., 1997) and temperature (Ni becomes compatible in MSS below temperatures of about 850; Mungall et al., 2005, Mungall, 2007). Copper and precious

metals (PGE, Au) partition strongly into the residual sulfide liquid (Fleet et al., 1993, Naldrett et al., 1999; Mungall, 2005, Mungall et al., 2005). As MSS cooled, it recrystallized to form pyrrhotite-pentlandite (+/- pyrite) with subordinate chalcopyrite, while the residual, fractionated Cu-rich liquid crystallized ISS which exsolved assemblages of chalcopyrite-cubanite with subordinate bornite, millerite, and other trace base metal sulfides and precious metal phases. Magnetite formed as either an early cumulus phase with MSS directly from the sulfide liquid, or exsolved from the cooling sulfide solid solution. Later hydrothermal remobilization resulted in ore grade modification and the redistribution of base and precious metals in the offsets (e.g. Carter et al., 2001; Rickard and Watkinson, 2001; Magyarosi et al., 2002).

The assimilation of country rocks into the early melt sheet, especially on the South Range, incorporated sufficient As into the SIC liquids to crystallize arsenide and sulfarsenide phenocrysts which sequestered precious metals and platinum-group elements (PGE) in solid solution, and in cases of higher PGE tenors, spatial associations and intergrowths of solid solution sulfarsenides with discrete platinum group minerals (PGM) (Cabri and LaFlamme, 1984; Cabri, 1988; Farrow and Lightfoot, 2002; Szentpeteri et al. 2002; Hem and Makovicky, 2004; Hem, 2006; Ames et al., 2008; Dare et al., 2010; LeFort et al., 2014 in press; *c.f.* Sinyakova and Kosyakov, 2012; Beziat et al., 1996). Discrete platinum group element minerals (PGM), like michenerite-merenskyite, create an often heterogeneous distribution of PGM inclusions (Li and Naldrett 1993) within cooling ISS or, less abundantly, in MSS cumulates. Arsenic-rich deposits are very common on the South Range of the SIC (Ames and Farrow, 2007), and discrete precious metal phases and PGE-rich Ni-Co arsenides and sulfarsenides often constitute the

majority of the PGM budget in South Range offsets, though sulfides like pentlandite and chalcopyrite can host some dissolved PGE as well.

Understanding the complexities and diversity of the processes responsible for the development and composition of ores in offset environments is integral to identifying which specific factors control the characteristics of each system. The unique characteristics of the McConnell ores (with respect to other South Range offsets) requires a comparison of a comprehensive data set to aid in identifying the intricacies of its formation and evolution which led to its current composition.

2.4.2 Comparison to other Sudbury offset deposits

The McConnell mineralization differs from other South Range offset deposits chemically in many ways, but notably its marked depletion in As, scarcity of arsenides and sulfarsenides within the ores, and relatively low Ni grade. Normative abundance diagrams (100% sulfide) show that McConnell ores have very similar PGE and Cu tenors as ores from Kelly Lake, Totten and Garson, but lower As, Ni and Co abundances (Figures 2.14, 2.15, 2.15). Arsenic concentrations at McConnell are low and narrow in range (Figure 2.14C), with sparse SSS occurring most often in MSS cumulates (Table 2.4). It should be noted that As levels in the McConnell deposit calculations were all increased to 5 ppm (detection limit of bulk rock assay) before re-normalization to 100% sulfide, and therefore may represent higher values than in actual McConnell samples. Ni/Co ratios in McConnell ores are unique and much lower than other South Range deposits (Figures 2.16, 2.17). The concentration of Ni within the McConnell ores is >60% lower than in other South Range deposits, while Co concentration within McConnell ores is generally 25% lower than, or comparable to, other deposits shown

(Figure 2.17). Copper shows trends similar to other deposits, while Pb is often low in McConnell ores compared to other deposits (Figures 2.16, 2.17).

Given the overall depletion of As, Ni, and to a lesser extent Co in the McConnell ores, it was expected that their PGE tenor would also be depleted if the pyrrhotite-rich ores represent MSS cumulates (*c.f.* Mungall et al. 2005). However the PGE tenor of McConnell ores is actually higher than deposits with comparable base metal concentration, showing higher Pd/Pt ratios than in other deposits (Figures 2.15, 2.18). Comparable Pd enrichment with lowest Pt/Pd ratios in the McConnell deposit than other South Range deposits is consistent with abundant arsenide separation, yet As abundance in the McConnell ores is very low. In addition to unique base and precious metal tenors, the McConnell ores also differ from other deposits in their pentlandite composition. McConnell pentlandite grains have the highest Co/Ni ratios, and highest dissolved Co + Pb concentration reported for South Range deposits (Figures 2.19, 2.20). Pentlandite grains from McConnell ores are also relatively high in Ag, have comparable As and Pd concentrations, and low Se concentrations compared to other South Range deposits (Figures 2.19, 2.20). It is difficult to explain a system that is depleted in Ni, Cu, and As, but enriched in Pd, with complications in using either equilibrium or fractional crystallization styles. These features suggest that the McConnell deposit either evolved in an atypical fashion than other offset deposits, or that the source controlling PGE was not associated with As or base metals.

2.4.3 Lead isotope ratios of pentlandite grains

Lead isotope ratios from the McConnell ores (pentlandite grains) form two distinct groups based on the intensity of alteration. Lead isotope ratios from the McConnell

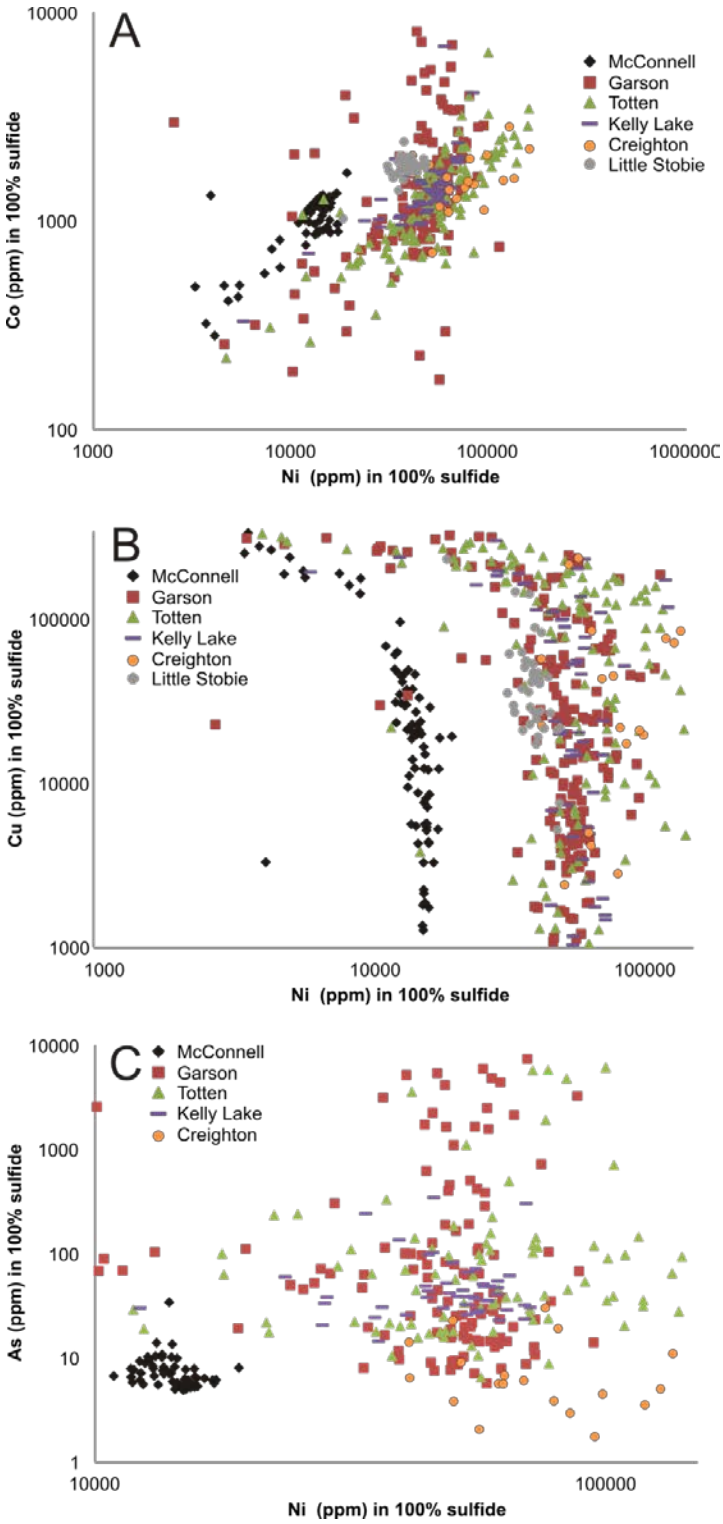

Figure 2.14 Base Metal tenors between South Range deposits calculated for 100% sulfide. Data from deposits; McConnell, this study; Garson, Lefort 2013; Totten, Warren 2013; Creighton, Dare et al., 2010a; Kelly Lake, Huminicki et al., 2005; Little Stobie, Hancock et al., 1979).

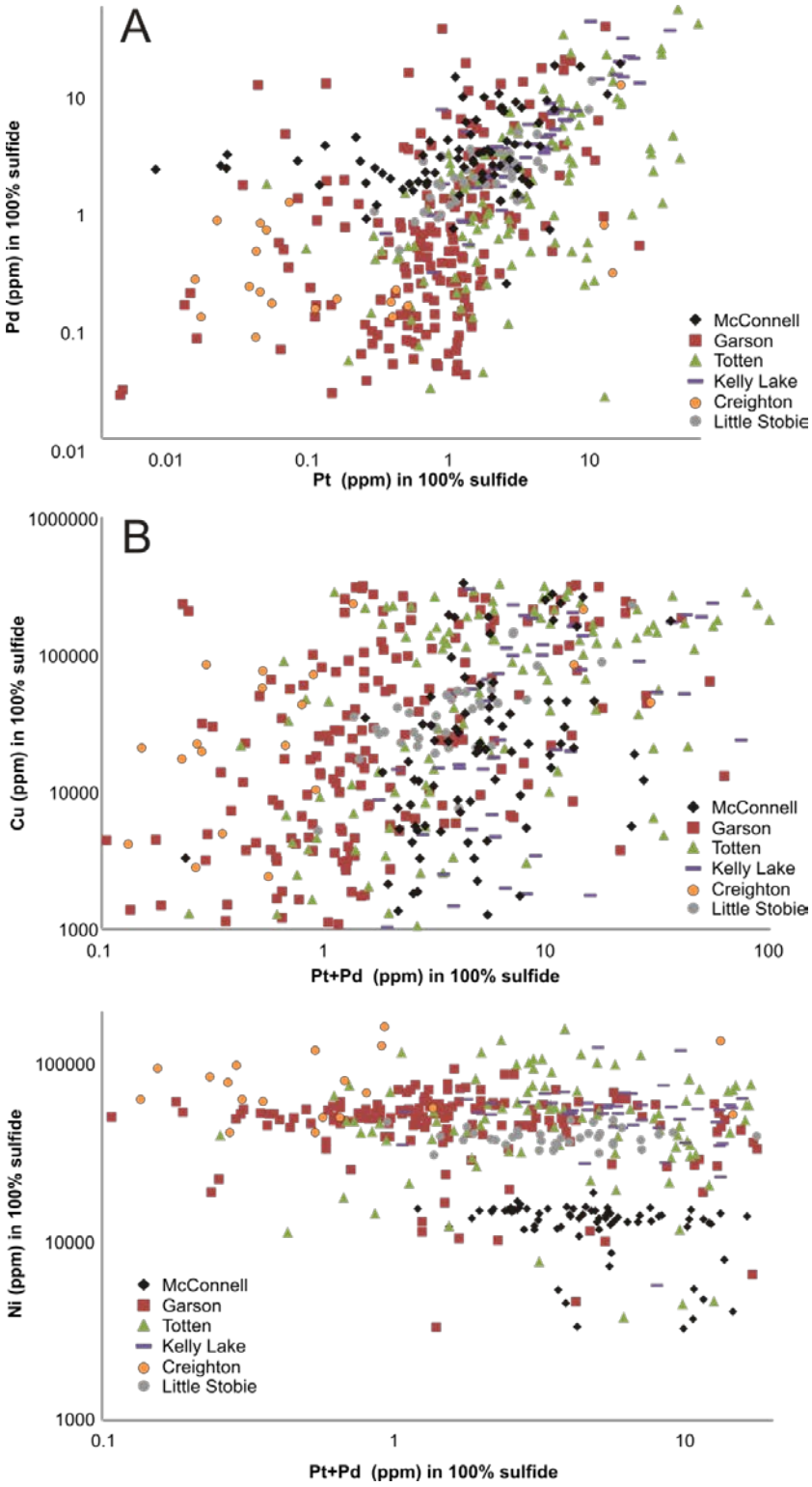

Figure 2.15 PGE in 100% sulfide from several South Range deposits. Data from deposits; McConnell, this study; Garson, Lefort 2013; Totten, Warren 2013; Creighton, Dare et al., 2010a; Kelly Lake, Huminicki et al., 2005; Little Stobie, Hancock et al., 1979).

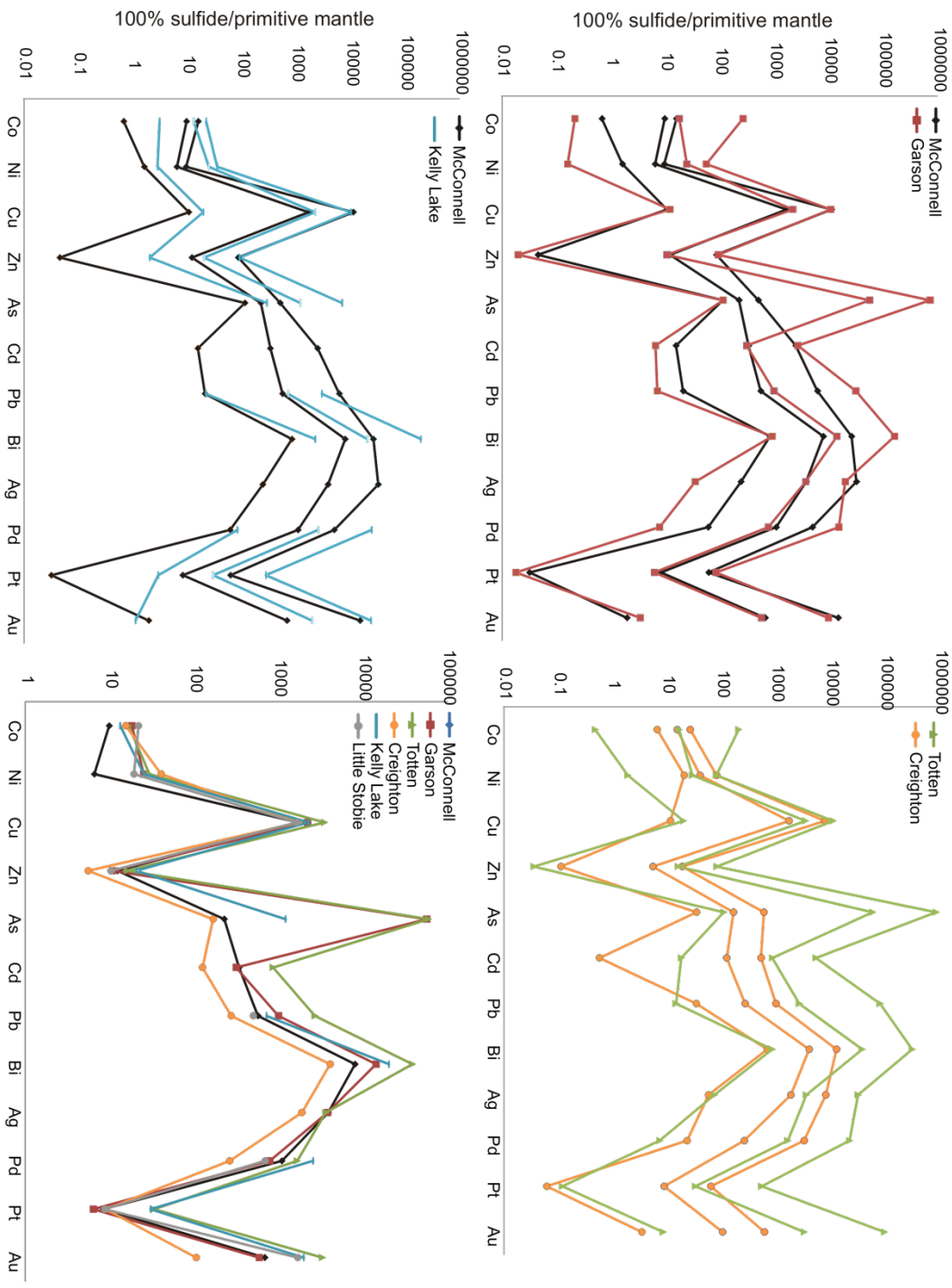

Figure 2.16 Bulk rock 100% sulfide concentrations of South Range deposits normalized to primitive mantle. Lines show maximum, minimum, and average concentrations from bulk rock assays. Data from deposits; McConnell, this study; Garson, Lefort 2013; Totten, Warren 2013; Creighton, Dare et al., 2010a; Kelly Lake, Huminicki et al., 2005; Little Stobie, Hancock et al., 1979).

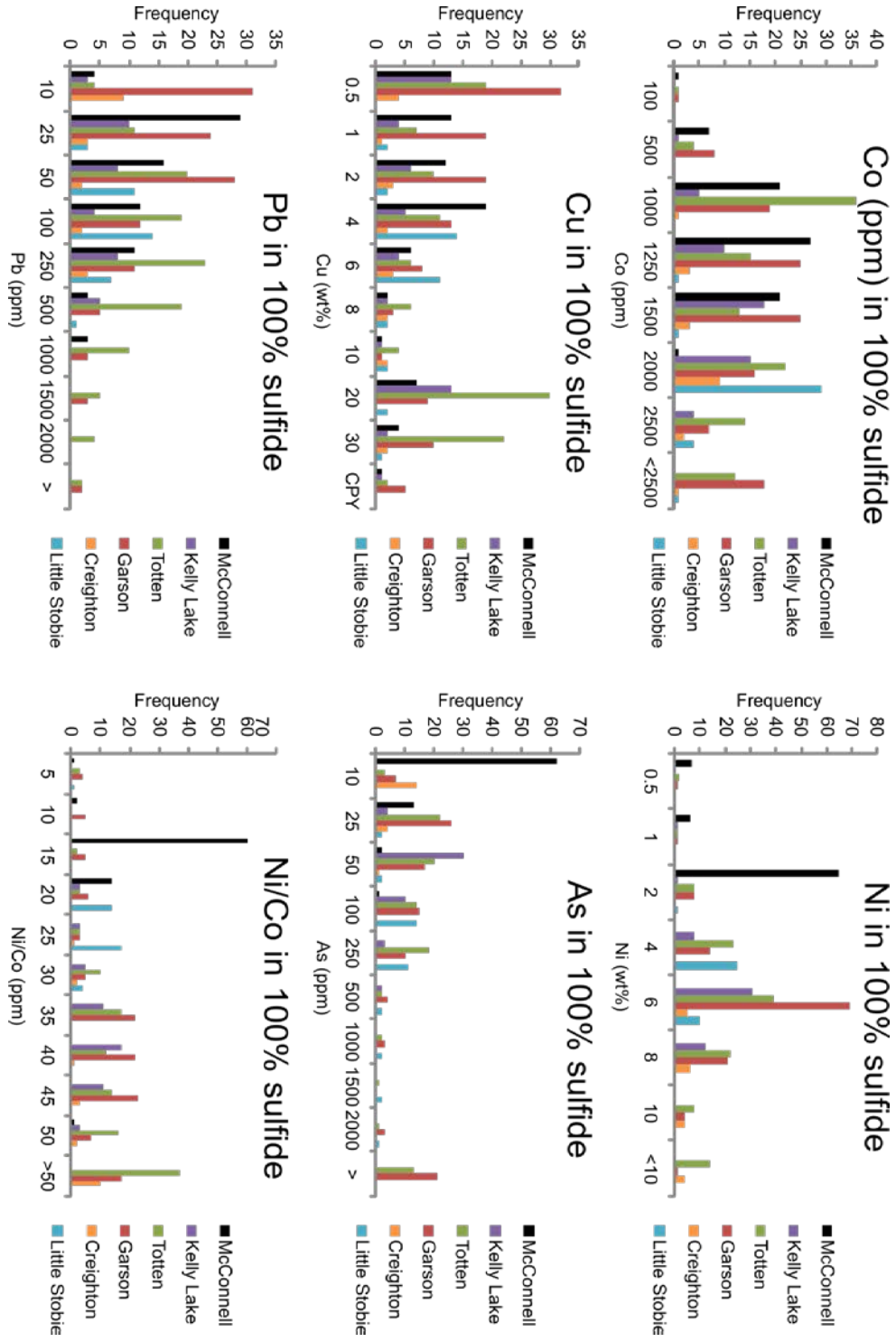

Figure 2.17 Histograms of assay concentrations in 100% sulfide from various South Range deposits. Data from deposits; McConnell, this study; Garson, Lefort 2013; Totten, Warren 2013; Creighton, Dare et al., 2010a; Kelly Lake, Huminicki et al., 2005; Little Stobie, Hancock et al., 1979).

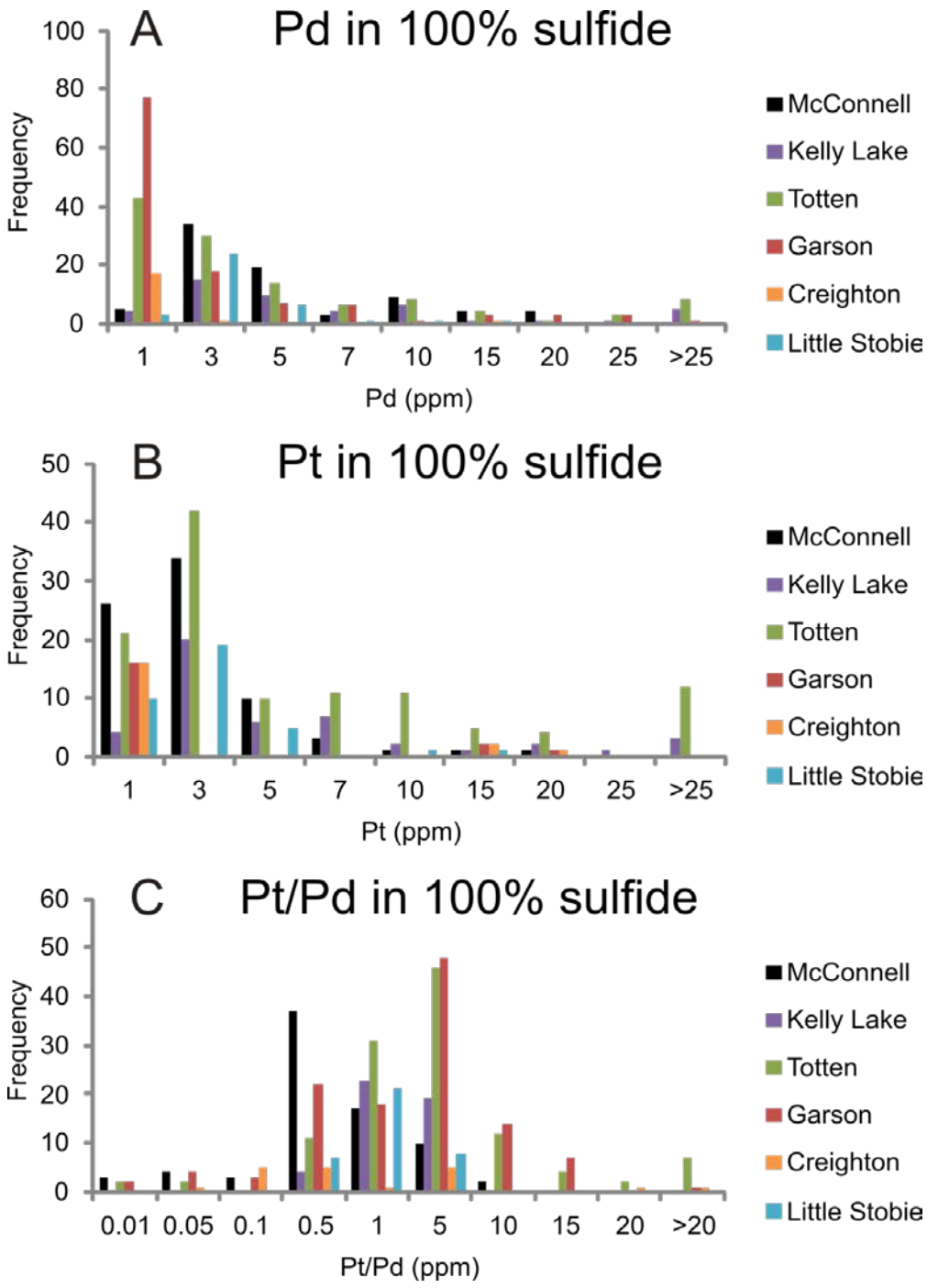

Figure 2.18 Histograms of PGE in 100% sulfide from various South Range deposits. A) Palladium concentration in the McConnell ores is comparable or higher to other South Range deposits. B) Platinum tenors in the McConnell ores show low but comparable values to other South Range deposits. C) The lowest Pt/Pd ratios in South Range deposits are from the McConnell ores, which either indicate removal of Pt in early arsenide phases, or a low concentration of Pt in the initial melt. Data from deposits; McConnell, this study; Garson, Lefort 2013; Totten, Warren 2013; Creighton, Dare et al., 2010a; Kelly Lake, Huminicki et al., 2005; Little Stobie, Hancock et al., 1979).

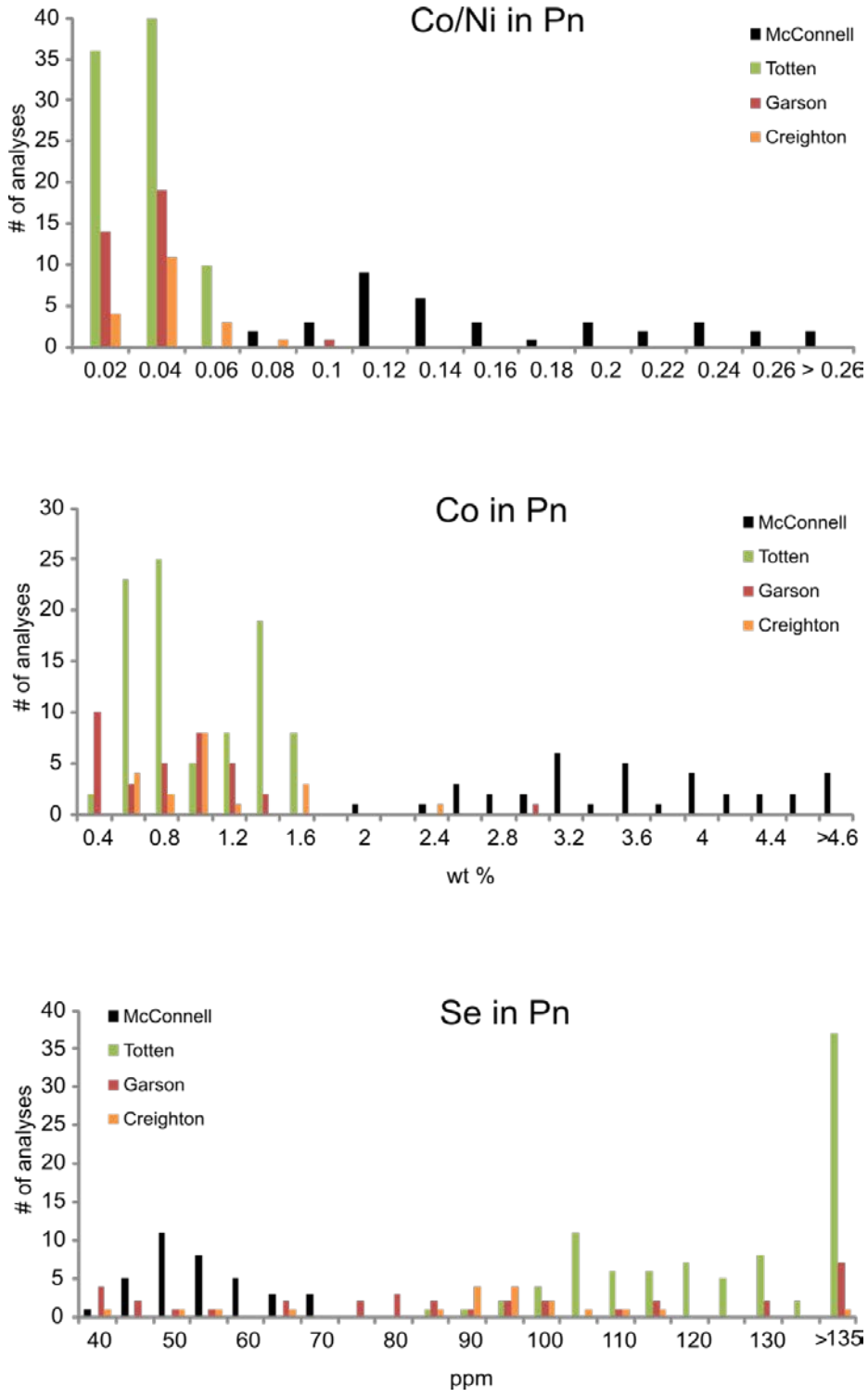

Figure 2.19 Co, Ni, and Se concentration of pentlandite grains from South Range deposits. Pentlandite grains from the McConnell ore body contain high Co and elevated Co/Ni ratios, with low Se concentration compared to other South Range deposits. Data from deposits; McConnell, this study; Garson, Lefort 2013; Totten, Warren 2013; Creighton, Dare et al., 2010a; Kelly Lake, Huminicki et al., 2005).

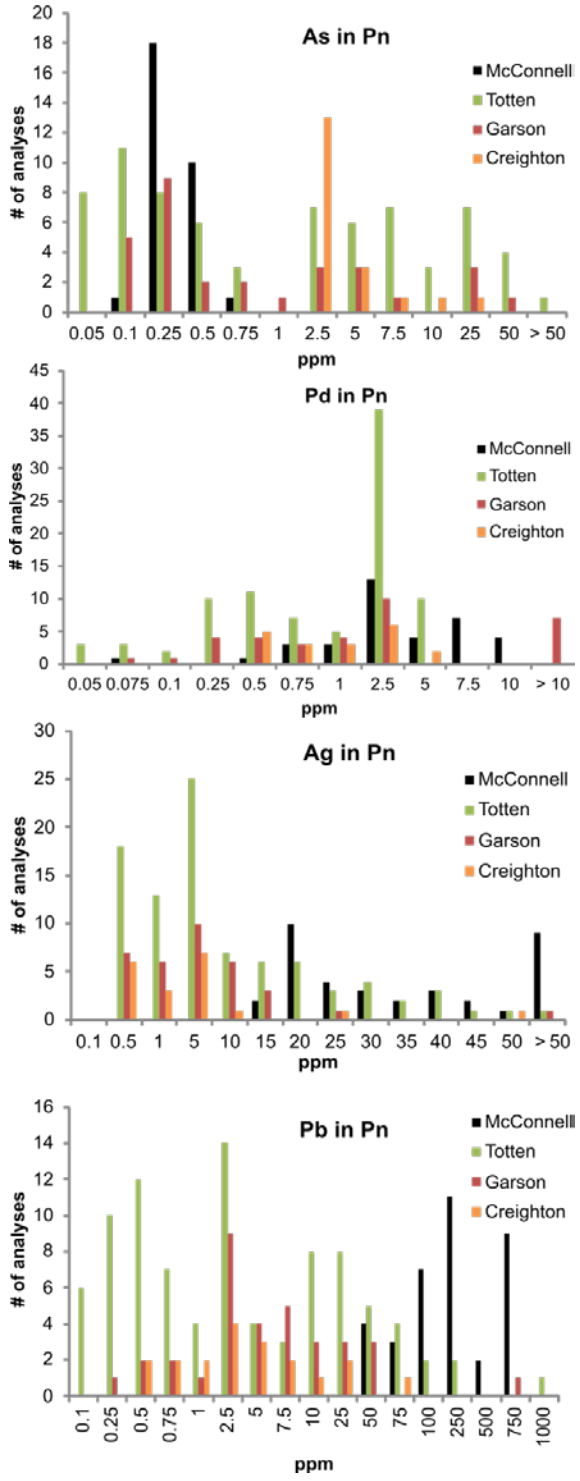

Figure 2.20 Concentrations of As, Pd, Ag, and Pb in pentlandite grains from South range deposits. Data from deposits; McConnell, this study; Garson, Lefort 2013; Totten, Warren 2013; Creighton, Dare et al., 2010a; Kelly Lake, Huminicki et al., 2005).

pentlandite grains fall between values for late stage veins from the Worthington offset, and isotope ratios from the overlying VMS deposits (Ames, pers comm 2014; Figure 2.21). The trend of $Pb^{207/204}$ and $Pb^{206/204}$ ratios for the McConnell system indicates that Pb may have been remobilized from hydrothermal fluids sourced from outside the McConnell system after emplacement, and was deposited during the late alteration of pentlandite (and other ores). An early external source of Pb may possibly have been remobilized from the norite contact near the McConnell offset as the SIC cooled and provided a source for hydrothermal fluids, though limited information (drill logs) on the region between the SIC basal nortie and the McConnell offset makes it difficult to prove this theory. A second possibility is that Pb was remobilized from VMS deposits forming in the overlying units, as isotope ranges for altered pentlandite appear to be intermediate between McConnell Pb (unaltered pentlandite) and VMS Pb (Figure 2.21), though this would require the fluids to migrate downward below the VMS deposits.

2.4.4 Post solidus alteration and down temperature recrystallization of sufides

Syn- and post-magmatic modification, metal solubility, transportation, and redistribution of economic base and precious metals (i.e.. Cu, Ni, Pt, Pd, Au) via hydrothermal fluids has long been considered in the literature as a key factor in modifying and/or forming zones of high-grade mineralization within Cu-Ni-PGE deposits (Crerar et al., 1985; Rowell and Edgar, 1986; Cook et al., 1992; Farrow et al., 1994; Molnar et al., 1997, 1999; Farrow and Watkinson, 1996, 1997, 1999; Wood, 2002; Barnes and Lightfoot, 2005; Audetat et al., 2008; Bursztyn and Olivo, 2010). Both primary (magmatic) volatiles and secondary (post-solidus) fluids may have altered metal concentrations and mineralogy in sulfide ores, and the redistribution of base and precious

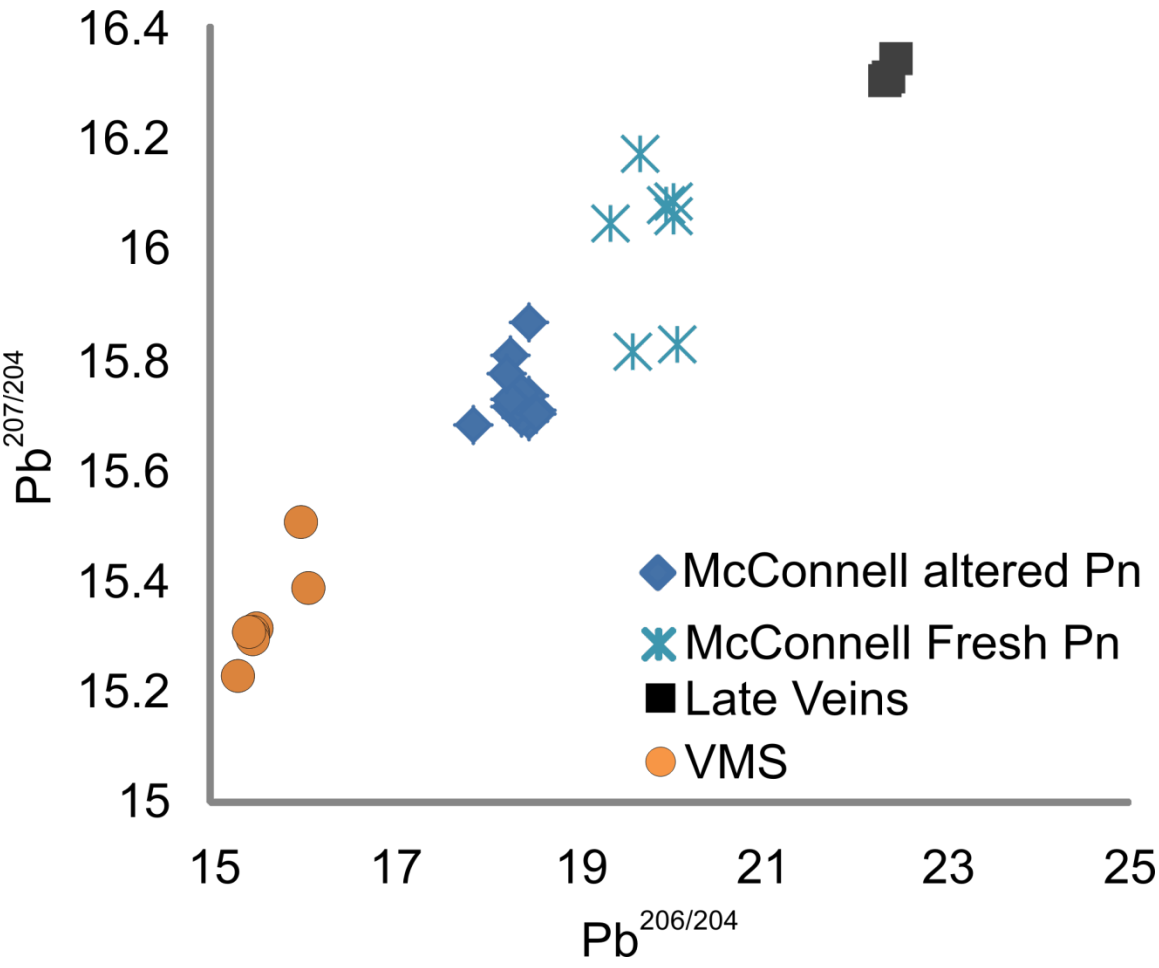

Figure 2.21 Lead isotope ratios from McConnell pentlandite, VMS environments and late alteration veins. Data for VMS and Late veins from Ames (2006; 2014 pers comm), McConnell data from this study.

metals by fluids is reported in many deposits associated with mafic-ultramafic intrusions, including the Coldwell Complex (Watkinson and Ohnenstetter, 1992), the Duluth Complex (Mogessie et al., 1991; Gál et al., 2011; Gál et al., 2013), the East Bull Lake Intrusive Suite (Peck et al., 2001; Easton et al., 2004) the Stillwater and Bushveld Complexes (Ballhaus and Stumpfl, 1985, 1986; Boudreau et al., 1986; Meurer et al., 1999; Willmore et al., 2000; Hanley et al., 2008), Lac des Iles (Hattori and Cameron, 2004; Hanley and Gladney, 2011), the Salt Chuck intrusion, Alaska (Watkinson and Melling, 1992) and New Rambler, Wyoming (McCallum et al., 1972; Nyman et al., 1999). The extensive role that fluids have played in the evolution of the SIC is also well documented, with fluids acting as a modifying agent in high-PGE footwall deposits (i.e.. Farrow and Watkinson, 1992; Jago et al., 1994; Farrow and Watkinson 1997; Marshall et al., 1999; Molnar and Watkinson, 2001; Molnar et al., 2001; Hanley and Mungall, 2003; Hanley et al., 2005;), the redistribution of PGE in offset and contact environments (Molnar et al., 1999; Carter et al., 2001), and the formation of economic Zn-Pb-Cu mineralization in overlying basin fill and fallback units (Ames et al., 2006, 2008).

At the McConnell offset, the transformation of pyrrhotite to secondary marcasite and/or pyrite by hydrothermal fluids through dissolution-reprecipitation reactions could be controlled by fluid pH, fO_2 and fS, T, and primary pyrrhotite chemistry (Fleet, 1978; Murowchick and Barnes, 1986; Putnis, 2002; Putnis, 2009; Qian et al., 2010; Qian et al., 2011). Replacement textures of pyrrhotite by pyrite and marcasite within McConnell ores follow orientations along original pyrrhotite crystallographic planes, or are present as polycrystalline intergrowths with highly variable random grain orientations within the original pyrrhotite grain boundaries. Areas of the deposit that have not been completely

altered to marcasite and pyrite show fractures within pyrrhotite that have begun to alter to pyrite, beginning at the fracture and radiating into the surrounding unaltered pyrrhotite (Figure 2.6C). Remobilization and deposition of Pb by hydrothermal fluids is apparent as fracture-filled galena occurs commonly within both altered pyrrhotite and pentlandite (Figure 2.6). Pyrrhotite and pentlandite (discussed below) alter to marcasite and violarite, respectively, under similar temperature and pH conditions (80 – 220°+, pH 1 – 5), and can be the result of either supergene or hypogene alteration (Xia et al., 2009; Qian et al., 2011).

In order for hydrothermal fluids to precipitate secondary sulfide minerals (marcasite, pyrite) a solvent must first dissolve pyrrhotite, liberating Fe and S into solution. Nicholson (1994) proposed an equation demonstrating the oxidation of pyrrhotite;

$$Fe_{(1-x)}S + (2 - \frac{x}{2})O_2 + (x)H_2O = (1-x)Fe^{2+} + SO_4^{-2} + (2x)H^+ \quad (1)$$

where monoclinic pyrrhotite (x = 0.125) was found to produce fluids with the lowest pH. Qian et al. (2011) investigated the dissolution of pyrrhotite beginning with a simplified equation;

$$Fe_8S_9 + 16H^+_{(aq)} = 8Fe^{2+}_{(aq)} + 8H_2S_{aq} + S^0 \quad (2).$$

In conditions where hydrothermal fluids provide an external oxidant, the dissolution of pyrrhotite and precipitation of marcasite using the equation of Murowchick (1992);

$$2Fe_{(1-x)}S_9 + (2 - 4x)H^+ + (1/2 - x)O_{2aq} = FeS_{2(s)} + (1 - 2x)Fe^{2+}_{(aq)} + (1 - 2x)H_2O \quad (3),$$

and pyrite using;

$$2Fe_8S_9 + 14H_2S + 7O_2 = 16FeS_2 + 14H_2O \quad (4)$$

occurring over a range of pH, fO_2, and availability of S^{2-}, with marcasite preferentially forming at lower pH and without the need of external S^{2-} (Qian et al., 2011). Heavily

altered samples within the McConnell mineralization contain large proportions of both marcasite and pyrite which may indicate an evolution in the fluid over a period of time.

It was initially presumed that the current form and chemical peculiarities of pentlandite grains within the McConnell system are a by-product of hydrothermal alteration. Indeed, pentlandite grains do show overprinting of hydrothermal processes, becoming almost indistinguishable in moderate to highly altered samples. However, pentlandite grains also show “alteration” while completely encapsulated in massive sulfide cumulates where no apparent hydrothermal alteration has taken place (Figures 2.6, 2.7, 2.10). It is therefore assumed, from this point forward, that the composition and physical features of pentlandite grains within McConnell ores are a function of their stability (and factors that control that stability) as MSS cooled, and not strictly a hydrothermal process.

End-member pentlandite $(Fe,Ni)S_8$ creates a continuous solid solution with cobalt-pentlandite (Co_9S_8) with the ideal formula of $Fe_{4.5}Ni_{4.5}S_8$, creating a cubic packing of 8 metal atoms oriented tetrahedral to sulfur, the metal atoms able to substitute freely with each other (Ni, Fe, Co) to have varying effect on the cell size of the crystal lattice (Riley, 1977; Hem, 2006). The shrinkage cracks, cleavage pits in-filled with pyrrhotite, and general enrichment of Co within McConnell pentlandite grains suggests that this phase may be the result of the transition of high pentlandite solid solution to that of stable pentlandite. High-pentlandite forms a solid solution series with MSS at temperatures much higher than usual pyrrhotite-pentlandite crystallization. The resulting pentlandite may also be a product of the Ni-poor MSS retaining too much Co and forming small intergrowths or exsolutions of cobalt-pentlandite. In addition to enrichment of chalcogenes, McConnell pentlandite contains high concentrations of Pd which remained

in solid solution.

Pentlandite within the McConnell deposit, and massive sulfides in general (both pyrite-bearing and pyrite-free) closely resemble those phases in the Thayer Lindsley (TL) deposit. Bailey et al. (2006) reported that pentlandite grains within the Thayer Lindsley deposit commonly are altered to pyrrhotite in the same fashion as those in McConnell, showing the same distinct pitting, fracturing, alteration textures, and chemical variations between the pentlandite of both deposits. The alteration of pentlandite to violarite is often attributed to hydrothermal fluids through dissolution-reprecipitation reactions such as:

$$Fe_xNi_{9-x}S_8 + 18H^+ + 0.5O_{2(aq)} = (9 - x)Ni^{2+} + xFe^{2+} + 8H_2S_{(aq)} + H_2O \quad (5)$$

$$2xFe^{2+} + (6 - 2x)Ni^{2+} + O_{2(aq)} + 8H_2S_{(aq)} = 2Fe_xNi_{3-x}S_4 + 12H^+ + 2H_2O \quad (6)$$

These reactions are dependent on pH and low temperature (1-6 and 80 - 220°C, respectively) (Xia et al., 2007, 2008, 2009). The leaching of Ni from the McConnell ores by hydrothermal fluids may explain the low metal tenors in altered intervals, though the precipitation of secondary sulfides from fluids sequestered some of the Ni lost during initial pentlandite and pyrrhotite dissolution. Notwithstanding differences in their composition, mineral assemblages between the deposits are extremely similar, showing variations only in the pentlandite abundance, and overall degree of alteration, and Co content. Similarities also exist between marcasite and pyrite within both deposits, although the Thayer Lindsley Mine typically shows lower degrees of alteration than that of McConnell. Alteration of the ores in the Thayer Lindsley mine was attributed primarily to hydrothermal fluids in the TL shear zone during a period of amphibolite- grade metamorphism (Bailey et al., 2006). Misra and Fleet (1974) discussed several assemblages of pentlandite-violarite with higher Fe:Ni ratios than the unaltered

pentlandite, with chemistries and textures similar to those in McConnell. Cobalt variation, infilling of fractures with silica, higher Fe content in pyrrhotite-rich samples, and discoloration of alteration products seems to be common in most samples that underwent violaritization. Within the McConnell deposit, alteration to Ni-rich pyrite/marcasite and Fe-rich Ni-depleted violarite is possible (eq.1-6). Bailey et al (2006) reported that no apparent correlation existed between pyrite and pentlandite alteration, and Craig (1973) showed the co-existence of pyrite-pentlandite pairs in equilibrium, but McConnell samples only appear to have significant pentlandite alteration in the presence of pyrite. Samples from the Gertrude ore body, Creighton deposit, show a similar form of very weak pentlandite alteration, with the distinctive pits in-filled by Ni-rich pyrrhotite, and partially replaced pyrrhotite by grains of rounded pyrite (Dare et al., 2010). In the McConnell deposit, fluids may have migrated along the contact between the metasediments and metabasalts, along the same structural weaknesses that the initial dyke was emplaced. Given the location and orientation of the McConnell offset, and the intervals effected by hydrothermal alteration (Figure 2.4), it may be possible that the fluids originated from the cooling SIC, and migrated through the host rocks from the norite contact (Figure 2.1C). Although the alteration of the McConnell ores does support this hypothesis, there is insufficient evidence to prove that this is the fluid source.

2.4.5 Arsenic and precious metal distribution

Arsenic is primarily concentrated in two trace phases, sperrylite (which is also the primary Pt-bearing phase), and sulfarsenides ranging in composition and crystal morphology (gersdorffite-cobaltite-glaucodot) that commonly display Pd zoning and intergrowths with or cores of PGM (hollingsworthite and irarsite). Sulfarsenide phases

most often occur hosted entirely within base metal sulfides (>90% of SSS grains are hosted in massive pyrrhotite). Rarely, sulfarsenides occur at grain boundaries between silicates and sulfides and are intergrown with discrete PGM like michenerite or sperrylite. The PGM (michenerite-merenskyite, sperrylite) occur most commonly in silicate gangue or along silicate-sulfide grain boundaries, as do other precious metal minerals (hessite, electrum) and may suggest locally fractionated areas.

Although South Range ores are typically more enriched in As than North Range deposits, primarily due to the assimilation of As from country rocks (Ames and Farrow, 2007), the McConnell deposit contains extremely low arsenic which segregates primarily into rare grains of sulfarsenides, compositionally falling between glaucadot-gersdorrfite-cobaltite end members. These sulfarsenides are typically very common in South Range deposits, often occurring as euhedral grains hosted in base metal sulfides (Carter et al., 2002; Huminicki et al., 2005; Dare et al., 2010a,b), containing small amounts of PGE in solid solution (Cabri and Laflamme, 1976; Cabri, 2002; Ames et al., 2008), and displaying zoning of both Ir and Rh (Dare et al., 2010a,b). The rhodium or iridium cores of these sulfarsenide grains may represent an intergrowth of hollingsworthite or irarisite, a common mineral in South Range ores (Cabri and Laflamme, 1984; Carter, 2000; Farrow and Lightfoot, 2002). Sulfarsenides within McConnell are small, uncommon, and distributed heterogeneously throughout the ores. Compared with some of the rarer discrete phases, however, sulfarsenide grains are found in every sample and are considered common in respect to hessite or sperrylite.

Pd-tellurides (Pd-Te-Bi, michenerite-merenskyite) within the ore body are larger and more common than sulfarsenides, and may be the result of either direct crystallization of

segregated Pd-rich blebs, or post-magmatic processes such as hydrothermal re-mobilization. Similar to McConnell ores, Pd-bearing discrete phases such as michenerite and merenskyite are often hosted along the boundaries of silicates and sulfides, or included entirely within silicate gangue, in other South Range Deposits (Totten, Farrow and Lightfoot, 2002; Creighton, Dare et al., 2010a,b; Kelly Lake, Huminicki et al., 2005). These discrete minerals often host a significant portion of Pd in McConnell samples, especially in altered or inclusion-rich massive ore, but a high proportion of Pd is also hosted by base metal sulfides, predominantly pentlandite. Although pentlandite occurs in only a few vol% in McConnell sulfide mineralization, it's still more abundant than discrete phases by several orders of magnitude. Due to the amount of Pd in unaltered pentlandite (Table 2.3), the addition of a few vol% pentlandite significantly shifts the mass balance of Pd from discrete phases to base metal sulfides.

Only one PGM (sperrylite) is considered to sequester significant Pt within McConnell ores, and concentrations of Pt in base metal sulfides are too low to significantly contribute to the overall PGE budget. Where they do, platinum is often hosted in chalcopyrite (<1 ppm), however, more often than not it is hosted almost entirely within sperrylite. Sperrylite is the primary host of Pt in South Range Ores (Cabri and Laflamme, 1984; Farrow and Lightfoot, 2002; Huminicki et al., 2005). Sperrylite grains are intergrown with sulfarsenides or occur as small isolated grains along sulfide-silicate boundaries. Sperrylite is extremely rare, though its heterogeneous distribution and overall Pt content in the ore body suggests that it occurs throughout the entire deposit.

2.4.6 Trace element distribution and effects on mass balance calculations

Distribution of elements between major phases in McConnell ores are demonstrated in

Figures 2.22-2.24 from LA-ICP-MS analyses. Since pentlandite within McConnell ores is very low, even in the best cases (<5 vol%), it is natural to assume that an appreciable portion of the Ni budget is provided by Ni- bearing pyrrhotite, which comprises the bulk of the ores. Mass balance calculations show that in most samples of both massive and disseminated sulfides, over 50% of the Ni reported from bulk rock assays is contributed by pyrrhotite (or marcasite and pyrite in altered intervals), while pentlandite contributes the remaining Ni. In cases where pentlandite is altered (pn II-III), pyrrhotite often contains a higher proportion of Ni (often ~1wt% compared to 0.6 – 0.8 wt%) while pentlandite is subsequently Ni depleted, thereby shifting Ni balance calculations toward pyrrhotite dominant. This has a huge effect on both Ni recovery and estimation of economic Ni contribution, as pyrrhotite is discarded during milling and concentration of the ores. Although only an accessory phase, pentlandite is the primary influence on Co concentration within the McConnell, and also contains an appreciable amount of Pd in unaltered grains (up to 8.5 ppm). In bulk rock, Co and Ni increase concurrently with high pairs often indicating the increased concentration of unaltered pentlandite grains. Intervals where pentlandite is altered show pyrrhotite controlling more Co, Ni, Pd, and often Pb than unaltered intervals, however, Pb is contained in both solid solution and as discrete grains and intergrowths of galena within pentlandite, so as alteration increases so too does the proportion of Pb associated with pentlandite. Arsenic is primarily controlled by sperrylite and sulfarsenides, but given the rarity and heterogeneous concentrations of these minerals, a sufficient amount of arsenic can also be influenced by pyrrhotite. Given that arsenic is ubiquitously low within the McConnell, and even lower within pyrrhotite (105 – 536 ppb), it is not considered a major contaminant. Where sperrylite is not

encountered, chalcopyrite controls the Pt budget of the sample. However, the addition of even a few discrete grains of sperrylite instantly shifts calculations toward sperrylite, and since sperrylite is the most common Pt-bearing PGM in South Range ores (Cabri and Laflamme, 1984; Farrow and Lightfoot, 2002), it is assumed that sperrylite is the main control on Pt. In one sample, pyrrhotite contained enough Pt for determination by LA-ICP-MS, and was comparable to hosting the same platinum concentration as a few discrete sperrylite grains. Platinum group minerals are the principle source for most platinum-group elements within McConnell ores (Pd is distributed between discrete PGM and pentlandite.

Where gangue-sulfide interaction was increased (INSM) or alteration of pentlandite had taken place, Pd was more commonly hosted within michenerite-merenskyite, and in one case, pyrrhotite. The distribution of palladium is very sensitive to the increase or decrease of discrete telluride phases, and is quite often hosted by PGMs in Sudbury ores, though sulfides and sulfarsenides can host a significant concentration of Pd (Cabri and Laflamme, 1984; Farrow and Lightfoot, 2002; Huminicki et al., 2005). The contribution of Pd from sulfarsenides in McConnell was <1%, and since LA-ICP-MS was not performed on McConnell sulfarsenides, only SEM could be used to determine relative concentrations. Given the lack of these phases, they are not considered a major influence on the Pd budget of the ores. Pentlandite loses Pd as it becomes altered, which appears to be slightly enriched in surrounding pyrrhotite. The composition of McConnell pentlandite grains of mild and intense alteration fall between ideal end-member minerals (Figure 2.25), impacting the distribution of elements between major phases as well as mass balance calculations. Although Pd is controlled by pentlandite in Pn-rich intervals where

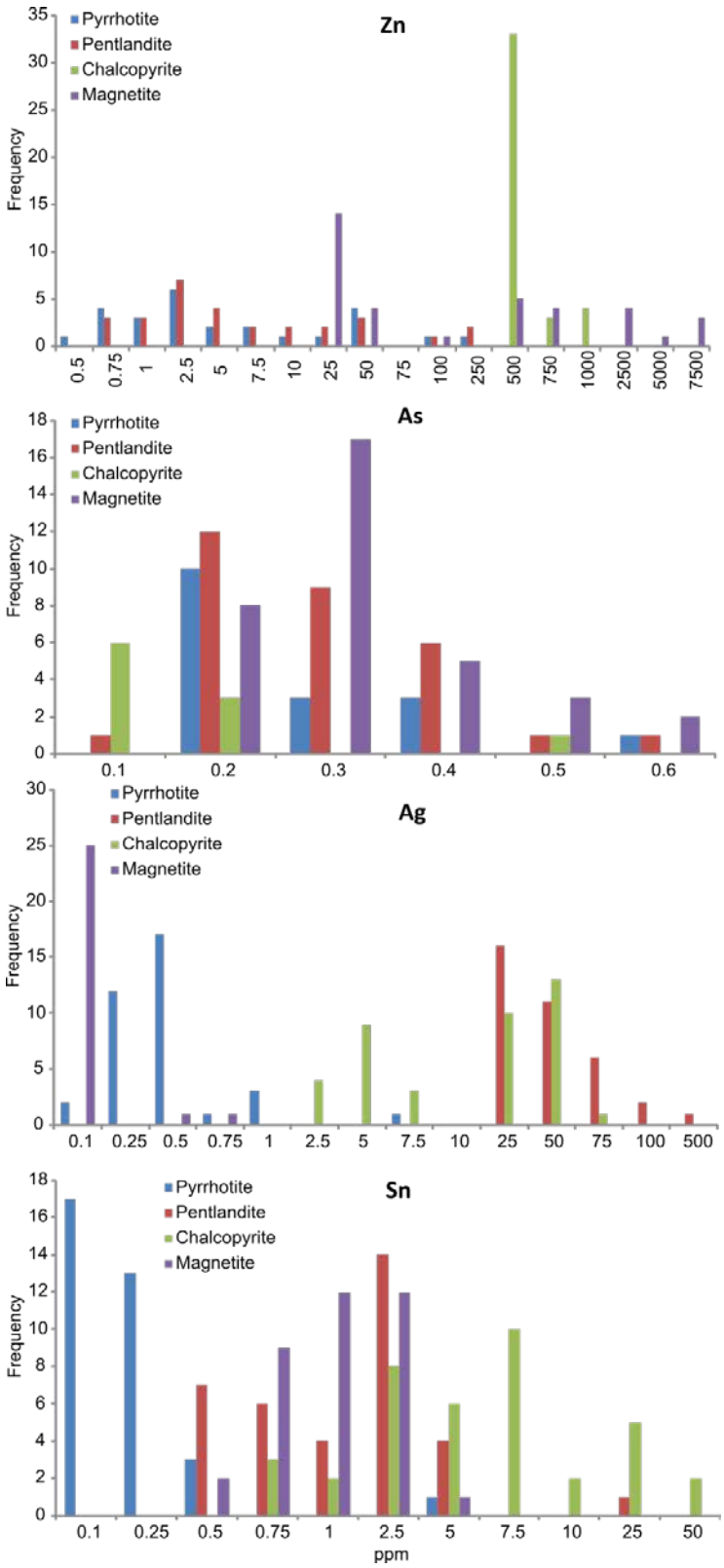

Figure 2.22 Distribution of Zn, Ag, Sn, and As between major phases in McConnell ores.

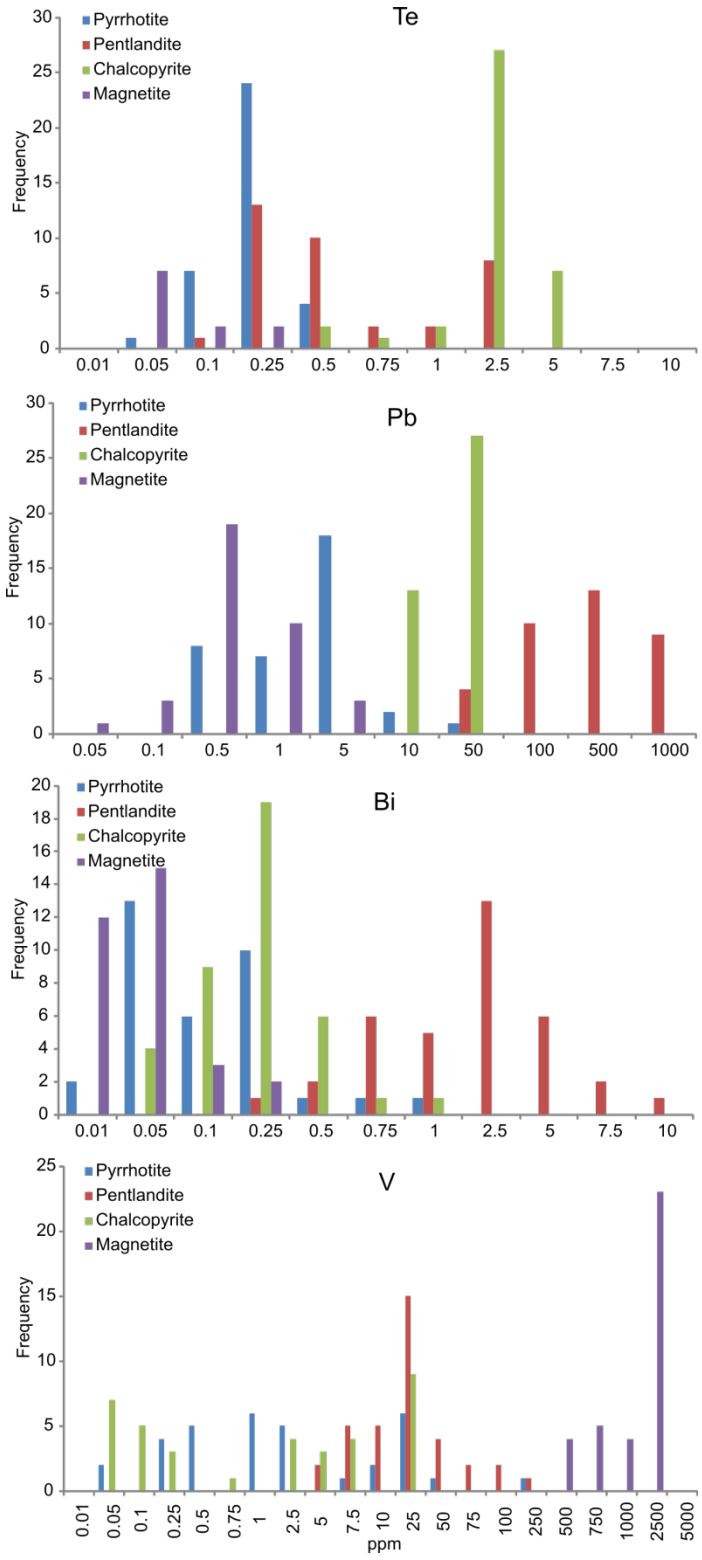

Figure 2.23 Distribution of Te, Pb, Bi, and V between major phases in McConnell ores.

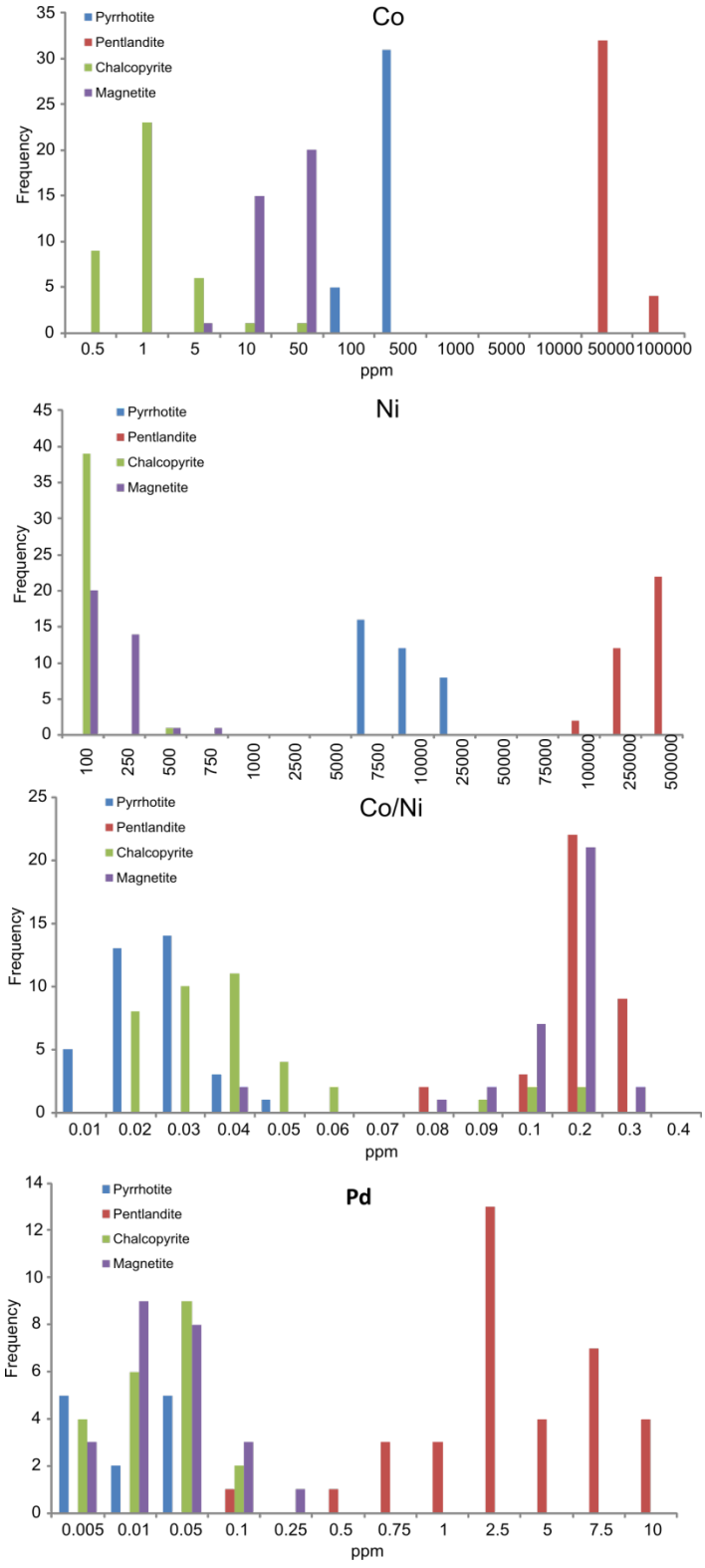

Figure 2.24 Distribution of Co, Ni, and Pd between major phases in McConnell ores.

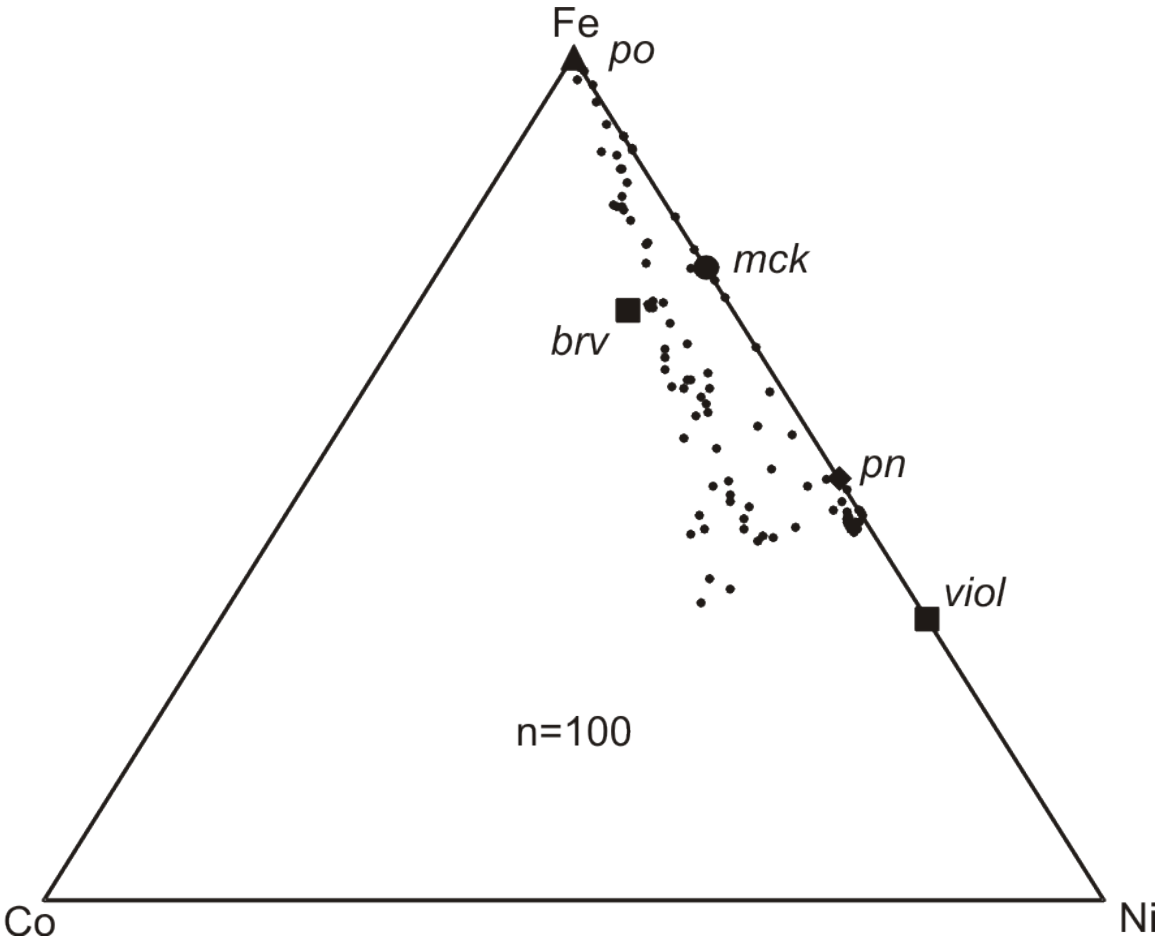

Figure 2.25 Pentlandite composition ternary of McConnell grains and ideal mineral formulas. SEM analyses show pentlandite grains from the McConnell ores vary in composition between ideal minerals; po (pyrrhotite), mck (mackinawite), brv (bravoite), pn (pentlandite), viol (violarite).

PGMs are rare, in general, mass balances conclude that the majority of Pt and Pd within the McConnell are hosted by discrete PGMs, a similar trend in Sudbury Ores, though the distribution of Pd is not fully established (Cabri and Laflamme, 1984; Cabri 1988; Li and Naldrett, 1993;Li et al., 1993; Farrow and Lightfoot, 2002; Huminicki et al., 2005).

2.4.7 Mineralogical and chemical models for the evolution of the McConnell deposit

Models for the evolution of the McConnell offset deposit must account for the following characteristics of the ores that are atypical for South Range offset-style deposits: i) a high volume (10-20%) of texturally-early magnetite hosted in cumulus MSS grains; ii) low Ni tenor, but where pentlandite occurs it contains very high concentrations of Pd and Co; iii) high Co/Ni ratios, but with low bulk Co tenor; iv) low As concentration (< 5 ppm) and very low abundance of arsenides and sulfarsenides; v) high Pt+Pd tenor and high Pd/Pt ratio but with typical Cu tenor; vi) areas of intense alteration that introduced secondary Pb into pentlandite (possibly remobilized from relatively late SIC-related VMS deposits); vii) areas of localized alteration that transformed pentlandite to Ni-rich pyrrhotite, pyrite, and marcasite with minor violarite.

2.4.7.1 Formation of an oxygen-rich sulfide liquid

Sulfide mineralization within the McConnell ore body contains a significant abundance of cumulus magnetite hosted in close spatial association with sulfides. This observation indicates that the sulfide melt was initially rich enough in O_2 to crystallize at or above a magnetite-saturated cotectic. Magnetite crystallized directly from the sulfide liquid prior to or during MSS crystallization in O-rich systems (Naldrett, 1969; Doyle and Naldrett, 1987; Fonseca et al., 2008). It has been shown that a high Ni/Fe ratio (and to a lesser extent Cu/Fe ratio) in a sulfide melt drastically reduces oxygen solubility in the melt (Mungall, 2007; Fonseca et al., 2008). This may account for the low Ni

concentration and high magnetite abundance in the McConnell ores. The McConnell deposit may have been emplaced into the offset before sufficient diffusion of oxygen from the sulfide liquid into the overlying melt sheet had occurred, though this would suggest an early sulfide emplacement. Alternately, if the McConnell sulfide liquid was formed relatively late (but prior to emplacement) it may have interacted with a silicate melt which was becoming progressively more oxidizing as it evolved over time. Although O_2 and fS_2 affect the composition of a melt through partition coefficients, it was found that these factors did not significantly lower the partitioning behaviour of the PGE from silicate to sulfide liquids (Peach et al., 1994; Bezmen et al., 1994), and evidence of high PGE tenors in low-Ni McConnell ores reflects this.

The sulfur fugacity and oxidation states of elements are two of the most important factors that control the partitioning behaviour of semimetals and chalcogenides between sulfide and silicate liquids, as S within MSS and sulfide melts is predominantly anionic (Helmy et al., 2010). As the sulfur fugacity of a system increases, the relative proportions of cation ratios of metals also tend to increase (Fe^{3+}/Fe^{2+}, Cu^{2+}/Cu^{+}), whereas metal/sulfur ratios of sulfides produced from these melts falls, and arsenic changes it's valence state from As^{-} to As^{+}, becoming increasingly incompatible in MSS (Helmy et al., 2010). A sulfide liquid rich in S crystallizes MSS with more defect concentrations than sulfide liquids that contain less S, allowing Ni and Cu to become more compatible in MSS (Ballhaus et al., 2001). Crystallization of magnetite from a sulfide liquid along the MSS-magnetite cotectic would effectively increase the S/metal concentration of the sulfide liquid.

A high O_2 concentration may account for the low As in McConnell ores if

fractionation had occurred and As partitioned into the residual sulfide liquid and away from the MSS cumulates. The limitations of a model which rely on oxygen-rich fractional crystallization depend mostly on the partition coefficients between MSS and residual sulfide liquid. If fractional crystallization had occurred then PGE would strongly partition into the sulfide liquid and become depleted in MSS. This is not seen in the McConnell ores, as PGE remains in MSS cumulates as discrete Pd-telluride grains, and fractionation based on ore texture and composition would have only occurred in minor amounts. In regards to fluctuating oxygen concentration, the sulfide liquid and silicate liquids would have been in equilibrium before injection, and could not vary significantly in oxygen content between the two liquids unless it was an early sulfide liquid, which is not reflected in the McConnell sulfide mineralogy. The effect that the R factor of the system has on the availibility of oxygen and metal content should also be considered. If the R factor of the system is relatively low, the concentration of metals that can partition into the sulfide liquid will also be low, allowing more oxygen to be incorporated into the sulfide melt. A low R factor associated with the McConnell sulfide system may be the cause of the high oxygen content of the sulfide liquid.

2.4.7.2 As-poor sulfide melt

The McConnell system did not attain the typical arsenic contamination that other South Range deposits share, as seen by low bulk As and low abundance of sulfarsenide grains within the McConnell ores. The sulfide liquid that formed the McConnell ores was still able to partition significant concentrations of PGE even though As partitioning was evidently hindered (Figure 2.26A). As a result, PGE within the cooling sulfide melt could not be sufficiently sequestered into early forming discrete sulfarsenide phases, and

instead formed Pd-Te-Bi composite grains (or alloys) along the boundaries of silicates and sulfides (figure 2.27). The low concentrations of As and Ni within the McConnell ores may have both been connected to the high oxygen content of the system, which inhibited partitioning of these elements from the silicate melt sheet to the sulfide liquid. The sulfide melt would only be able to incorporate these elements in abundance after magnetite had begun crystallizing, sometime after injection into the offset. Although the exact source, timing, and mechanisms of arsenic introduction and contamination into sulfide melts is unclear, it can be concluded that a South Range sulfide melt can achieve economic PGE tenors without the associated contamination of arsenic. If the McConnell deposit does indeed reflect an uncontaminated sulfide melt, it may be more representative of the composition of the early silicate melt than other ores which indicate high degrees of contamination.

If partitioning was not greatly affected by O content, the low concentration of As in McConnell ores may be a result of the initial sulfide liquid interacting with a locally depleted silicate melt (Figure 2.26B). If the incorporation of As-bearing host rock was responsible for As contamination into the melt sheet (Figure 2.26A), then locally elevated or depleted sections of the melt sheet could have interacted with different proportions or lithologies of host rock, altering the composition of the sulfide liquid that interacted with it (Darling et al., 2012). A difference in the composition of South Range ores may also reflect a variance in O_2 and fS_2 between the sulfide liquids that formed from the melt sheet, altering portioning behaviour of elements between sulfide and silicate melts. Once the sulfide had been emplaced into the dyke, early arsenide phases may have formed and depleted the sulfide liquid in As, Ni, Co, and PGE (Figure 2.26B), but a limited amount

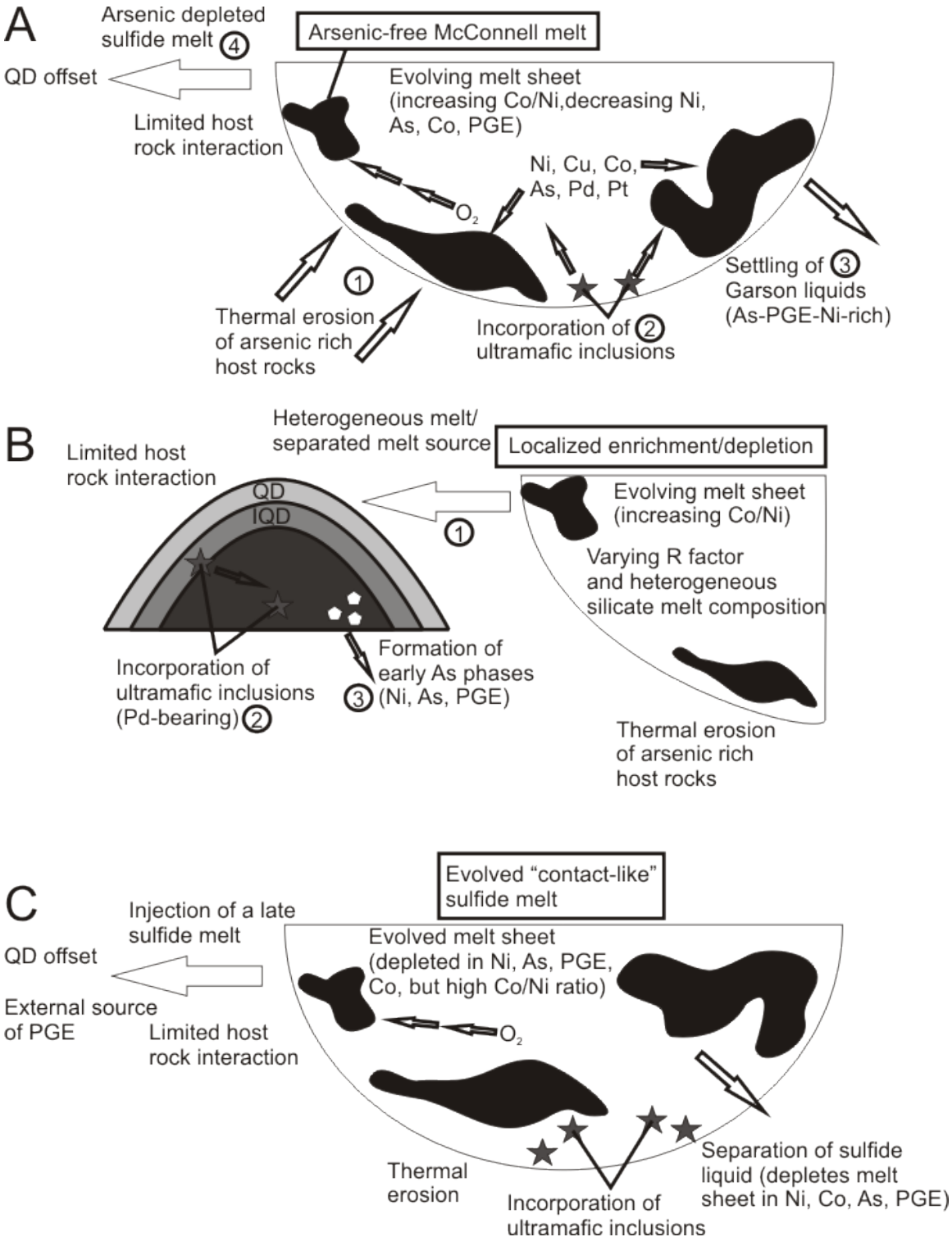
A
Arsenic depleted sulfide melt ④
Arsenic-free McConnell melt
QD offset
Limited host rock interaction
Evolving melt sheet (increasing Co/Ni,decreasing Ni, As, Co, PGE)
Ni, Cu, Co, As, Pd, Pt
O2
Settling of ③ Garson liquids (As-PGE-Ni-rich)
①
Thermal erosion of arsenic rich host rocks
Incorporation of ② ultramafic inclusions
B
Heterogeneous melt/ separated melt source
Localized enrichment/depletion
Limited host rock interaction
QD
IQD
①
Evolving melt sheet (increasing Co/Ni)
Varying R factor and heterogeneous silicate melt composition
Formation of early As phases ③ (Ni, As, PGE)
Incorporation of ultramafic inclusions (Pd-bearing) ②
Thermal erosion of arsenic rich host rocks
C
Evolved "contact-like" sulfide melt
Injection of a late sulfide melt
QD offset
External source of PGE
Limited host rock interaction
Evolved melt sheet (depleted in Ni, As, PGE, Co, but high Co/Ni ratio)
O2
Thermal erosion
Incorporation of ultramafic inclusions
Separation of sulfide liquid (depletes melt sheet in Ni, Co, As, PGE)

Figure 2.26 Proposed models to explain compositions of McConnell sulfide ores. A) 1)The bulk As budget of the melt sheet increases as incorporation of As-bearing country rocks through thermal erosion occurs on the South Range. 2) Incorporation and partial melting of xenolithic inclusions provides a possible source for PGE. 3) As the melt sheet begins to cool and promotes sulfide saturation, As partitions into sulfide melt from the silicate melt sheet, along with base and precious metals. Settling of Garson liquids depletes melt sheet in metals, most prominently As and Ni. 4) The McConnell melt is derived from a melt that contains less metals and more oxygen than the Garson sulfide melt. The McConnell sulfide liquid avoids significant As contamination but attains sub-economic metal tenors with elevated Co/Ni ratios. B) The McConnell sulfide liquid is locally As and Ni depleted due to the size and composition its silicate melt reservoir. The McConnell sulfide liquid had far less volume than other systems, limiting its potential to interact with a greater volume of silicate melt and thus incorporating lower concentrations of metals. Other sulfide liquids were able to incorporate larger proportions of these elements due to their greater volume and interaction with the silicate melt sheet. 1) Emplacement of a depleted sulfide melt and inclusion-rich quartz diorite (IQD) silicate liquid is injected into quartz diorite (QD). This creates an envelope around the sulfide liquid that prevents it from assimilating As-bearing host rocks. 2) The incorporation of silicate inclusions may have provided additional metals in low concentrations to the McConnell melt. 3) Formation of sulfarsenides would have sequestered Ni, Co, As, and PGE from the cooling sulfide liquid, depleting it in these metals if they had formed and separated from the system. C) Late-stage sulfide liquid is left to scavenge a depleted silicate reservoir, thus limiting available metal concentrations. Elevated Co/Ni ratios, low base and precious metals, and far less thermal erosion due to cooler silicate melts are all factors which would reflect a later sulfide melt source. An external source of Pt and Pd would have had to been introduced into the McConnell sulfide melts in order to account for its elevated PGE content while coming from a depleted source.

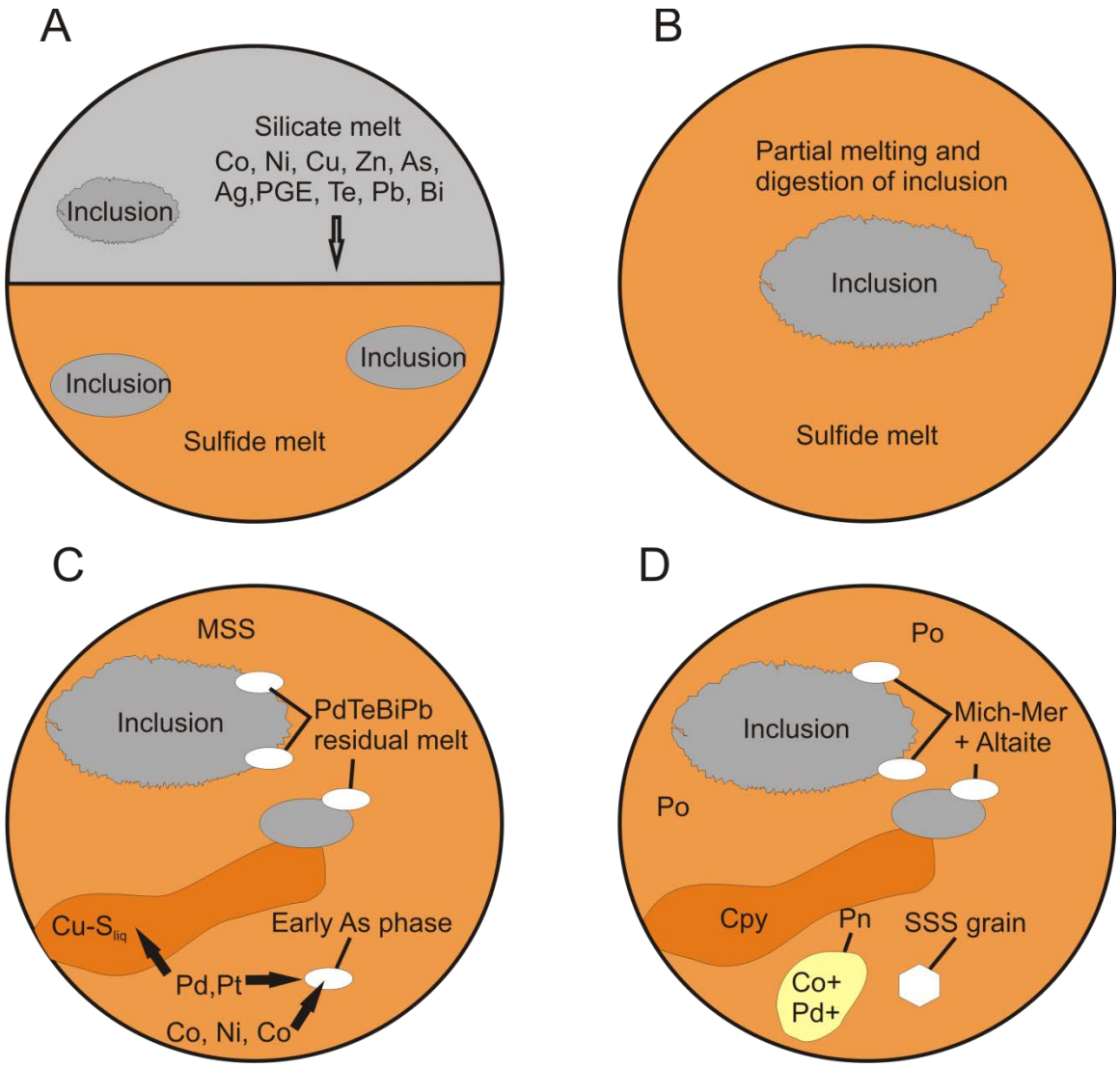

Figure 2.27 Proposed cooling history of McConnell ores. A) Sulfide melt forms from the superheated silicate melt sheet at and scavenges base and precious metals. McConnell sulfide melt was not able to attain significant concentrations of most elements (Ni, Cu, Zn, As) as it contained high concentrations of O_2. Inclusions of country rock and exotic fragments were incorporated and partially melted by superheated silicate melt. B) Sulfide liquid and some silicate melt (IQD) was injected into the McConnell offset structure. Inclusions of country rock and exotic fragments continued to be partially melted by sulfide liquid. C) MSS cumulates form and accumulate, with interstitial residual sulfide liquid occurring between MSS grains. Early forming arsenide phases sequestered Co and Ni, as well as PGE (Pd, Pt), while composite grains of Pd-tellurides formed on the boundaries of MSS and silicate inclusions, as well as along MSS-sulfide liquid. PGEs partition strongly from MSS into residual sulfide liquid. D) McConnell ores contain PGM (michenerite-meresnkyite) and precious metal phases (hessite, electrum) between grain boundaries of sulfides and silicates, and along pyrrhotite (po) chalcopyrite (cpy) boundaries. Sulfarsenide solid solution (SSS) grains are rare in McConnell ores, reflecting low initial As concentrations. Pentlandite (pn) grains are also very rare, but have high concentrations of Co and Pd.

of As in the segregated sulfide melt only allowed for the formation of sparse arsenides and sulfarsenides. As a result, Co and the PGE were left to accumulate in MSS or residual sulfide liquid without As. Local depletion of the melt sheet may have also occurred if the McConnell system was emplaced later than other deposits from an evolved source.

If the low As concentrations in McConnell ores are not related to partitioning between the melt sheet and sulfide liquid at supersolidus conditions, they may instead reflect post-emplacement depletion of As from the cooling sulfide liquid. The formation of an As-rich liquid or early forming mineral phases could efficiently deplete the sulfide liquid in As and Ni, as is reported for other South Range deposits (Cabri and Laflamme, 1984; Magyarosi et al., 2002; Huminicki et al., 2005; Dare et al., 2010; Lefort, 2014). If early forming As-rich phases did form and separate from the sulfide liquid, they would have also sequestered PGE thus depleting the liquid and any formed cumulates (Figure 2.26B). In addition, Co would also sequester into As-rich phases, lowering Co concentration in MSS and residual sulfide liquid as temperatures fell. Due to the high PGE tenors and elevated Co/Ni ratios of McConnell ores, it is unlikely that early forming As phases separated from the sulfide liquid.

The small size of the McConnell system may have led to the inability to melt and incorporate a sufficient amount of As-bearing host rocks to reach similar arsenic contamination as other systems, though a bolide impact would cause whole scale melting of crustal rocks during the formation of the initial melt sheet. The regional bulk As concentrations of sulfide liquids would have been dictated by partition coefficients, fugacities, and the size and composition of the silicate reservoir in equilibrium with the initial sulfide liquid at sulfur saturation (Naldrett, 1969; Keays and Lightfoot, 1999;

Farrow and Lightfoot, 2002; Keays and Lightfoot, 2004; Mungall et al., 2005; Mungall, 2007), and before injection into structures or host rocks (Lightfoot et al. 2001). Sulfide liquid and silicate melt (IQD) that formed economic offset deposits were injected either partially or entirely into the cores of QD offsets, thus creating a system that restricted the interaction of sulfide liquid with As-bearing host rocks after injection (Figure 2.26B). The size of the offset should therefore have minimal influence on the As content of the sulfide melt, as the composition of the injected melt would be dictated by the melt sheet (Figure 2.26A), unless As contributions from the melt sheet are negligible and only represent incorporation of local As-bearing country rock.

One limitation to this model is the inexplicable fact that only As was rejected from the sulfide liquid. Although other metal concentrations are indeed low, they are still present in sufficient amount to explain lower partition coefficients between silicate and sulfide liquids, possibly due to a low R factor, but only As occurs in such low concentrations as to assume negligible partitioning from the melt sheet to the sulfide liquid. This model relies on either impeding As partitioning exclusively, or a portion of the melt sheet that is devoid of As; the former may be explained by elevated O_2 of the McConnell system, while the latter requires a locally depleted or evolved (late) silicate reservoir.

2.4.7.3 Heterogeneous sulfide/silicate melts and local enrichment

If the composition of a sulfide melt depends on the concentration of the silicate reservoir, then the difference in metal tenors between McConnell ores and other offset systems must be due to heterogeneity in the silicate melt sheet while sulfide liquids were being accumulated (Darling et al., 2012; Figure 2.26B). If the sulfide liquid interacted with an As-Ni-poor region of the melt sheet, it may explain the low concentrations of

these elements in the McConnell ores. A lack of As within the cooling sulfide melt precluded the formation of sulfarsenide phenocrysts, which left Co relatively enriched in MSS, concentrating into pentlandite as it later crystallized (Figure 2.27). Co/Ni ratios are higher in McConnell ores than other South Range deposits, as is the elevated concentration of Co in pentlandite. However, whole rock Co is lower in McConnell ores than other deposits, and may indicate a more evolved silicate reservoir than other South Range systems. The excess Co in the ores without significant Ni or As in the offset suggests that the source melt may have been initially depleted in these elements, as early-forming sulfarsenide grains would have sequestered most Co at high temperatures (Hem et al., 2001; Hem, 2006; Dare et al., 2010; Lefort et al., 2014). The sulfide liquid which formed the McConnell deposit may have interacted with a smaller, or a metal-depleted (late), silicate reservoir which may have resulted in a smaller R factor (e.g. Theriault et al., 1997, Mungall et al., 2005) than other South Range offsets. This may suggest that local contamination and heterogeneous composition of the initial melt sheet were pivotal factors in contributing to the unique mineralogy of the McConnell ores. The degree of heterogeneity within the melt sheet and subsequent sulfide liquids is not well known, but it is thought to be responsible for localized variations in ore geochemistry of South Range deposits (Darling et al., 2012).

It is yet unclear whether sulfide melts which originated in close proximity to each other were sourced from large pools in equilibrium together, or if they were hosted as separate systems which reflect localized assimilation and contamination separated by vast amounts of silicate melt (Mungall, 2002; Darling et al., 2012). A sulfide melt may have originated from higher, or lower in the melt sheet under conditions very different from

where it settled, mixing with sulfide liquids sourced from other parts of the melt sheet. Although the assimilation of country rocks is known to alter liquid compositions, the exact contribution and rheology of crustal material is still highly debated (i.e. Faggart et al., 1985; Mungall et al., 2004; Darling et al., 2010), as is the precise timing of offset formation (Wood and Spray, 1998; Murphy and Spray, 2002; Tuchscherer and Spray, 2002; Riller, 2005).

2.4.7.4 Late-stage sulfide liquid emplacement

If larger offset systems were emplaced before the McConnell sulfide liquid had even formed, they would have depleted regions of the silicate melt sheet in base and precious metals leaving a more evolved reservoir for any later sulfide melts (Figure 2.26C). The collection and formation of sulfide liquids that formed contact deposits would further deplete the melt sheet in metals. With no significant source of Ni, the McConnell sulfide melt was able to assimilate a large concentration of O_2 before emplacement into QD. The negligible As contributed from the melt sheet was not changed after emplacement, as the sulfide melt would have had very limited interaction with any As-bearing host rock. The depleted Ni and As, mediocre Cu and Co, and high Co/Ni ratios in McConnell ores may all reflect an evolved, metal depleted silicate melt source that signifies a later collection and emplacement of McConnell sulfide liquids than other South Range offsets. The introduction of PGE into the McConnell system may have occurred before or after emplacement into QD; the silicate melt sheet either locally assimilated some source of PGE before emplacement, or the silicate inclusions that were incorporated into the McConnell system contained enough PGE to significantly raise tenors (Figures 2.26B, 2.27). If the source of the McConnell sulfide liquid was a later fractionated silicate melt,

mineralization should reflect high Cu/Ni and Pd/Ir ratios, and although Cu/Ni ratios are elevated, Ir data was not collected for McConnell mineralization.

Another possibility is that McConnell sulfide liquid began to form at the same time as sulfide saturation of larger offset systems. Initially, the composition of the McConnell sulfide melt may have been very similar to Ni-rich melts, but where the Ni-rich offsets were emplaced quickly after sulfide saturation, the McConnell sulfide liquid remained in equilibrium with the melt sheet, possibly losing Ni to the silicates while increasing its oxygen concentration. This scenario would account for the similar PGE tenors of McConnell and larger South Range systems, as PGE should remain within sulfide liquid during crystallization of the silicate mass.

The exact timing of offset formation and sulfide saturation of the SIC is in constant debate, but it is widely agreed that offsets and the sulfides which they host represent the most primitive compositions of melts in the SIC, being emplaced very early but still after a huge assimilation of crustal material and some degree of cooling in the overlying melt sheet (e.g. Wood and Spray, 1998; Farrow and Lightfoot, 2002). Timing is very important for a number of reasons, but the most obvious is the effect of temperature on a system. Temperature not only affects the amount of metals available to a sulfide liquid from a silicate liquid (if the cooling silicate reservoir begins fractional crystallization, R factor quickly falls), but also strongly affects the partitioning behaviour of most elements (Naldrett et al., 1979; Mungall et al., 2005). In addition, sulfide liquids that remain in equilibrium with silicate liquids for a long period of time will efficiently deplete the silicate reservoir in chalcophile elements, effectively limiting the contributions of the silicate to a later sulfide liquid.

Interaction with a slightly later (more evolved) depleted silicate melt would explain the McConnell system, were it not for the elevated PGE. If a silicate melt is even slightly depleted in Ni from a previous sulfide liquid, it should presumably be extremely depleted in PGE, as partitioning of PGE between sulfide and silicate melt is orders of magnitude higher than that of Co, Cu, and even Ni. The only way that a late stage sulfide melt could interact with a depleted silicate reservoir and still achieve the same PGE tenor as an early melt is to require some outside source of PGE to enrich the later melt, as relying on R factor, Nernst partition coefficients, and equilibrium coefficients of typical sulfide-silicate systems cannot adequately account for this anomaly. Although there is no positive conclusive evidence to support the following speculation, the outside source of PGE that is required to prove this model may in fact be the anomalous inclusions that are associated with nearly all South Range offsets and deposits. If these xenolithic ultramafics were sourced from a complex which was present before the Sudbury impact event, they may actually be carriers and contributors of PGE, as nearby intrusions have been shown to contain very rich palladium concentrations (East Bull Lake intrusive suite, James et al., 2002). The partial-melting and incorporation of silicate inclusions is present in almost all McConnell ores at some scale. Whether these inclusions were melted and incorporated before or after emplacement does not change the fact that most PGM in McConnell ores occur hosted between the boundaries of silicates and sulfides. This does not appear to be a coincidence and may support the fact that these inclusions are the source of Pd within McConnell sulfides.

2.4.7.5 Late stage alteration of ores

Hydrothermal fluids have only affected a small segment of the McConnell ores, a

Table 2.6 Summary of models

	Uncontaminated sulfide melt	Local enrichment/depletion	Late stage sulfide melt
High oxygen fugacity	Excess oxygen in sulfide liquid inhibits assimilation of arsenic	Lower concentrations of available Ni allow higher solubility of oxygen in sulfide liquid	Depleted silicate reservoir contributes higher concentrations of oxygen to sulfide liquid than base metals
Low Ni/Co ratios	Elevated oxygen fugacity affects Ni concentration but not Co	Nickel distribution in silicate melt sheet may be more heterogeneous than Co distribution	Early forming sulfide liquid scavenges more Ni than Co, depleting silicate reservoir and raising Co/Ni ratio
Low Arsenic contamination	Arsenic partitioning was inhibited by some factor during formation of sulfide	Arsenic-bearing rocks were not assimilated into local silicate or sulfide liquid	Arsenic partitioned into earlier formed sulfide melts, depleting silicate reservoir
High PGE tenor	PGE are often associated with As, but always partition strongly into sulfide liquid regardless of fO_2	Country rocks containing PGE were assimilated into local silicate and sulfide liquids	Silicate liquid would be depleted in PGE, requires an external source or a recharge of PGE rich silicate liquid
Unstable/anomalous pentlandite composition	Lack of As inhibits sulfarsenide formation, sequestering Co in pentlandite	Cobalt and Pb substitute for Ni in early high temperature pentlandite, becoming unstable during cooling	Cobalt-rich pentlandite incorporates Pb and is altered by late stage hydrothermal fluids

ltering primary minerals to pyrite and marcasite where hydrothermal processes were most intense. These fluids introduced Pb into the McConnell system, contributing to the already Pb-rich pentlandite that was present in the ores. Fluids that altered the McConnell system may have been sourced from (or mixed with) overlying VMS systems that formed during the cooling of the main mass (Figure 2.21). Although fluids have altered pentlandite grains, high Co/Ni ratios and Pd enrichment also occur in pentlandite that is not associated with hydrothermal alteration, indicating these features precede alteration. Pentlandite grains also display instability within unaltered intervals, and are a result of the initial composition and cooling history of the McConnell sulfide system.

2.5 Conclusions

The characteristics of McConnell ores reflect a much different evolutionary history than other offset or South Range environments. The textural and geochemical peculiarities of the McConnell offset deposit, especially concerning the PGE, reflect the difficulty in attributing these factors to one event or process. The effect of O_2 concentration in a sulfide liquid may explain preferential partitioning of elements between silicate and sulfide liquid, but the reason O_2 solubility was so high is not well established. The relationship between Ni and O_2 solubility in the McConnell sulfide melt is not fully understood; was the initial low Ni content of the McConnell sulfide melt responsible for the high O solubility, allowing it to collect more oxygen from the surrounding silicate melt, or did the oxygen-rich liquid effectively alter the partitioning behaviour of Ni between sulfide and silicate melt so as to make it incompatible in sulfide liquid. What is clear is that the higher than normal abundance of magnetite hosted entirely within McConnell sulfides compared to other offsets or South Range systems

implies that the oxygen content of this system was different than other similar sulfide melts.

A late-stage sulfide liquid would explain the depleted metal tenors and elevated Co/Ni ratios of McConnell ores, but would require that PGE were introduced from another source to account for the elevated Pt+Pd tenors. The local depletion of Ni and As from surrounding silicate reservoirs is most difficult to explain, especially given the elevated PGE tenors in McConnell ores. The low metal tenors and As contamination in McConnell ores may be explained by its size and limited ability to digest country rock or silicate inclusions, though the composition of the ores should still be similar to other South Range deposits since PGE tenors are comparable. Two models require that PGE be provided by a source other than the melt sheet; one model requires that the melt sheet contain negligible As contamination (presumably from a limited digestion of As-bearing country rocks by the superheated silicate melt previous to sulfide segregation), but still contain very high PGE concentrations. The alternative to an As-free melt sheet is that As partitioning into sulfide liquid was efficiently inhibited, while the partitioning behaviour of other elements was simply reduced, presumably by the elevated O_2 content of the system. A low R factor of a sulfide system has a very large effect on base and precious metal concentrations, and would account for most of these features, though the PGE content of the McConnell mineralization would also be greatly depleted.

References

Arndt, N.T., C.M. Lesher, G.K. Czamanske, 2005; Mantle-derived magmas and magmatic NiCu-(PGE) deposits; Economic Geology, 100th Anniversary volume, 5-2

Ames, D.E., 1999, Geology and regional hydrothermal alteration of the crater-fill, onaping formation: association with Zn-Pb-Cu mineralization, Sudbury Structure, Canada; PhD thesis, Carleton University.

Ames, D.E., and Farrow, C.E.G., 2007, Metallogeny of the Sudbury mining camp, Ontario, in Goodfellow, W.E., ed., Mineral deposits of Canada: A synthesis of major deposit-types, District Metallogeny, the evolution of geological provinces, and exploration methods; Geological association of Canada, mineral deposits division, special publication no. 5, p. 329-350.

Ames, D.E., Davidson, A., and Wodicka, N., 2008; Geology of the Giant Sudbury Polymetallic Mining Camp, Ontario, Canada; Economic Geology, v.103, p.1057-1077.

Ames, D. E., Golightly, J. P., Lightfoot, P. C. & Gibson, H. L., 2002; Vitric compositions in the Onaping Formation and their relationship to the Sudbury Igneous Complex, Sudbury Structure; Economic Geology, v.97,p .1541–1562.

Audetat, A., Pettke, T., Heinrich, C.A., and Bodnar, R.J., 2008, The composition of magmatic-hydrothermal fluids in barren and mineralized intrusions; Economic Geology, v. 103, p. 877-908

Bailey, J., McDonald, A., Lafrance, B., and Fedorowich, J., 2006, Variations in Ni content in sheared magmatic sulfide ore at the Thayer Lindsley Mine, Sudbury, Ontario; The Canadian Mineralogist, v. 44, p. 1063-1077.

Ballhaus, C., Tredoux, M., and Späth, A., 2001, Phase relations in the Fe–Ni–Cu–PGE–S system at magmatic temperature and application to massive sulphide ores of the Sudbury Igneous Complex; Journal of Petrology, v. 42, p. 1911–1926

Barnes, S-J., van Achterbergh, E., Makovicky, E., and Li, C., 2001, Prton microprobe results for the partitioning of platinum-group elements between monosulphide solid solution and sulphide liquid; South African Journal of Geology, v. 104, p. 275-286.

Barnes, S-J. and Lightfoot, P.C. (2005). Formation of magmatic nickel-sulfide ore deposits and processses affecting their copper and platinum-group element contents. In Hedenquist, J.W., Thompson, J.F.H., Goldfarb, R.J. and Richards, J.P. (eds.) Economic Geology 100th Anniversary Volume, p. 179-213

Barnes, S.J., Makovicky, E., Karup-Moller, S., Makovicky, M., Rose-Hanson, J., 1997, Partition coefficients for Ni, Cu, Pd, Pt, Rh and Ir between monosulfide solid solution and sulfide liquid and the implications for the formation of compositionally zoned Ni–Cu

sulfide bodies by fractional crystallization of sulfide liquid; Canadian Journal of Earth Sciences, v. 34 p. 366–374

Becker, M., de Villers, J., Bradshaw, D., 2010, The flotation of magnetic and non-magnetic pyrrhotite from selected nickel ore deposits; Minerals Engineering, v. 23, p. 1045- 1052

Bennett, G., Dressler, B.O., and Robertson, J.A., 1991, The Huronian Supergroup and associated intrusive rocks: Ontario Geological Survey Special Volume 4, p. 549–592.

Béziat, D., Monchoux, P., and Tollon, F., 1996, Cobaltite-gersdorffite solid solution as a primary magmatic phase in spessartite, Lacune area, Montagne Noire, France; The Canadian mineralogist, v. 34, p. 503-512.

Boudreau, A.E., Mathez, E.A., and McCallum, I.S., 1986, Halogen geochemistry of the Stillwater and Bushveld complexes: Evidence from hydrous silicates and fluid inclusions; Journal of Petrology, v. 27, p. 967-986.

Boudreau, A.E., and Meurer, W.P., 1999, Concentration of platinum-group elements by magmatic fluids in layered intrusions; Economic Geology, v. 94, p. 1830-1848.

Buck, W .K. (1968): Nickel, Canada and the world. Dep. Of Energy, Mines and Resources, Canada, Mineral Resources Div., Mineral Rep. 16.

Bursztyn, N., and Olivo, G., 2010, PGE-Rich Ni-Cu sulfide mineralization in the Flin Flon Greenstone Belt, Manitoba, Canada: Implications for hydrothermal remobilization of Platinum Group Elements in basic-ultrabasic sequences; Economic Geology, v. 105 (8), p., 1469-1490.

Cabri, L.J., 2002; The platinum-group minerals: Canadian Institute of Mining, Metallurgy and Petroleum, Special Volume 54, p. 13-129

Cabri, L.J., and Laflamme, L.H.G., 1976; The Mineralogy of the Platinum Group Elements from Some Copper-Nickel Deposits of the Sudbury Area, Ontario; Economic Geology, v. 71, p.1159-1195.

Cabri, L.J., and Laflamme, L.H.G., 1984; Mineralogy and distribution of platinum-group elements in mill products from Sudbury, *in* Park. W.C., Hausen, D.M., and Hagni, R.D., ads., Applied Mineralogy: Proceedings of the second international congress on applied mineralogy in the minerals industry: Warrendale, PA, Metallurgical Society of AIME, p. 911-922

Campbell, I.H., and Naldrett, A.J., 1979, The influence of silicate:sulfide ratios on the geochemistry of magmatic sulfides; Economic Geology, v. 74, p. 1503-1506.

Campbell, I.H., Naldrett, A.J., and Barnes, S.J., 1983, A model for the origin of the platinum group rich sulphide horizons in the Bushveld and Stillwater complexes; Journal of Petrology, v. 24, p. 133–165

Campos-Alvarez, N.O., Samson, I.M., Fryer, B.J., and Ames, D.E., 2010, Fluid sources and hydrothermal architecture of the Sudbury Structure: Contrains from femtosecond LA-MC-ICP-MS Sr isotopic analysis of hydrothermal epidote and calcite; Chemical Geology, v., 278, p. 131-150.

Candela, P.A., and Holland, H.D., 1984, The partitioning of copper and molybdenum between silicate melts and aqueous fluids; Geochimica et Cosmochimica Acta, v., 48, p. 373-380.

Candela, P.A., and Piccoli, P.M., 1995, An experimental-theoretical model of brine-vapor-silicate melt equilibria with applications to geothermal and ore-forming systems, *in* Thompson, J.F.H., ed., Magmas, Fluids and Ore Deposits; Mineralogical Association of Canada Short Course Series, v., 23, p. 101-127.

Card, K.D., 1994, Geology of the Levack gneiss complex, the northern footwall of the Sudbury structure, Ontario *in* Current Research 1994-C; Geological Survey of Canada, p.269-278.

Card, K.D., Church, W.R., Franklin, J.M., Frarey, M.J., Robertson, J.A., West, G.F., and Young, G.M., 1972, The Southern province: Geological Association of Canada Special Paper 11, p. 335–380

Card, K.D., and Innes, D.G., 1981, Geology of the Benny area, district of Sudbury; Ontario Geological Survey Report 206, 117 p

Card, K.D., Gupta, V.K., McGrath, P.H., and Grant, F.S., 1984, The Sudbury Structure: Its regional geological geophysical setting, *in* Pye, E.G., Naldrett, A.J., and Giblin, P.E., eds., The geology and ore deposits of the Sudbury structure; Ontario geological survey, special volume 1, p. 57-82.

Card, K.D., and Poulsen, K.H., 2000, Archean and Paleoproterozoic geology and metallogeny of the southern Canadian Shield: Exploration and Mining Geology, v. 7, p. 181–215

Carter, W.M., 2000, Sulfide, sulfarsenide, and platinum-group minerals from the 740 deposit, Kelly Lake orebody of the Copper Cliff offset, Sudbury, Canada; Unpublished B.Sc. thesis, Ottawa, Ontario, Carleton University, 95 p

Carter, W.M., Watkinson, D.H., and Jones, P.C., 2001, Post-magmatic remobilization of platinum-group elements in the Kelly Lake Ni-Cu sulphide deposit, Copper cliff offset, Sudbury; Exploration and Mining Geology, v. 10, p. 95−110.

Chanturiya, V., Makarov, V., Forsling, W., Makarov, D., Vasil'eva, T., Trofimenko, T., Kuznetsov, V., 2004, The effect of crystallochemical peculiarities of nickel sulphide minerals on flotation of copper-nickel ore; International Journal of Mineral Processing, v. 74, p. 289-301.

Cline, J.S., and Bodnar, R.J., 1991, Can economic porphyry copper mineralization be generated by a typical calc-alkaline melt?; Journal of Geophysical Research, v., 96 (B5), p. 8113-8126.

Cochrane, L.B., 1984, Ore deposits of the Copper Cliff offset, *in* Pye, E.G., Naldrett, A.J., and Giblin, P.E., eds., The geology and ore deposits of the Sudbury structure: Toronto, Ontario Geological Survey, Special Volume 1, p. 347–359

Cook, N.J., Wood, S.A., and Zhang, Y., 1992, Transport and fixation of Au, Pt and Pd around the Lac Sheen Cu-Ni-PGE occurrence in Quebec, Canada; Journal of Geochemical Exploration, v. 46, p. 187-228.

Corfu, F., and Lightfoot, P.C., 1997, U-Pb geochronology of the Sublayer Igneous Complex, Ontario: Economic Geology 91, p. 1263-1269.

Craig, J.R., 1973; Pentlandite-Pyrrhotite and Other Low-Temperature Relations in the Fe-Ni-S System; American Journal of Science, Volume 273-A, p.496-510.

Crerar, D., Wood, S., Brantley, S., and Bocarsly, A., 1985, Chemical controls on solubility of ore forming minerals in hydrothermal solutions; Canadian Mineralogist, v., 23, p. 333-352.

Crocket, J.H., Fleet, M.E., and Stone, W.E., 1997, Implications of composition for experimental partitioning of platinum-group elements and gold between sulfide liquid ans basalt melt: The significance of nickel content; Geochimica et Cosmochimica Acta, v. 61, p. 4139-4149

Dare, S.A.S., Barnes, S.J., Prichard, H.M., 2010, The distribution of platinum group elements (PGE) and other chalcophile elements among sulfides from the Creighton Ni-Cu-PGE sulfide deposit, Sudbury, Canada, and the origin of palladium in pentlandite; Minerallium Deposita, v. 45, p. 765-793

Dare, S.A.S., Barnes, S.-J., and Beaudoin, G., 2012, Variation in trace element content of magnetite crystallized from a fractionating sulfide liquid, Sudbury, Canada: Implications for provenance discrimination; Geochimica et Cosmochimica Acta, v. 88, p. 27–50

Darling, J.R., Hawkesworth, C.J., Lightfoot, P.C., Storey, C.D., and Tremblay, E., 2010a, Isotopic heterogeneity in the Sudbury impact melt sheet; Earth and Planetary Science Letters, v. 289, p. 347-356

Darling, J.R., Hawkesworth, C.J., Storey, C.D., and Lightfoot, P.C., 2010b, Shallow impact: isotopic insights into crustal contributions to the Sudbury impact melt sheet; Geochimica et Cosmochimia acta, v. 74, p. 5680-5696

Darling, J.R., Storey, C.D., Hawkesworth, C.J., and Lightfoot, P.C., 2012, In-situ Pb isotope analysis of Fe-Ni-Cu sulphides by laser ablation multi-collector ICPMS: New insights into ore formation in the Sudbury impact melt sheet; Geochimica et Cosmochimica Acta, v. 99, p. 1-17

Deutsch, A., Grieve, R.A.F., Avermann, M., Bischoff, L., Brockmeyer, P., Buhl, D., Lakomy, R., Muller-Mohr, V., Ostermann, M., and Stöffler, D., 1995, The Sudbury Structure (Ontario, Canada): A tectonically deformed multi-ring impact basin: Geologische Rundschau v. 84, pp. 697-709.

Dickin, A.P., Artan, M., and Crocket, J., 1996, Isotopic evidence for distinct crustal sources of North and South Range ores, Sudbury Igneous Complex; Geochimica et Cosmochimica Acta, v. 60, p. 1605-1613

Dickin, A.P., Nguyen, T., and Crocket, J., 1999, Isotopic evidence for a single impact melting origin of the Sudbury Igneous Complex, *in* Large meteroirte impacts and planetary evolution II, Dressler, B., and Sharpton, V., eds.; Special paper 339, Geological Society of America, p. 361-371

Dietz, R.S., 1964, Sudbury structure as an astrobleme: The Journal of Geology, v.72, pp. 412-434.

Doyle, C.D., Naldrett, A.J., 1987, The oxygen content on “sulfide” magma and its effect on the partitioning of nickel between coexisting olivine and molten ores; Economic Geology, v. 82, p. 208-211

Dressler, B.O., 1984; Chapter 4, General Geology of the Sudbury Area, p.58-78 in The Geology and Ore Deposits of the Sudbury Structure, Pye, E.G., Naldrett, A.J., Giblin, P.E. (Eds.), The Geology and Ore Deposits of the Sudbury Structure, Special vol. 1. Ontario Geological Survey, pp 58-78.

Easton, R.M., Jobin-Bevans, L.S., and James, R.S., 2004, Geological guidebook to the Paleoproterozoic East Bull Lake intrusive suite plutons at East Bll Lake, Agnew Lake and River Valley, Ontario; Ontario Geological Survey, Open File Report 6135, p. 84.

Ebel, D.S., and Naldrett, A.J., 1996, Fractional crystallization of sulfide ore liquids at high temperature; Economic Geology v. 91, p. 607-621.

Eckstrand, O.R., Good, D.J., Yakubchuk, A., and Gall, Q., comp., 2004; World dstribution of Ni, Cu, PGE, and Cr deposits and camps: Geological Survey of Canada, unpublished update of Open File 3791a.

Eckstrand, O.R., and Hulbert, L.J., 2007, Magmatic nickel-copper-platinum group element deposits, in Goodfellow, W.D., ed., Mineral Deposits of Canada: A Synthesis of Major Deposit Types, District Metallogeny, the Evolution of Geological Provinces, and Exploration Methods: Geological Association of Canada, Mineral Deposits Division, Special Publication No. 5, p. 205-222.

Ernst, R.E., and Buchan, K.L., 2001, Large mafic magmatic events through time and links to mantle-plume heads: Geological Society of America Memoir 352, p. 483–575.

Everest, J.O., 1999, The relationship of Cu-Ni-PGE veins in the Levack Gneiss Complex to hanging wall magmatic ore at the McCreedy West Mine, Sudbury; M.Sc. thesis, Carlton University.

Faggart, B.E., Basu, A.R., and Tatsumoto, M., 1985, Origin of the Sudbury complex by meteoric impact: neodymium isotope evidence; Science, v.230, p.436-439.

Farrow, C.E.G., 1994, Geology, alteration, and the role of fluids in Cu-Ni-PGE mineralization of the footwall rocks to the Sudbury Igneous Complex, Levack and Morgan townships, Sudbury District, Ontario; PhD. thesis, Carlton University.

Farrow, C.E.G., Watkinson, D.H., and Jones, P.C., 1994, Fluid inclusions in sulfides from North and South Range Cu-Ni-PGE deposits, Sudbury structure, Ontario; Economic Geology, v. 89, p. 647-655.

Farrow, C.E.G., and Watkinson, D.H., 1992, Alteration and the role of fluids in Ni, Cu and platinum-group element deposition, Sudbury Igneous Complex Contact, Onaping-Levack area, Ontario; Mineralogy and Petrology, v., 46, p. 67-83.

Farrow, C.E.G., and Watkinson, D.H., 1996, Geochemical characteristics of the Epidote Zone: its development and associated Ni-Cu-PGE remobilization by saline fluids, Fraser mine, Sudbury, Ontario; Exploration Mining Geology, v. 5, p. 17-31.

Farrow, C.E.G., and Watkinson, D.H., 1997, Diversity of precious metal mineralization in footwall Cu-Ni-PGE deposits, Sudbury, Ontario: Implications for hydrothermal models of formation; The Canadian mineralogist, v. 35, p. 817-839.

Farrow, C.E.G., and Lightfoot, P.C., 2002; Sudbury PGE revisited: Toward an integrated model: Canadian Institute of Mining, Metallurgy and Petroleum Special Volume 54, p. 579-617.

Farrow, C.E.G., Everest, J.O., King, D.M., and Jolette, C., 2005, Sudbury Cu(-Ni)-PGE systems: refining the classification using McCreedy West Miner and Podolsky project case studies *in* Mungall, J.E., ed., Mineralogical association of Canada, short course, 35.

Fahrig, W. F., 1987, The tectonic settings of continental mafic dyke swarms: Failed arm and early passive margin: Geological Association of Canada Special Paper 34, p. 331–348

Fleet, M.E., Chryssoulis, S.L., Stone, W.E., and Weisener, C.G., 1993, Partitioning of platinum-group elements and Au in the Fe-Ni-Cu-S system: Experiments on the fractional crystallization of sulphide melt; Contributions to Mineralogy and Petrology, v. 115, p. 36−44

Fleet, M.E., Crocket, J.H., and Stone, W.E., 1996, Partitioning of platinum-group elements (Os, Ir, Ru, Pt, Pd) and gold between sulfide liquid and basalt melt; Geochimica et Cosmochimica Acta v. 60, p. 2397-2412

Fonseca R. O. C., Campbell I. H., O'Neill H. S. C. and Fitzgerald J. D. (2008) Oxygen solubility and speciation in sulphide-rich mattes. Geochimica et Cosmochimica Acta, v. 72, p. 2619–2635

French, B.M., 1972. Shock-metmorphic features in the Sudbury structure, Ontario: a review. In: Guy-Bray, J.V. (Ed.), New Developments in Sudbury Geology. Geological Association of Canada Special Paper 10, pp. 19– 28.

Gál, B., Molnár, F., and Peterson, D.M., 2011, Cu-Ni-PGE mineralization in the South Filson Creek area, South Kawishiwi Intrusion, Duluth Complex: Mineralization styles and magmatic and hdrothermal processes; Economic Geology, v. 106, p. 481-509.

Grant, R.W., and Bite, A., 1984; Sudbury Quartz Diroite Offset Dikes, *in*: Pye, E.G., Naldrett, A.J., Giblin, P.E. (Eds.), The Geology and Ore Deposits of the Sudbury Structure, Special vol. 1. Ontario Geological Survey, pp 276-289.

Greenman, L., 1970. The petrology of the footwall breccias in the vicinity of the Strathcona mine, Levack, Ontario; Unpublished PhD dissertation, Toronto, University of Toronto, 153 p

Grieve, R.A.F., Stöffler, D., and Deutsch, A., 1991, The Sudbury Structure: Controversial or Misunderstood? : Journal of Geophysical research, v. 96, pp. 22753 – 22754.

Grieve, R.A.F., 1994, An impact model of the Sudbury structure. In: Lightfoot, P.C., Naldrett, A.J. (eds.), Proceedings of the Sudbury-Noril'sk symposium: Ontario Geol. Surv. Spec. Pap., v.5, p.119-132.

Guy-Bray, J.G., 1966. Shatter cones at Sudbury. Journal of Geology 74, 243–245

Hawley, J.E., and Stanton, R.L., 1962; The Facts, The Ores, Their Minerals, Metals and Distribution; p.30-145 In; The Sudbury Ores: Their Mineralogy and Their Origin, Canadian Mineralogist, v.7.

Hanley, J.J., and Mungall, J.E., 2003, Chlorine enrichment and hydrous alteration of the Sudbury Breccia hosting footwall Cu-Ni-PGE mineralization at the Frasier Mine, Sudbury, Ontario, Canada; The Canadian Mineralogist, v. 41, p. 857-881.

Hanley, J.J., Mungall, J.E., Bray, C.J., and Gorton, M.P., 2004, The origin of bulk and water soluble Cl and Br enrichments in ore-hosting Sudbury breccias in the Fraser copper zone, Strathcona embayment, Sudbury, Ontario, Canada; The Canadian Mineralogist, v. 42, p. 1777-1798.

Hanley, J.J., Mungall, J.E., Pettke, T., Spooner, E.T.C., and Bray, C.J., 2005, Ore metal redistribution by hydrocarbon-brine and hydrocarbon-halide melt phases, North Range footwall of the Sudbury Igneous Complex, Ontario, Canada; Mineralium Deposita, v. 40, p. 237-256.

Hanley, J.J., and Bray, C.J., 2009, The trace metal content of amphibole as a proximity indicator for Cu-Ni-PGE mineralization in the footwall of the Sudbury Igneous Complex, Canada; Economic Geology, v. 104, p. 113-125.

Hanley, J.J., and Gladney, E.R., 2011, The presence of carbonic-dominant volatiles during the crystallization of sulfide-bearing mafic pegmatites in the North Roby Zone, Lac des Iiles Complex, Ontario; Economic Geology, v. 106 (1), p. 33-54.

Hanley, J.J., Ames, D., Barnes, J., Sharp, Z., and Guillong, M., 2011, Interaction of magmatic fluids and silicate melt residues with saline groundwater in the footwall of the Sudbury Igneous Complex, Ontario, Canada: New evidence from bulk rock geochemistry, fluid inclusions and stable isotopes; Chemical Geology, v. 281, p.1-25.

Harris, A.C., Kamenetsky, V.S., White, N.C., van Achterbergh, E., and Ryan., C.G., 2003, Melt inclusions in veins: Linking magmas and porphyry Cu deposits; Science, v., 302 (5653), p. 2109-2111.

Hattori, K.H., and Cameron, E.M., 2004, Using the high mobility of palladium in surface media in exploration for platinum group element deposits: Evidence from the Lac ds Iles region, Northwestern Ontario; Economic Geology, v. 99, p. 157-171.

Heaman, L.M., 1997, Global magmatism at 2.45 Ga: Remnants of an ancient large igneous province?: Geology, v. 25, p. 299–302.

Hedenquist, J.W., and Lowenstern, J.B., 1994, The role of magmas in the formation of hydrothermal ore deposits.; Nature v. 370, p. 519-527

Helmy, H.M., Ballhaus, C., Wohlgenmuth-Ueberwasser, C., Fonseca, R.O.C., and Laurenz, V., 2010, Partitioning of Se, As, Sb, Te and Bi between monosulfide solide solution and sulfide melt – Application to magmatic sulfide deposits; Geochimica et Cosmochimica Acta, v. 74, p. 6174-6179

Hem, S.R., Makovicky, E., and Gervilla, F., 2001; Compositional Trends in Fe, Co, and Ni Sulfarsenides and their Crystal-Chemical Implications: Results From the Arroyo De La Cueva Deposits, Ronda Peridotite, Southern Spain : The Canadian Mineralogist, v. 39, p. 831 – 853

Hem, S., 2006, Solid solutions in the Fe-Co-Ni-As-S system; Chemical Geology, v. 225, p. 291-303

Hem, S.R., Makovicky, E., 2004, The system Fe–Co–Ni–As–S: I. Phase relations in the (Fe, Co, Ni)$As_{0.5}S_{1.5}$ section at 650 °C and 500 °C; Canadian Mineralogist, v. 42, p. 43–62

Hoffman, P.F., 1989, Precambrian geology and tectonic history of North America: Geological Society of America, Decade of North American Geology, Volume A, p. 447–512.

Holm, D.K., Schneider, D.A., O'Boyle, C., Hamilton, M.A., Jercinovic, M.J., and Williams, M.L., 2001, Direct timing constraints on Paleoproterozoic metamorphism, southern Lake Superior region: results from SHRIMP and EMO U-Pb dating of metamorphic monazites; Geological Society of America, Abstracts with Program, v. 33 (6), p. A-401.

Holzheid, A., 2010, Separation of sulfide melt droplets in sulfur saturated silicate liquids; Chemical Geology, v. 274, p. 127-135

Howard -White, F .B. (1963): Nickel, an historical review. Longmans Canada, Toronto, Ontario

Huminicki, M.A.E., 2003, Geology, mineralogy, and geochemistry of the Kelly Lake Ni-Cu-PGE deposit, Sudbury, Ontario; Unpublished M.Sc. thesis, Sudbury, Ontario, Laurentian University

Huminicki., M.A.E., Sylvester, P.J., Cabri, L.J., Lesher, C.M., and Tubrett, M., 2005, Quantitative mass balance of platinum-group elements in the Kelly Lake Ni-Cu-PGE deposit, Copper Cliff offset, Sudbury: Economic Geology, v. 100, p. 1631-1646

Huminicki, M.A.E., Shaffer, M., Wilton, D.H.C., Evans-Lamswood, D., and Wheeler, R.I., 2012, Systematic and integrative ore characterization of massive sulfide deposits: An example from Voisey's Bay Ni-Cu-Co ovoid orebody, Labrador, Canada; Exploration and Mining Geology, v. 20, p. 53-86

Ivanov, B.A., and Deutsch, A., 1999, Sudbury impact event: Cratering mechanics and thermal history: Geological Society of America Special Paper 339, pp. 389-397.

Jago, B.C., Morrison, G.G., and Little, T.L., 1994, Metal zonation patterns and microtextural and micromineralogical evidence of alkali- and halogen-rich fluids in the genesis of the Victor Deep and McCreedy East footwall copper orebodies, Sudbury

Igneous Complex, *in* Proceedings of the Sudbury-Noril'sk Symposium, Lightfoot, P.C., and Naldrett, A.J., eds., O.G.S. Special Volume 5, p. 65-75.

James, R.S., Easton R.M., Peck D.C., and Hrominchuk J.L., 2002, The East Bull Lake intrusive suite: Remnants of a ~2.48 Ga large igneous and metallogenic province in the Sudbury area of the Canadian Shield; Economic Geology, v. 97, p. 1577−1606.

Jana, D., and Walker, D., 1997, The influence of sulfur on partitioning of siderophile elements; Geochimica et Cosmochimia Acta, v. 61, p. 5255-5277

Kamenetsky, M.B., Sobolev, A.V., Kamenetsky, V.S., Maas, R., Danyushevsky, L.V., Thomas, R., Sobolev, N.V., and Pokhilenko, N.P., 2004, Kimberlite melts rich in alkali chlorides and carbonates: a potent metasomatic agent in the mantle; Geology, v. 32, p. 845-848.

Keays, R., and Lightfoot, P.C., 2004, Formation of Ni-Cu-Platinum group element sulfide mineralization in the Sudbury Impact melt sheet; Contributions to Mineralogy and Petrology, v.82, p. 217-258

Krogh, T., Davis, D., and Corfu, F., 1984, Precise U-Pb zircon and baddeleyite ages for the Sudbury area, *in* The geology and ore deposits of the Sudbury structure special volume 1; Ontario geological survery, p. 431-446

Langford, F.E., 1960, Geology of Levack township and the northern part of Dowling township, district of Sudbury; Ontario Department of Mines, Preliminary Report

Lakomy, R., 1990, Implications for cratering mechanics from a study of the footwall breccia of the Sudbury impact structure, Canada; Meteorics, v. 25, p. 195-207

Lesher, C.M., and Keays, R.R., 1984, Metamorphically and hydrothermally mobilized Fe-Ni-Cu sulphides at Kamblada, Western Australia; Sulphide deposits in mafic and ultramafic rocks, Institute of Mining and Metallurgy, London, p. 62-69.

Li, C., Naldrett, A.J., Coats, C.J.A., and Johannessen, P., 1992, Platinum, palladium, gold and copper-rich stringers at the Strathcona mine, Sudbury: their enrichment by fractionation of a sulfide liquid; Economic Geology, v. 87, p. 1584-1598.

Li, C., and Naldrett, A.J., 1992, PGE studies in the footwall at Sudbury, Ontario; Ontario Geological Survey, Open file report 5830.

Li, C., and Naldrett, A.J., 1993, Platinum-group minerals from the Deep Copper zone of the Strathcona deposit, Sudbury, Ontario: Canadian Mineralogist, v. 31, p.31-44

Li, C., and Naldrett, A.J., 1994, A numerical model for the compositional variations of Sudbury sulfide ores and its application to exploration. Economic Geology, v. 89, p. 1599–1607

Li, C., Naldrett, A.J., Rucklidge, J.C., and Kilius, L.R., 1993, Concentrations of platinum-group elements and gold in sulfides from the Strathcona deposit, Sudbury, Ontario: Canadian Mineralogist, v. 30, p.523-531

Lightfoot, P.C., Keays, R., Morrison, G., Bite, A., and Farrell, K., 1997a, Geochemical relationships in the Sudbury Igneous Complex: origin of the Main Mass and Offset Dikes; Economic Geology and the Bulletin of the Society of Economic Geologists, v. 92, p. 289-307

Lightfoot, P.C., Doherty, W., Farrell, K., Keays, R., Moore, M., and Pekeski, D., 1997b, Geochemistry of the Main Mass, Sublayer, Offsets and inclusions from the Sudbury Igneous Complex, Ontario; Open file report 5959, Ontario Geological Survey

Lightfoot, P.C., Naldrett, A.J., and Morrison, G., 1997c; Sublayer and Offsets Dikes of the Sudbury Igneous Complex—an Introduction and Field Guide, Ontario Geological Survey, Open File Report 5956, 37p.

Lightfoot, P.C., and Farrow, E.G., 2002, Geology, Geochemistry, and Mineralogy of the Worthing Offset Dike: A Genetic Model for Offset Dike Mineralization in the Sudbury Igneous Complex; Economic Geology v. 97, p. 1419-1446.

Lightfoot, P.C., 2007, Advances in Ni-Cu-PGE sulphide deposit models and imlications for exploration technologies, *in* Proceedings of Exploration 07: Fifth Decennial International Conference on Mineral Exploration (ed. Milkereit, B.) p. 629-646.

Lowenstern, J.B., Mahood, G.A., Rivers, M.L., and Sutton, S.R., 1991, Evidence for extreme partitioning of copper into a magmatic vapor phase; Science, v. 252, p. 1405-1409.

Lowenstern, J.B., 1995, Applications of silicate melt inclusions to the study of magmatic volatiles, *in* Thompson, J.F.H., ed., Magmas, Fluids and Ore Deposits; Mineralogical Association of Canada Short Course, v. 23, p. 71-99.

Maclean, W.H., and Shimazaki, H., 1976, The partition of Co, Ni, Cu and Zn between sulfide and silicate liquids; Economic Geology and the Bulletin of the Society of Economic Geologists, v. 71, p. 1049-1057.

Magyarosi, Z.,Watkinson, D.H. and Jones, P.C., 1999, Mineralogy and chemistry of silicates and sulphides in different types of ore in the Copper Cliff South Mine; Geological Association of Canada-Mineralogical Association of Canada Joint Annual Meeting. Program with Abstracts, 24, p. 78.

Magyarosi, Z., Watkinson, D.H., and Jones, P.C., 2002, Mineralogy of Ni-Cu-platinum group element sulfide ore in the 800 and 810 orebodies, Copper Cliff South mine, and P-

T-X conditions during the formation of platinum group minerals: Economic Geology, v. 97, p. 1471−1486

Marshall, D., Watkinson, D., Farrow, C.E.G., Molnar, F., Fouillac, A.M., 1999, Multiple fluid generations in the Sudbury Igneous Complex: fluid inclusions, Ar, O, H, Rb and Sr evidence; Chemical Geology, v. 154, p. 1-19

Mathez, E.A., 1999, Factors controlling the concentrations of platinum-group elements in layered instrusions and chromitites, *in* Dynamic Processes in Magmatic Ore Deposits and their Application to Mineral Exploration; GAC Short Course Notes, v. 13, p. 251-286.

McCallum, M.E., Loucks, R.R., Carlson, R.R., Cooley, E.F., and Doerge, T.A., 1976, Platinum metals associated with hydrothermal copper ores of the New Rambler Mine, Medicine Bow Mountains, Wyoming; Economic Geology, v. 71, p. 1429-1450.

Melosh, H., 1989, Impact cratering: a geological process; Oxford University Press, New York

Mogessie, A., Stumpfl, E.F., and Weiblen, P.W., 1991, The role of fluids in the formation of platinum-group-minerals, Duluth Complex, Minnesota: Mineralogic, textural and chemical evidence; Economic Geology, v. 86, p. 1506-1518.

Molnar, F., and Watkinson, D.H., 2001, Fluid-inclusion data for vein-type Cu-Ni-PGE footwall ores, Sudbury Igneous Complex and their use in establishing an exploration model for hydrothermal PGE-enrichment around mafic-ultramafic intrusions; Exploration and Mining Geology, v. 10, p. 125-141

Molnar, F., Watkinson, D.H., and Jones, P.C., 2001, Multiple hydrothermal processes in the footwall units of the North Range, Sudbury Igneous Complex, Canada, and implications for the genesis of vein-type Cu-Ni-PGE deposits; Economic Geology, v. 96, 1645-1670

Morris, W.A., 1982, A paleomagnetic investigation of the Sudbury basin offsets, Ontario, Canada; Tectonophysics, v. 85, p. 291-312.

Morrison, G.G., 1984. Morphological features of the Sudbury Structure in relation to an impact origin. In: Pye, E.G., Naldrett, A.J., Giblin, P.E. (Eds.), The Geology and Ore Deposits of the Sudbury Structure. Ontario Geological Survey Special Volume 1, pp. 513– 520.

Morrison, G.G., Jago, B.C., and White, T.L., 1994, Footwall mineralization of the Sudbury Igneous Complex *in* Proceedings of the Sudbury-Noril'sk Symposium, Lightfoot, P.C., and Naldrett, A.J., eds., O.G.S. Special Volume 5, p. 57-64.

Mountain, B.W., and Wood, S.A., 1988, Chemical controls on the solubility, transport, and deposition of platinum and palladium in hydrothermal solution: a thermodynamic approach; Economic Geology v. 83, p. 492-510.

Mungall, J.E., 2001; Kinetic Controls on the Partitioning of Trace Elements Between Silicate and Sulfide Liquids, Journal of Petrology, v.45, p.749-768.

Mungall, J.E., 2002, Late-stage sulfide liquid mobility in the main mass of the Sudbury Igneous Complex: examples from the Victor Depp, McCreedy East, and Trillabelle deposits; Economic Geology, v. 97, p. 1563-1576

Mungall, J.E., Ames, D.E. and Hanley, J.J., 2004, Geochemical evidence from the Sudbury structure for crustal redistribution by large bolide impacts: Nature, v. 429, p. 546-548.

Mungall, J.E., 2005, Magmatic Ores, in Mining Geology, p. 637-645

Mungall, J.E., Andrews, D.R.A., Cabri, L.J., Sylvester, P.J., and Tubrett, M., 2005, Partitioning of Cu, Ni, Au, and platinum group elements between monosulfide solid solution and sulfide melt under controlled oxygen and sulfur fugacities; Geochimica et Cosmochimica Acta, v. 69, p. 4349–4360

Mungall, J.E., 2007, Crystallization of magmatic sulfides: An empirical model and application to Sudbury ores: Geochimica et Cosmochimica Acta, v. 71, p. 2809–2819

Murphy, A.J., and Spray, J.G., 2002, Geology, Mineralization, and Emplacement of the Whistle-Parkin Offset Dike, Sudbury; Economic Geology v. 97, p. 1399-1418

Murowchick, J.B., and Barnes, H.L., 1986, Formation of cubic FeS; American Mineralogist, v. 71, p. 1243-1246

Murowchick, J.B., and Barnes, H.L., 1986, Marcasite precipitation from hydrothermal solutions; Geochimica et Cosmochimica Acta, v. 50, p. 2615-2629.

Naldrett A. J. (1969) A portion of the system Fe–S–O between 900 and 1080 °C and its application to sulfide ore magmas; Journal of Petrology, v. 10, v. 171–201

Naldrett, A.J., 1979, Partitioning of Fe, Co, Ni and Cu between sulfide liquid and basaltic melts and the composition of Ni-Cu sulfide deposits - a reply and further discussion; Economic Geology, v. 74, p. 1520-1528.

Naldrett, A.J., 1984; Mineralogy and Composition of the Sudbury Ores, In : Pye, E.G., Naldrett, A.J., Giblin, P.E. (Eds.), The Geology and Ore Deposits of the Sudbury Structure, Special vol. 1. Ontario Geological Survey, pp 310-314.

Naldrett, A.J., Hewins, R.H., Dressler, B.O., and Rao, B.V., 1984, The contact sublayer of the Sudbury Igneous Complex, *in* The geology and ore deposits of the Sudbury structure, Pye, E., Naldrett, A., Giblin, P., eds.; Special volume 1, Ontario Geological Survery, Ch. 11, p. 253-274

Naldrett, A.J., Rao, B.V., and Evenson, N.M., 1986, Contamination at Sudbury and its role in ore formation, *in* Metallogeny of Basic and Ultrabasic rocks, Gallagher, M.J., Ixer, R.A., Neary, C.R., and Pritchard, H.M., eds., Institution of Mining and Metallurgy, London, U.K., p. 75-91.

Naldrett, A.J., Pessaran, R., Asif, M., and Li, C., 1994, Compositional varation in the Sudbury ores and prediction of the proximity of footwall copper-PGE orebodies, *in* Proceedings of the Sudbury-Noril'sk Symposium, Lightfoot, P.C., and Naldrett, A.J., eds., O.G.S. Special Volume 5, p. 133-146.

Naldrett, A.J., 2004; Magmatic sulfide deposits; Geology, geochemistry and exploration, Heidelberg, Springer Verlag, 728 p.

Naldrett, A.J., Bray, J.G., Gasparrini, E.L., Podolsky, T., and Rucklidge, J.C., 1970; Cryptic Variation and the Petrology of the Sudbury Nickel Irruptive; Economic Geology, v. 65, p. 122-155.

Naldrett, A.J. and Hewins, R.H., 1984; Chapter 10, The main mass of the Sudbury Igneous Complex, In: Pye, E.G., Naldrett, A.J., Giblin, P.E. (Eds.), The Geology and Ore Deposits of the Sudbury Structure, Special vol. 1. Ontario Geological Survey, pp 235-251.

Naldrett, A.J., Hewins, R.H., Dressler, B.O., Rao, B.V., 1984; Chapter 11, The Contact Sublayer of the Sudbury Igneous Complex, In: Pye, E.G., Naldrett, A.J., Giblin, P.E. (Eds.), The Geology and Ore Deposits of the Sudbury Structure, Special vol. 1. Ontario Geological Survey, pp 253-274.

Naldrett, A.J., and Kullerud, G., 1967; A study of the Strathcona Mine and Its Bearing on the Origin of the Nickel-Copper Ores of the Sudbury District; Journal of Petrology, V.8, p.453-531.

Naldrett, A.J., Asif, M., Schandl, E., Searcy, T., Morrison, G.G., Binney, W.P., and Moore, C., 1999, Platinum group elements in the Sudbury ores: Significance with respect to the origin of different ore zones and to the exploration for footwall ores: Economic Geology, v. 94, p. 185− 210.

Noble, S.R., and Lightfoot, P.C., 1992, U-Pb baddeleyite ages for the Kerns and Triangle Mountain intrusions, Nipissing Diabase, Ontario: Canadian Journal of Earth Sciences, v. 29, p. 1424–1429.

Nyman, M.W., Sheets, R.W., and Bodnar, R.J., 1990, Fluid-inclusion evidence for the physical and chemical conditions associated with intermediate-temperature PGE mineralization at the New Rambler deposit, southeastern Wyoming; Canadian Mineralogist, v. 28, p. 629-638.

Pan, P., and Wood, S.A., 1994, Solubility of Pt and Pd sulfides and Au metal in aqueous bisulfide solutions: II Results at 200° to 350° C and saturated vapor pressure; Mineralium Deposita, v. 29, p. 373-390.

Peach, C.L., and Mathez, E.A., 1993, Sulfide melt-silicate melt distribution coefficients for nickel and iron and implications for the distribution of other chalcophile elements; Geochimica et Cosmochimica Acta, v. 57, p. 3013–3021

Peach, C.L., Mathez, E.A., Keays, R.R., and Reeves, S.J., 1994, Experimentally determined sulfide melt-silicate melt partition coefficients for iridium and palladium; Chemical Geology, v. 117, p. 361-377

Peck, D.C., Keays, R.R., James, R.S., Chubb, P.T., and Reeves, S. J., 2001, Controls on the formation of contact-type platinum-group element mineralization in the East Bull Lake intrusion; Economic Geology, v. 96 , p. 559-581

Péntek, A., Molnar, F., Watkinson, D.H., and Jones, P.C., 2008, Footwall-type Cu-Ni-PGE mineralization in the Broken Hammer area, Winser Township, North Range, Sudbury structure; Economic Geology, v. 103, p. 1005-1028

Peredery, W.V., 1972. Chemistry of fluidal glasses and melt bodies in the Onaping Formation. In: Guy-Bray, J.V. (Ed.), New Developments in Sudbury Geology. Geological Association of Canada Special Paper 10, pp. 49–59.

Peredery, W.V., Morrison, G.G., 1984. Discussion of the origin of the Sudbury Structure. In: Pye, E.G., Naldrett, A.J., Giblin, P.E. (Eds.), The Geology and Ore Deposits of the Sudbury Structure, Special vol. 1. Ontario Geological Survey, pp. 491–512.

Putnis, A., 2002, Mineral replacement reactions: from macroscopic observations to microscopic mechanisms; Mineralogical Magazine, v. 66, p. 689–708.

Putnis, A., 2009, Mineral replacement reactions, *in* Oelkers, E.H., and Schott, J., eds., Thermodynamics and Kinetics of Water-Rock Interaction, Reviews in Mineralogy and Geochemistry; Mineralogical Society of America, v. 70, p. 87–124

Pye, E.G., Naldrett, A.J., and Giblin, P.E., eds., 1984, The geology and ore deposits of the Sudbury structure; Ontario Geological Survey, special publication 1

Qian, G., Xia, F., Brugger, J., Skinner, W.M., Bei, J., Chen, G., and Pring, A., 2011, Replacement of pyrrhotite by pyrite and marcasite under hydrothermal conditions up to

220 °C: An experimental study of reaction textures and mechanisms; American Mineralogist, v. 96, p. 1878-1893

Qian, G., Brugger, J., Skinner, W.M., Chen, G.R., and Pring, A., 2010, An experimental study of the mechanism of the replacement of magnetite by pyrite up to 300 °C; Geochimica et Cosmochimica Acta, v.74, p. 5610–5630

Rajamani, V., and Naldrett, A.J., 1978, Partitioning of Fe, Co, Ni and Cu between sulfide liquids and basaltic melts and the composition of Ni-Cu sulfide deposits; Economic Geology, v. 73, p. 82-93

Reed, M.H., 1998, Hydrothermal alteration and its relationship to ore fluid composition, *in* Barnes, H.L., ed., Geochemistry of Hydrothermal Ore Deposits, 3rd edition; John Wiley and Sons, New York, p. 303-365.

Rickard, J.H., 2000, Petrological and mineralogical study of Cu-Ni-PGEbearing ores within the 100 orebody, Copper Cliff North mine, Sudbury, Ontario; Unpublished M.Sc. thesis, Carleton University, 113 p

Rickard, J.H., and Watkinson, D.H., 2001, Cu-Ni-PGE Mineralization within the Copper Cliff Offset Dike, Copper Cliff North Mine, Sudbury, Ontario: Evidence for Multiple Stages of Emplacement; Exploration and Mining Geology, V.10, p. 111-124.

Riller, U., 2005, Structural characteristics of the Sudbury impact structure, Canada: Impact-induced versus orogenic deformation—a review; Meteoritics and Planetary Science, v. 40, p. 1723−1740

Rousell, D.H., 1981. Sudbury and the meteorite theory. Geoscience Canada 8, 167– 169.

Rousell, D.H., 1984. Structural geology of the Sudbury basin. In: Pye, E.G., Naldtrett, A.J., Giblin, P.E. (Eds.), The Geology and ore deposits of the Sudbury structure. Ontario Geological Survey, Special Volume 1, pp. 83 – 95.

Rousell, D.H., Fedorowich, J.S., and Dressler, B.O., 2003, Sudbury Breccia (Canada): a product of the 1850 Ma Sudbury Event and host to footwall Cu-Ni-PGE deposits; Earth-Science Reviews, v. 60, p. 147-174.

Rowell, W.F., and Edgar, A.D., 1986, Platinum-group element mineralization in a hydrothermal Cu-Ni sulfide occurrence, Rathbun Lake, northeastern Ontario; Economic Geology, v. 81, p. 1272-1277.

Rusk, B.G., Lowers, H.A., and Reed, M.H., 2008, Trace elements in hydrothermal quartz: Relationships to cathodoluminescent textures and insights into vein formation; Geology, v. 36, p. 547-550.

Scribbins , B., Rae, D.R., and Naldrett, A.J., 1984, Mafic and ultramafic inclusions in the sublayer of the Sudbury Igneous Complex; Canadian Mineralogist, v.22, p. 67-75

Senior, G.D., Smith, L.K., Silvester, E., and Bruckard, W.J., 2009, The flotation of gersdorffite in sulphide nickel systems - A single mineral study; International Journal of Mineral Processing, v. 93, p. 165-171/

Shinohara, H., 1994, Exsolution of immiscible vapor and liquid phases from a crystallizing silicate melt: Implications for chlorine and metal transport; Geochimica et Cosmochimica Acta, v. 58 (23), p. 5215-5221.

Sinyakova, E.F., and Kosyakov, V.I., 2012, The bahavior of nobel-metal admixtures during fractional crystallization of As- and Co-containing Cu-Fe-Ni sulfide melts; Russian Geology and Geophysics, v. 53, p. 1055-1076.

Simonds C. and Kieffer S. (1993) Impact and volcanism – a momentum scaling law for erosion; J. Geophys Res. Solid Earth, v. 98, p. 14321–14337.

Spray, J.G., 1998. Localized shock- and friction-induced melting in response to hypervelocity impact. In: Grady, M.M., Hutchinson, R., McCall, G.J.H., Rothery, D.A. (Eds.), Meteorites: Flux with Time and Impact Effects. Geological Society, London, Special Publications 140, pp. 195– 204.

Stevenson, J.S., 1972. The Onaping ash-flow sheet, Sudbury, Ontario. In: Guy-Bray, J.V. (Ed.), New Developments in Sudbury Geology. Geological Association of Canada Special Paper 10, pp. 41– 48.

Stewart, M., 2002, Petrology and mineralogy of Cu-Ni-PGE ore, Totten area, Worthington Offset, Sudbury Igneous Complex; M.Sc. thesis, Carleton University, Ottawa, Ontario, p. 164.

Stewart, M.C., Watkinson, D.H., and Jones, P.C., 1999, Petrology of the sulphides within the Copper Cliff offset, south of Kelly Lake, Sudbury [abs.]: Geological Association Canada-Mineralogical Association Canada Joint Annual Meeting, Sudbury, Program with Abstracts, p. 78

Stöffler, D., Deutsch, A., Avermann, M., Bischoff, L., Brockmeyer, P., Buhl, D., Lakomy, R., Müller-Mohr, V., 1994, The formation of the Sudbury structure, Canada: Toward a unified impact model; Geological Society of America Special Paper 293, pp. 303-318.

Su, S., and Lesher, C.M., 2012, Genesis of PGE mineralization in the Wengeqi mafic-ultramafic complex, Guyang County, Inner Mongolia, China; Mineralium Deposita, v. 47, p. 197-207.

Szabó, E., Halls, H.C., 2006, Deformation of the Sudbury structure: Paleomagnetic evidence from the Sudbury breccia. Precambrian Research, 150, 27-48.

Szentpéteri, K., 1999, Mineralogical-petrological study of the Copper Cliff North mining area, Sudbury, Canada; Unpublished M.Sc. thesis, Eotvos L. University, Budapest, Hungary, 117 p

Szentpéteri, K., Watkinson, D.H., Molnar, F., and Jones, P.C., 2002, Platinum-group elements-Co-Ni-Fe sulfarsenides and mineral paragenesis in Cu-Ni-platinum-group element deposits, Copper Cliff north area, Sudbury, Canada: Economic Geology, v. 97, p. 1459−1470

Theriault, R.D., Barnes, S.-J., Severson, M.J., 1997, The influence of country rock assimilation and silicate to sulfide ratios (R factor) on the genesis of the Dunka Road Cu–Ni–platinum-group element deposit, Duluth Complex, Minnesota; Canadian Journal of Earth Sciences, v. 34, p, 375–389

Thompson, L.M., and Spray, J.G., 1996. Pseudotachylyte petrogenesis: constraints from the Sudbury impact structure. Contributions to Mineralology and Petrology 125, 359–374.

Tuba, G., Molnár, F., Watkinson, D.H., Jones, P.C., and Mogessie, A., 2010, Hydrothermal vein and alteration assemblages associated with low-sulfide footwall Cu-Ni-PGE mineralization and regional hydrothermal processes, North and East Ranges, Sudbury structure, Canada; Society of Economic Geologists Special Publication, v. 15, p. 573-598.

Tuba, G., Molnár, F., Ames, D.E., Péntek, A., Watkinson, D.H., and Jones, P., 2013, Multi-stage hydrothermal processes involved in “low-sulfide” Cu(-Ni)-PGE mineralization in the footwall of the Sudbury Igneous Complex, Canada: Amy Lake PGE zone, East Range: Mineralium Deposita, v. 49, p. 7-47

Tuchscherer, M., and Spray, J., 2002, Geology, mineralization, and emplacement of the Foy Offset dike, Sudbury impact structure; Economic Geology and the Bulletin of the Society of Economic Geologists, v. 97, p. 1377-1397

Watkinson, D.H., and Melling, D.R., 1992, Hydrothermal origin of platinum-group mineralization in low-temperature copper sulfide-rich assemblages, Salt Chuck intrusion, Alaska; Economic Geology, v. 87, p. 47-57.

Watkinson, D.H., and Ohnenstetter, D., 1992, Hydrothermal origin of platinum-group mineralization in the Two Duck Lake intrusion, Coldwell Complex, northwestern Ontario; Canadian Mineralogist, v., 30, p. 121-136.

Wood, S.A., 1987, Thermodynamic calculations of the volatility of the platinum-group elements (PGE): the PGE content of fluids at magmatic temperatures; Geochimica et Cosmochimica Acta, v. 51, p. 3041-3050.

Wood, S.A., Mountain, B.W., and Fenlon, B., 1989, Thermodynamic constraints on the solubility of platinum and palladium in hydrothermal solutions: reassessment of hydroxide, bisulfide and ammonia complexing; Economic Geology, v. 84, p. 2020-2028.

Wood, S.A., Mountain, B.W., and Pan, P., 1992, The aqueous geochemistry of platinum, palladium and gold: Recent experimental constraints and a re-evulation of theoretical predictions; Canadian Mineralogist, v. 30, p. 955-982.

Wood, C.R., and Spray, J.G., 1998; Origin and emplacement of Offset Dykes in the Sudbury impact structure: Constraints from Hess; Meteoritics and Planetary Science, v.33, p.337-347)

Wood, C.R., and Samson, I.M., 1998, Solubility of ore minerals and complexation of ore metals in hydrothermal solutions, *in* Richards, J.P., and Larson, P., eds., Techniques in Hydrothermal Ore Deposit Geology, Reviews in Economic Geology; Society of Economic Geologists, v. 10, p. 33-80.

Wood, S.A., 2002, The aqueous geochemistry of the platinum-group elements with applications to ore deposits, *in* Cabri, L.J., ed., The geology, geochemistry, mineralogy and mineral beneficiation of platinum-group elements: Montreal, Canadian Institute of Mining, Metallurgy and Petroleum, p. 211−249

Yates, A.B., 1948; Properties of International Nickel Company of Canada; p.596-617 in Structural Geology of Canadian Ore Deposits, Canadian Institute of Mining and Metallurgy, Montreal.

Young, G.M., 1983, Tectono-sedimentary history of Early Proterozoic rocks of the northern Great Lakes area: Geological Society of America Memoir 160, p. 15–32.

Young, G., Long, D., Fedo, C., and Nesbitt, H., 2001, Paleoproterozoic Huroian basin: product of a Wilson cycle punctuated by glaciations and a meteorite impact; Sedimentary Geology, v. 141, p. 233-254

Zieg, M., and Marsh, B., 2005, The Sudbury Igneous complex: viscous emulsion differentiation of a superheated impact melt sheet; Geological Society of America Bulletin, v. 117, p. 1427-1450

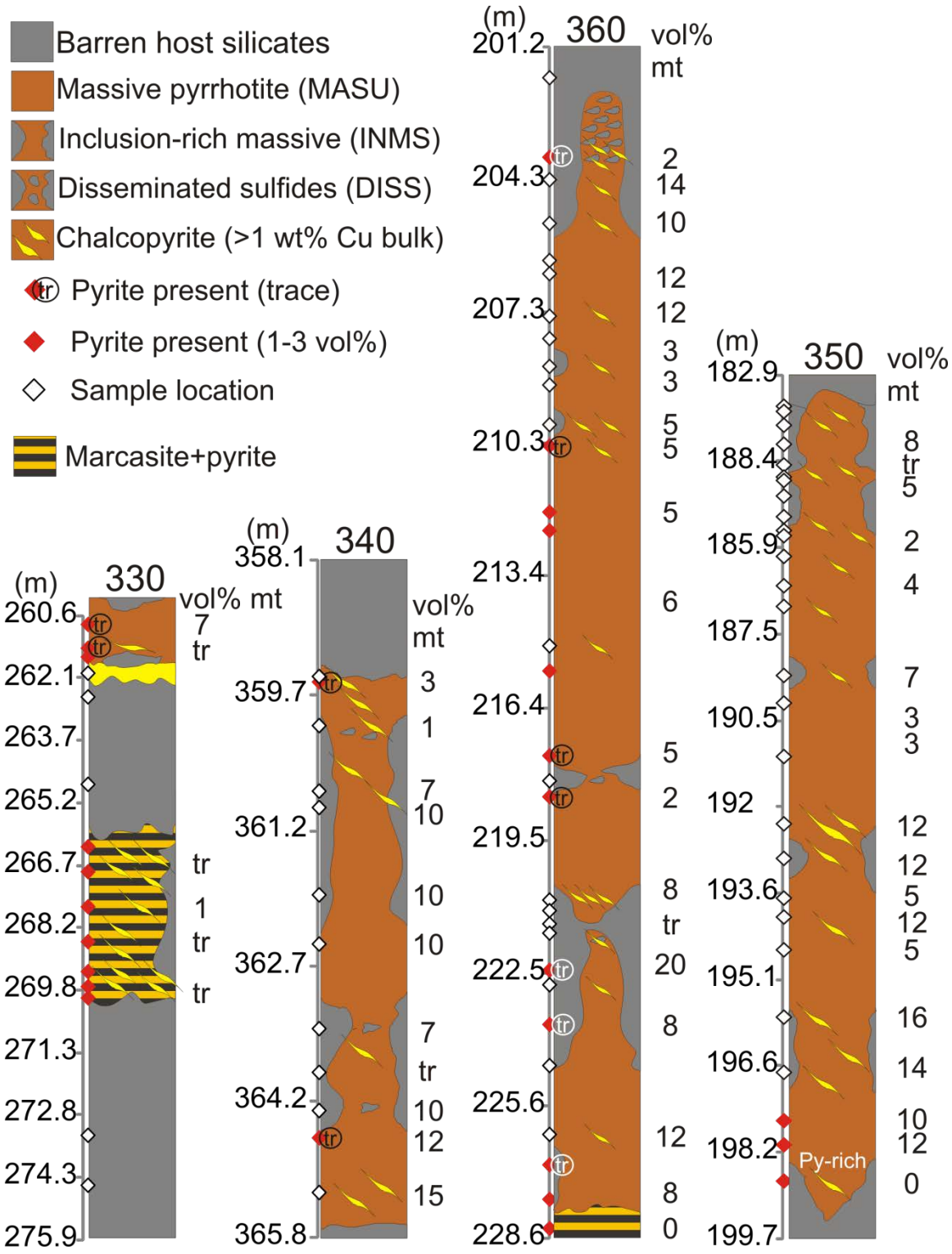

Figure A1) Magnetite abundance and pentlandite alteration in each sample. tr = trace amount (<1 vol%)

Table A1. Designation, depth down hole, and size of McConnell drill hole samples

Core ID	Depth (ft)	Size (in)	Core ID	Depth (ft)	Size (in)
1276360-BB22	662.4	4	1276350-1	577	4
1276360-BB23	668.4	3	1276350-2	582.1	5
1276360-BB24	670.1	3.2	1276350-3	586.4	5
1276360-BB25	673.4	5	1276350-4	593.1	4
1276360-BB26	676.2	4	1276350-5	595.7	4
1276360-BB27	677.2	5	1276350-6	597.6	5
1276360-BB28	680.4	6	1276350-7	600.4	5
1276360-BB29	682.1	3.5	1276350-8	600.8	6
1276360-BB30	684.2	3.5	1276350-9	601.8	5
1276360-BB31	685.6	4	1276350-10	602.1	6
1276360-BB32	688.6	4.5	1276350-11	602.9	3
1276360-BB1	690.2	5	1276350-12	604	5
1276360-BB2	695.2	5	1276350-13	605.2	4
1276360-BB3	696.6	4.5	1276350-14	605.9	3
1276360-BB4	705.3	5	1276350-15	606.1	5
1276360-BB5	707.2	5	1276350-16	607	5
1276360-BB6	713.6	3.5	1276350-17	608.2	4
1276360-BB7	715.5	6	1276350-18	609	5
1276360-BB8	716.7	3.5	1276350-19	609.3	5
1276360-BB9	724.5	4	1276350-20	610.5	5
1276360-BB10	725.3	5	1276350-21	612.2	4
1276360-BB11	726.3	3.5	1276350-22	613.4	5
1276360-BB12	727	4	1276350-23	617.4	5
1276360-BB13	729.8	4	1276350-24	619	4
1276360-BB14	730.9	3.5	1276350-25	622.1	5
1276360-BB15	733.9	6	1276350-26	626	5
1276360-BB16	737	2.5	1276350-27	628	4
1276360-BB17	742.2	3.5	1276350-28	630.3	5
1276360-BB18	744.5	4	1276350-29	631.4	5
1276360-BB19	747.1	3	1276350-30	633.3	4
1276360-BB20	749.3	5.5	1276350-31	637.2	4
1276360-BB21	759	5	1276350-32	640.4	4
			1276350-33	643.2	5
			1276350-34	644.6	4
1276360-BB33	523.2	3	1276350-35	646.7	3
1276360-BB34	530	5.5	1276350-36	647	5
1276360-BB35	403.5	5	1276350-37	650.2	4
1276360-BB36	397.8	7	1276350-38	660	3
1276360-BB37			1276350-39	668.6	5
1276360-BB38	382.5	4	1276350-40	671.7	4
1276360-BB39	196.2	4	1276350-41	679	4
1276360-BB40	~160	5			
1276360-BB41	112	6			

Table A1 Cont.

Core ID	Depth (ft)	Size (in)	Core ID	Depth (ft)	Size (in)
1276340-1	1145.7	5	1276330-1	837	4
1276340-2	1151.6	4	1276330-2	844	3
1276340-3	1158	4	1276330-3	854	3
1276340-4	1159.3	3	1276330-4	855.7	3
1276340-5	1163	4	1276330-5	857.6	2
1276340-6	1170.6	3	1276330-6	858.3	4
1276340-7	1171.6	3	1276330-7	859.6	4
1276340-8	1176.8	5	1276330-8	861.5	2
1276340-9	1178.6	5	1276330-9	868.5	3
1276340-10	1179.3	3	1276330-10	873.5	4
1276340-11	1179.5	3	1276330-11	875.5	4
1276340-12	1181.1	4	1276330-12	878.3	4
1276340-13	1183.5	4	1276330-13	881.1	4
1276340-14	1184.1	3	1276330-14	883.5	4
1276340-15	1187.3	4	1276330-15	884.7	3
1276340-16	1189.1	3	1276330-16	885.6	3
1276340-17	1192.2	3	1276330-17	896.6	3
1276340-18	1193.8	3	1276330-18	900.6	4
1276340-19	1195.2	3	1276330-19	912.6	4
1276340-20	1196.2	3			
1276340-21	1198.2	3			
1276340-22	1201.8	3			
1276340-23	1208.6	4			
1276340-24	1210.6	4			

Table A4. Reported SEM analyses (in wt%) of base metal sulfides

	S	Fe	Co	Ni
Pentlandite (unaltered-light alteration)				
Avg	38.0	27.0	1.4	33.5
Stdev	0.5	0.7	0.5	0.8
Max	39.1	29.9	2.6	34.6
Min	37.4	25.6	0.4	30.9
(Co unreported)				
Avg	38.6	27.3	-	34.0
Stdev	0.6	0.6	-	0.7
Max	40.6	30.1	-	35.1
Min	37.7	26.3	-	31.2
Pentlandite (moderate alteration)				
Avg	42.6	26.4	6.9	23.8
Stdev	3.3	5.2	3.1	2.4
Max	47.1	39.3	13.7	29.6
Min	33.6	16.5	0.9	20.0
(Co unreported)				
Avg	43.4	31.2	-	25.2
Stdev	3.2	4.0	-	2.8
Max	48.0	37.6	-	28.7
Min	38.8	24.6	-	19.9
Pentlandite (strong alteration)				
Avg	43.1	36.4	5.1	15.2
Stdev	2.9	5.3	2.0	2.7
Max	46.4	51.5	10.0	19.8
Min	30.1	24.7	0.7	10.4
(Co unreported)				
Avg	42.1	43.4	-	13.8
Stdev	3.7	2.5	-	2.5
Max	46.9	48.7	-	17.6
Min	36.4	40.6	-	10.7
Alteration products				
Avg	43.8	48.2	1.9	6.0
Stdev	2.5	4.3	1.2	2.4
Max	45.3	59.6	4.6	9.4
Min	32.6	40.9	0.3	1.0
(Co unreported)				
Avg	44.6	49.5	-	5.8
Stdev	1.8	2.6	-	2.1
Max	47.0	57.3	-	10.0
Min	34.6	44.6	-	1.9

Table A4. Cont

	S	Fe	Ni	Cu
Pyrrhotite (Ni reported)				
Avg	44.3	54.8	0.9	
Stdev	0.3	0.4	0.1	
Max	45.0	55.8	1.2	
Min	43.6	54.1	0.6	
Pyrrhotite (Ni unreported)				
Avg	44.5	55.5	-	
Stdev	0.4	0.4	-	
Max	45.4	55.9	-	
Min	44.1	54.6	-	
Pyrite (early and late)				
Avg	57.4	38.6	4.1	
Stdev	0.5	1.2	1.1	
Max	58.4	42.4	8.6	
Min	54.8	34.2	2.2	
Marcasite (Ni reported)				
Avg	57.5	41.2	1.3	
Stdev	0.5	0.5	0.3	
Max	58.3	42.3	2.0	
Min	56.4	40.3	0.8	
Marcasite (Ni unreported)				
Avg	57.8	42.2	-	
Stdev	0.6	0.6	-	
Max	60.0	44.7	-	
Min	55.4	40.0	-	
Chalcopyrite				
Avg	39.9	28.8		31.3
Stdev	0.5	0.6		0.6
Max	41.5	30.3		33.0
Min	38.5	26.2		29.1

Chapter 3: Geochemical investigation of magnetite from the McConnell offset Ni-Cu-PGE mineralization by LA-ICP-MS: implications for timing and provenance of magnetite grains in a cooling sulfide assemblage

Abstract

The composition, form, and volume of magnetite within sulfide ore deposits yields valuable information about the emplacement and evolution of sulfide liquids. The initial sulfide liquid composition is dictated by sulfur fugacity and silicate reservoir size and composition, affecting the oxygen content of the system, which can be approximated based on co-existing sulfide-oxide minerals in equilibrium. Factors such as metal solubility, element valence state, element partitioning, and timing of MSS crystallization are dependent on the oxygen content of the initial sulfide liquid. Magnetite within massive and inclusion-rich massive sulfide of the McConnell orebody occurs in locally moderate to high concentrations (10-20 vol%) and shows exsolution of Al-, Ti-, and Cr-spinel. Analyses show that magnetite within these ores was formed before or during the crystallization of MSS, indicating that the sulfide liquid which formed the McConnell contained high concentrations of oxygen. The oxygen content of a sulfide melt has an inverse correlation with Ni solubility in the melt, though the relationship between the two is not fully understood.

3.0 Introduction

The chemical composition of coexisting ilmenite-magnetite-spinel group minerals can be used to determine the oxygen fugacity of a system during crystallization, reflect the original composition of the host melt, and monitor changes in the evolution of both silicate and sulfide assemblages with which these minerals form (Buddington and Lindsley, 1964; Dasgupta, 1967; Naldrett, 1969; Gasparrini and Naldrett, 1972; Knecht et al., 1977; Powell and Powell, 1977; Sack, 1982; Klemm et al., 1985; Von Gruenewaldt et al., 1985; Hill and Sack, 1987; Ghiorso and Sack, 1991; Haggerty, 1991; Lattard, 1995; Krasnova and Krezer, 1995; Zhou et al., 1997; Barnes and Roeder, 2001; Mücke, 2003; Lattard et al., 2005; Sauerzapf et al., 2008; Dupuis and Beaudoin, 2011; Dare et al., 2012). Although several studies have been undertaken on the partitioning of major and trace elements between silicate liquid and oxide phases (Horn et al., 1994; Nielsen et al., 1994; Toplis and Carroll, 1995; Nielsen and Beard, 2000; Toplis and Corgne, 2002; Righter et al., 2006), very little is known about trace element partitioning between sulfide and oxide liquids and mineral solid solutions. This contrasts greatly to numerous studies focusing on trace element partitioning behaviour of elements between monosulfide solid solution (MSS) and residual Cu-rich sulfide liquid, or silicate and sulfide melts (e.g. Fleet et al., 1993; Fleet and Pan, 1994; Li et al., 1996; Barnes et al., 1997; Jana and Walker, 1997; Fleet et al., 1999; Barnes et al., 2001; Mungall et al., 2005). Generalizations concerning trace element partitioning behaviour between co-crystallizing oxide-sulfide solid solution (MSS or ISS) systems are made by measuring the concentrations of trace elements in texturally coeval magnetite and ilmenite and associated sulfide phases (e.g., Naldrett, 1969; Dare et al., 2012). Oxides hosted within such magmatic sulfides can

form: i) as titanomagnetite crystallized from silicate melt and settled into sulfide liquid accumulations, or were entrained into the sulfides during cosettling of the phases in an oxide and sulfide saturated silicate melt (the gravity settling process), or ii) oxides formed directly from the initial sulfide liquid or later-forming solid solutions (MSS and ISS) during cooling (the exsolution process) (Fonseca et al., 2008). The texture and chemical composition of the spinel may be indicative of the source melt (or solid solution) composition from which they formed (Dare et al., 2012).

Magnetite is common in magmatic sulfide deposits associated with mafic-ultramafic rocks (e.g., Sudbury Igneous Complex, Ontario; Gasparrini and Naldrett, 1972) or Voisey's Bay, Newfoundland and Labrador (Naldrett et al., 2000). The compositional and textural relationship (and timing) of magnetite and other oxide minerals is a complex function of oxygen content, fS_2, parental magma composition, and partitioning behaviour of major and trace elements between oxides and source liquid + co-existing phases. Structural controls on cation substitution in the magnetite-spinel structure and the valence state of particular elements of interest (i.e. V) also impact oxide chemistry (Toplis and Corgne, 2002; Dupuis and Beaudoin, 2011). In typical magmatic sulfide deposits, magnetite co-crystallizes with MSS from a sulfide liquid at temperatures between 1000–1100 °C depending on the composition of the melt and O_2 content of the system, in addition to other factors (Naldrett, 1969; Naldrett et al., 1972; Gruenewaldt et al., 1985; Fleet et al., 1993; Toplis and Carroll, 1995; Naldrett et al., 2000; Mungall et al., 2004). Since this is above the temperature at which ISS begins to crystallize (800-940 °C, Fleet and Pan, 1994; Fleet et al., 1993), the MSS and the magnetite which forms from it (or with it) is generally enriched in lithophile and some siderophile (V, Cr, Ti) trace elements

and relatively depleted in the chalcophile elements, as they would partition into the residual fractionated sulfide liquid (Dare et al., 2012). Magnetite that co-crystallized with MSS from a sulfide liquid, or exsolved from MSS, should show an enrichment of compatible lithophile elements (V, Cr, Ti) and a depletion of chalcophile elements (Ni, Sn) compared to magnetite grains that crystallized from a lower temperature Cu-rich fractioned liquid or ISS component (Dare et al., 2012). If the oxygen content within the initial sulfide liquid is very high, magnetite may begin to crystallize directly from the sulfide liquid before MSS (Fonseca 2008). If this were the case, magnetite should presumably show chemical compositions that overlap with grains that exsolved from an MSS and ISS source, as the initial sulfide liquid would be unfractionated and representative of both solid solution systems. Although very little is known about partition coefficients for elements between sulfide melt and oxides, it is reasonable to assume that elements will partition similarly between MSS-oxide and ISS-oxide if the oxygen content and sulfur fugacities of the system are not greatly perturbed. The O_2 and *f*S2 of most sulfide systems shouldn't change a large degree during MSS-magnetite crystallization (Mungall et al., 2005). Following this line of reasoning, the concentration of trace elements within magnetite are related to the composition of the crystallizing host phase (MSS or ISS), and therefore, can be used to determine relative timing and provenance of magnetite formation. It should be noted, however, that the experiments of Fonseca et al. (2008) concluded that most systems which crystallized massive sulfides represented open systems in respect to O_2 content. Major oxygen loss from sulfide melt to associated silicate phases may account for bands of chromite and very little magnetite within some massive ores (e.g., Heath et al., 2001; Fonseca et al., 2008).

The oxygen content and oxygen solubility of an Fe-rich sulfide liquid dictate whether or not magnetite forms before MSS begins crystallization, with higher Ni and Cu contents of the melt displaying a negative effect on oxygen solubility and causing crystallization of MSS before crystallization of magnetite in Ni- and Cu-rich sulfide liquids (Doyle and Naldrett, 1987; Mungall et al., 2005; Mungall, 2007; Fonseca et al., 2008). During cooling of the sulfide liquid, oxygen concentration increases as MSS crystallizes, and magnetite (often Ti-poor) forms within the massive ores (Fonseca et al., 2008). At oxygen fugacities typical of crustal environments (QFM), Fe-rich sulfide liquids often contain higher proportions of oxygen than sulfur, which alter its composition on the magnetite-MSS cotectic so that magnetite crystallizes first, though this is not usually the case in most natural Ni-bearing systems (Naldrett, 1969; Doyle and Naldrett, 1987; Fonseca et al., 2008; Dare et al., 2012). Fonseca et al. (2008) reported that the largest effect on the oxygen solubility of a sulfide liquid was its Ni/Fe ratio, lowering solubility by almost 50% in Ni-rich systems. The following study will attempt to characterize McConnell magnetite origins by their trace element compositions, thus contributing to the current dataset on Sudbury magnetite. As analyses through LA-ICP-MS are becoming increasingly common, it is possible to be very selective and precise with trace element compositions of mineral grains. By comparing the compositions of magnetite and its host sulfide phase, generalizations can be made about the partitioning behaviour of trace elements between co-existing sulfide-oxide solid solutions. Using similar techniques as previous studies (e.g. Dare et al., 2012), it is possible that the composition of magnetite grains within the McConnell deposit can help determine properties of the original sulfide melt that formed the ore body. The goals of this study are to; i) investigate the

relationship between magnetite and sulfide hosts; ii) determine timing of McConnell magnetite crystallization using trace elements and textures; and iii) use trace element concentrations to help determine partitioning behaviour and original melt properties.

3.1 Local Geology

The McConnell sulfide occurrence is hosted within a concentric offset dike on the South Range of the Sudbury Igneous Complex, located near the township of Garson (Figure 3.1). Meta-basalt and meta-sediment rocks of the Huronian supergroup host a quartz-diorite dike that encapsulates most of the known sulfide mineralization. The McConnell offset hosts Ni-Cu-PGE mineralization that contains Ni-poor Fe-sulfides with unusually elevated Pd (avg 3-5 ppm in 100% sulfide). Its ores consist primarily of MSS cumulates, with massive pyrrhotite hosting small amounts of pentlandite and variable chalcopyrite (Figures 3.2, 3.3). Hydrothermal alteration (chloritization) has been recorded in some intervals, though this feature appears to be confined to the base of the mineralization. Nickel grades in the McConnell sulfides are low, with bulk rock concentrations often near or below 1 wt%. Ores are also depleted in As, especially when compared to some ore bodies in other South Range deposits, with bulk rock As contents below 5 ppm for most samples. Magnetite is ubiquitous throughout McConnell ores (avg 7-10 vol%), occurring in variable concentrations throughout the ore body from trace amounts to up to 20 vol% (Figure 3.2). Hydrothermally altered intervals contain very little magnetite, presumably removed by the fluid. The textures and chemical characteristics of magnetite grains indicate they formed with MSS cumulates, either as exsolution products from MSS, or as a result from the direct crystallization from an oxygen-rich sulfide melt.

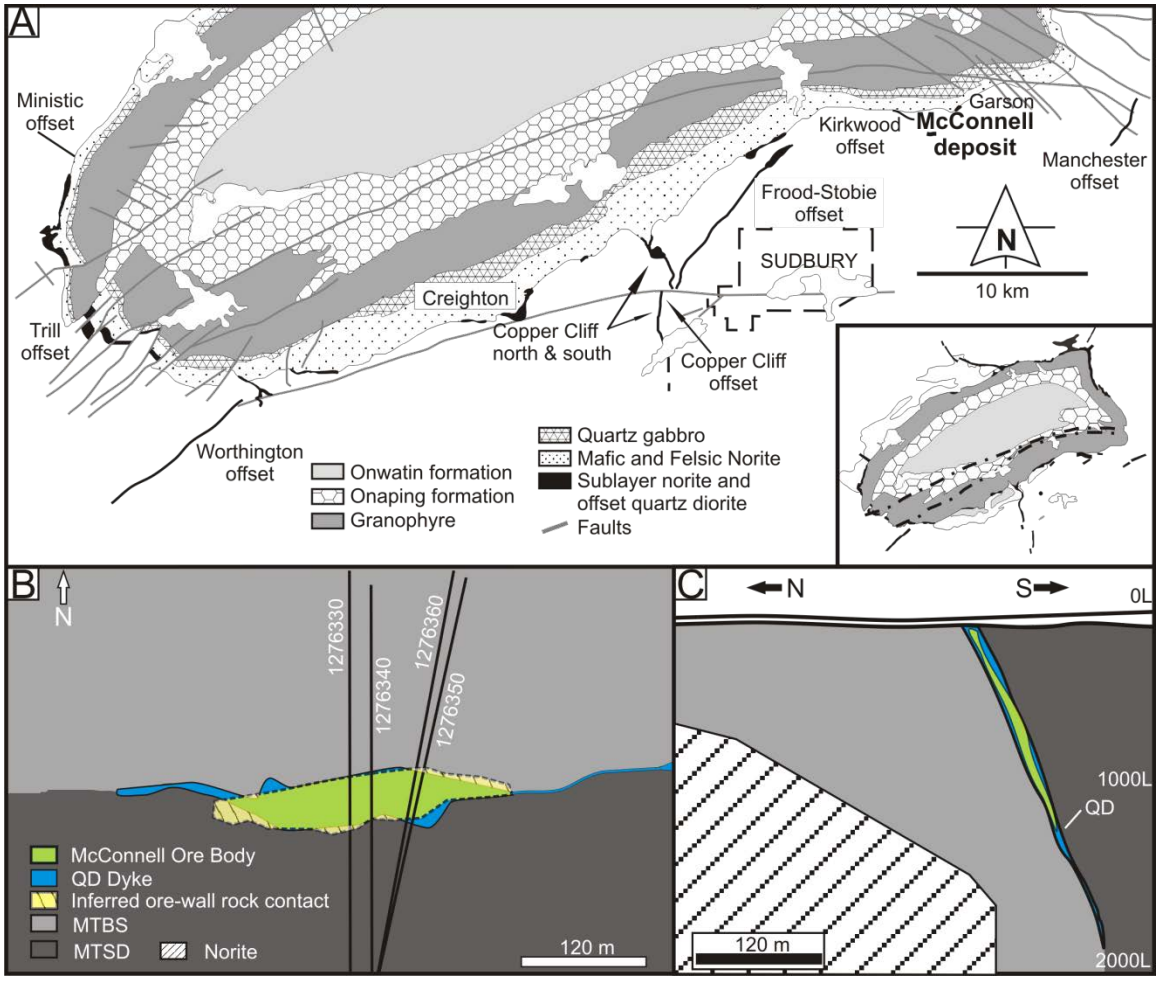

Figure 3.1. Location and Plan view of the McConnell concentric offset. (Top) The South Range of the Sudbury Igneous Complex showing faults and offset dike locations and orientations, the McConnell offset is located between the Garson and Kirkwood systems. (Inset) The entire SIC including the North Range Levack Gneiss Complex (black), South Range igneous intrusive rocks (pink), and the South Range Shear Zone (dashed lines). (Bottom) The McConnell ore body is situated at the contact between metabasalts and metasediments, and is (mostly) encapsulated within Quartz Diorite.

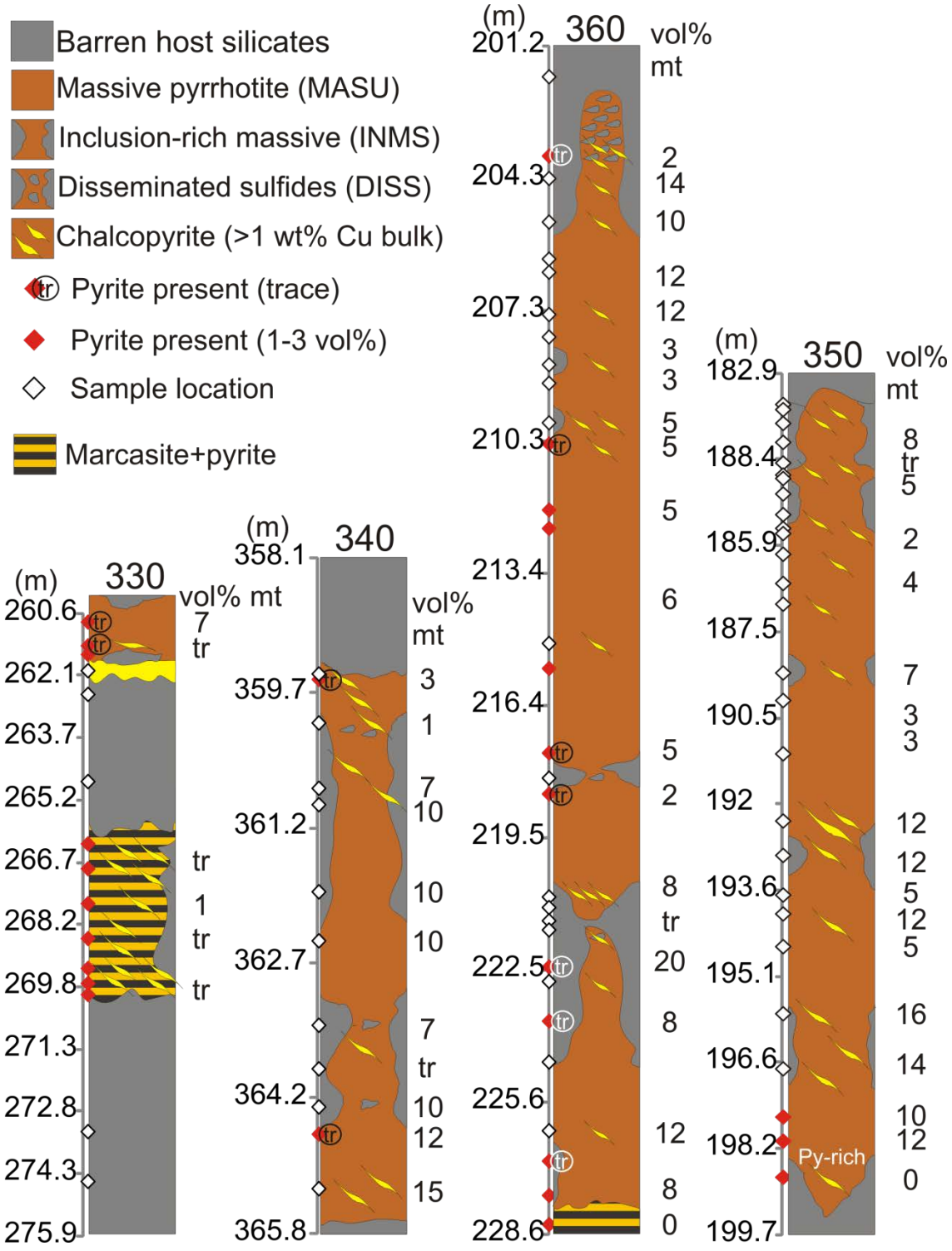

Figure 3.2. Graphic logs show the mineralogy of drill core from the McConnell ore body. Shorter columns have been stretched to help illustrate mineral domains.

3.2 Samples and Analytical methods

3.2.1 Sample collection

4 drill holes intersect the McConnell deposit (DDH-1276330, 1276340, 1276350, 1276360, Figure 3.1B). A total of 125 samples, each approximately 12 cm in length, were collected from BQ drill core provided by past Vale and Inco drilling programs. Samples were chosen at intervals showing mineralogical and textural representivity and changes (e.g. the appearance of pyrite as an alteration phase). Core samples were cut into 140 blocks for creation of polished thick and thin sections, and prepared into pulverized powders (100 g batches) for bulk rock assays (ALS Minerals, Sudbury, Ontario). 140 polished thick sections were made, resulting in a large suite of representative host rocks and sulfide mineralization sections which pass through the McConnell deposit (Figure 3.1). The drill core was logged and labelled with increasing depth to create graphic logs of mineralogical observations, separating zones of massive sulfide (MASU), inclusion-rich massive sulfide (INMS), disseminated sulfide (DISS), and host rock (metasediments, metabasalts, quartz diorite).

3.2.2 Optical and scanning electron microscopy

Petrographic analyses observations were accomplished using a Nikon Eclipse H550L microscope with reflected and transmitted light capabilities. These observations were augmented by scanning electron microscopy using a LEO 1450 VP Scanning Electron Microscope (Saint Mary's University) with a maximum resolution up to 3.5 nm at 30 kV. EDS analyses were performed at 25 kV accelerating voltage and 5 nA beam current. The SEM was used to help quantify mineral composition and identify discrete trace and accessory phases. The SEM uses INCA™ software to quantify X-ray spectra using a standard-enhanced semi quantitative routine, and to create element distribution maps

which were made for selected pentlandite and pyrite grains to better understand Ni, Fe, Co, and S distribution in altered samples. To discriminate monoclinic from hexagonal pyrrhotite, a magnetic colloid (powdered magnetite-hematite blend mixed into a solution with methanol) was applied to 10 representative polished thin sections of MASU and INMS. The magnetic colloid is strongly attracted to monoclinic pyrrhotite and magnetite grains (though the two are easily distinguishable from each other by optical properties), and is not attracted to hexagonal pyrrhotite, pentlandite, pyrite, or chalcopyrite.

3.2.3 Laser ablation inductively-coupled plasma mass spectrometry

Trace element analysis of minerals by laser ablation ICP-MS was conducted at the Geological Survey of Canada (Ottawa, Ontario) using an Agilent 7700 quadrupole inductively-coupled plasma mass spectrometer coupled to a 193 nm Ar-F Excimer laser for sample aerosol introduction. Ablation was performed at a 43 micron spot size (ablation pit diameter) and at a 10 Hz repetition (pulse) rate at 40% of 5 mJ (attenuated) output energy (Table 3.1). A 40 second gas blank was collected before each mineral analysis, followed by 65 seconds of mineral ablation (Figure 3.2). Standard reference materials were used to calibrate analyte sensitivities to account for instrument drift and for quality control, analyzed before and after blocks of 11 mineral analyses. Standards utilized at the GSC were synthetic pyrrhotite (Po726 from Memorial University, Saint Johns, Newfoundland and Labrador) for Au and PGE, a granitic glass (GSE-1G from USGS) for base metals and S, and a pressed sulfide pellet (MASS-1 from USGS). Ablation sites were selected in the centers of large grains, avoiding any cracks or grain boundaries (mixed matrices) with adjacent minerals. Collected spectra were observed in real time to make note of the presence of mineral inclusions in larger analyzed grains or

Table 1: LA-ICP-MS operating conditions

LA	
Model	Photon Machines Analyte.193
Wavelength	193 nm
Pulse duration (FWHM)	4 ns
Repetition rate	10 Hz
Spot diameter	32-86 µm
Energy density	ca. 4 J/cm^2
Primary (calibration) standards	**Po726** (synthetic, PGE and Au doped pyrrhotite, Sylvester et al., 2005; reference values from certificate) **MASS-1**(synthetic, doped, precipitated sulfide; reference values from Wilson et al., 2002, except Te from Dare et al., 2010b, and Ni (98 ppm) and Pb (73 ppm) determined in house)
Secondary (QC) standard	**GSE-1** (synthetic silicate glass; provided by GSC) **JB Sulfide** (synthetic sulfide [University of Toronto] reference values from Mungall and Brenan, 2014)
ICP-MS	
Model	Agilent 7700x with additional interface rotary pump which approximately doubles instrument sensitivity
Forward power	1550 kW
Shield torch	Used
Sampling depth	7 mm
Gas flows (He carrier mixed downstreamn from cell with Ar make up):	
Carrier (He)	0.6 L/min
Make up (Ar)	1.08 L/min
ThO^+/Th^+	<0.3%
U^+/Th^+ (NIST 612)	ca. 1.05
Data acquisition parameters	
Data acquisition protocol	Time Resolved Analysis
Scanning mode	Peak hopping, 1 point per blank
Dwell time per isotope	10 ms for all masses (earlier analyses) or as indicated below
Detector mode	Pulse counting except analogue for isotopes in italics below
Isotopes determined (dwell time ms)	^{34}S(5), ^{51}V(10), ^{53}Cr(10), ^{57}Fe(5), ^{59}Co(10), ^{60}Ni(5), ^{61}Ni(10), ^{65}Cu(10), ^{65}Cu(10),^{66}Zn(10), ^{75}As(10), ^{77}Se(10), ^{88}Sr(5), ^{89}Y(5), ^{90}Zr(5), ^{99}Ru(15),^{101}Ru(15), ^{102}Ru(15), ^{103}Rh(15), ^{105}Pd(15), ^{106}Pd(15), ^{107}Ag(15), ^{108}Pd(15), ^{109}Ag(15), ^{111}Cd(10), ^{118}Sn(15), ^{121}Sb(10), ^{125}Te(10), ^{181}Ta(5), ^{193}Ir(15), ^{195}Pt(15), ^{197}Au(15),^{205}Tl(10), ^{206}Pb(10), ^{208}Pb(10),^{209}Bi(10)
Quadrupole settling time	1-5 ms depending upon mass jump
Analysis time	100 s: ~40 s gas blank, up to ~60 s of ablation

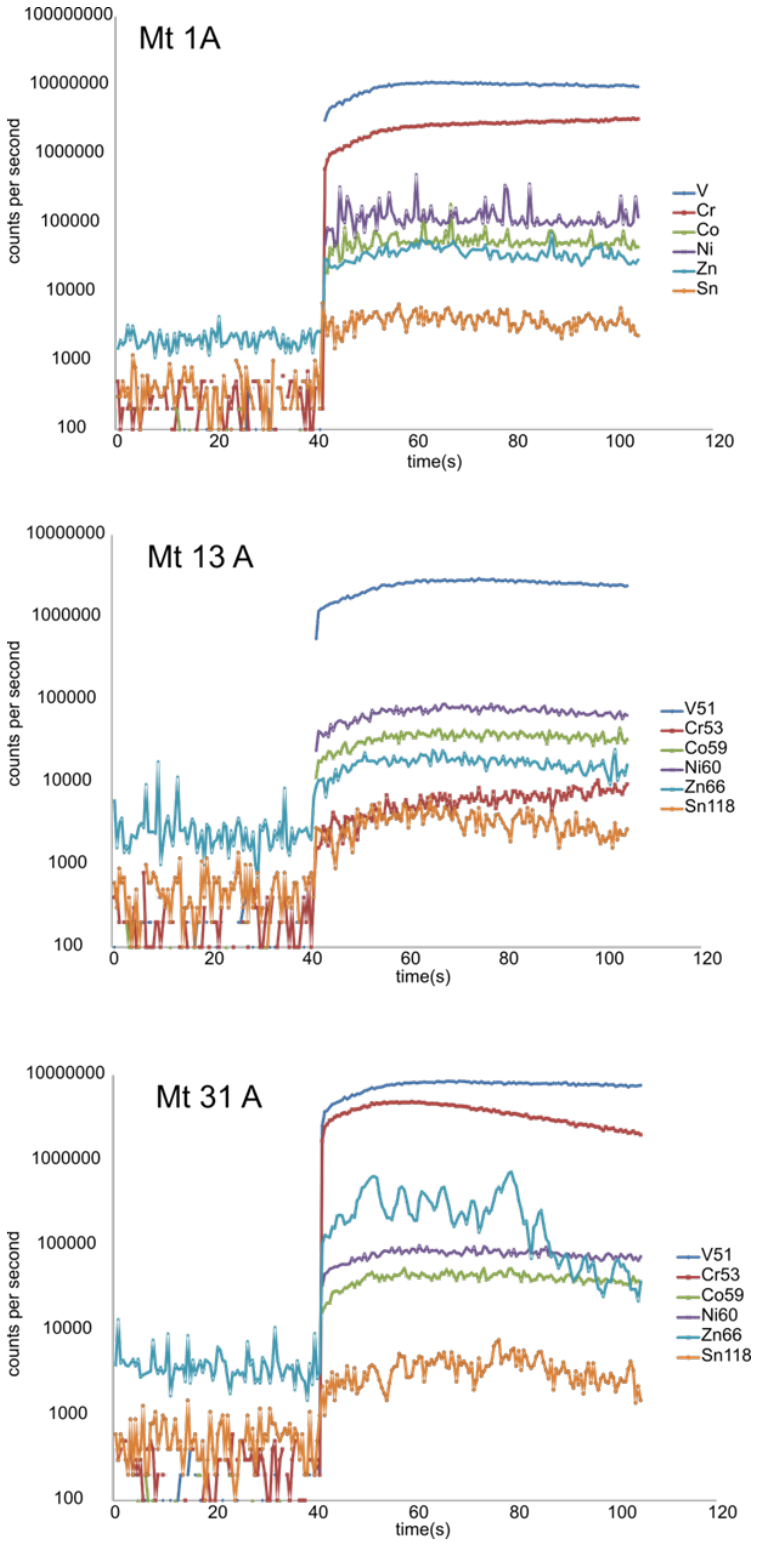

Figure 3.3. LA-ICP-MS signals for 3 representative magnetite grains over the course of a 60 second ablation with a 40 second gas blank.

inhomogeneous grains, allowing for scrutiny of raw data prior to data reduction. Figure 3 (time-resolved signals) demonstrates distribution of elements through magnetite grains during ablation. Isotopes measured were ^{34}S, ^{51}V, ^{53}Cr, ^{57}Fe, ^{59}Co, ^{60}Ni, ^{61}Ni, ^{65}Cu, ^{66}Zn, ^{75}As, ^{77}Se, ^{99}Ru, ^{101}Ru, ^{102}Ru, ^{103}Rh, ^{105}Pd, ^{106}Pd, ^{107}Ag, ^{108}Pd, ^{111}Cd, ^{118}Sn, ^{121}Sb, ^{125}Te, ^{181}Ta, ^{193}Ir, ^{195}Pt, ^{197}Au, ^{205}Tl, ^{206}Pb, ^{208}Pb, and ^{209}Bi (Table 3.2).

3.3 Results

3.3.1 Petrographic characteristics of magnetite

Magnetite is heterogeneously distributed in the McConnell ores in concentrations between <1 – 20 vol% (Figure 2), except in areas which have undergone intense hydrothermal alteration, in which magnetite is either extremely scarce or entirely absent (hole 330, bottom of 360). Magnetite grains occur as small (< 1 mm) single subhedral to rounded inclusions hosted in pyrrhotite and, less commonly, chalcopyrite (Figure 3.4). Magnetite grains also occur as crystal aggregates or clusters, possibly representing a cumulate phase (Figure 3.4D). Magnetite is hosted along grain boundaries of pyrrhotite and pyrrhotite-chalcopyrite in massive sulfide samples (MASU), along grain boundaries of chalcopyrite-pyrrhotite-gangue in inclusion-rich massive sulfide samples (INMS), and as inclusion within pyrrhotite and chalcopyrite in massive to inclusion-rich massive ore, typically when the host grain size is much larger (3-5x) than the magnetite inclusion. Magnetite grains may occur within silicates and are commonly enclosed by very thin silicate rims when hosted in sulfides (Figure 3.4D). Figure 3.4 shows typical magnetite morphology and inclusion type (grain hosted or grain-boundary hosted) for massive pyrrhotite-dominant ore (Figure 3.4C) in which grains are typically smaller, hosted along boundaries, and occur more frequently than larger grained massive samples (Figure 3.4D). Chalcopyrite-bearing massive (Figure 4A) and inclusion-rich massive

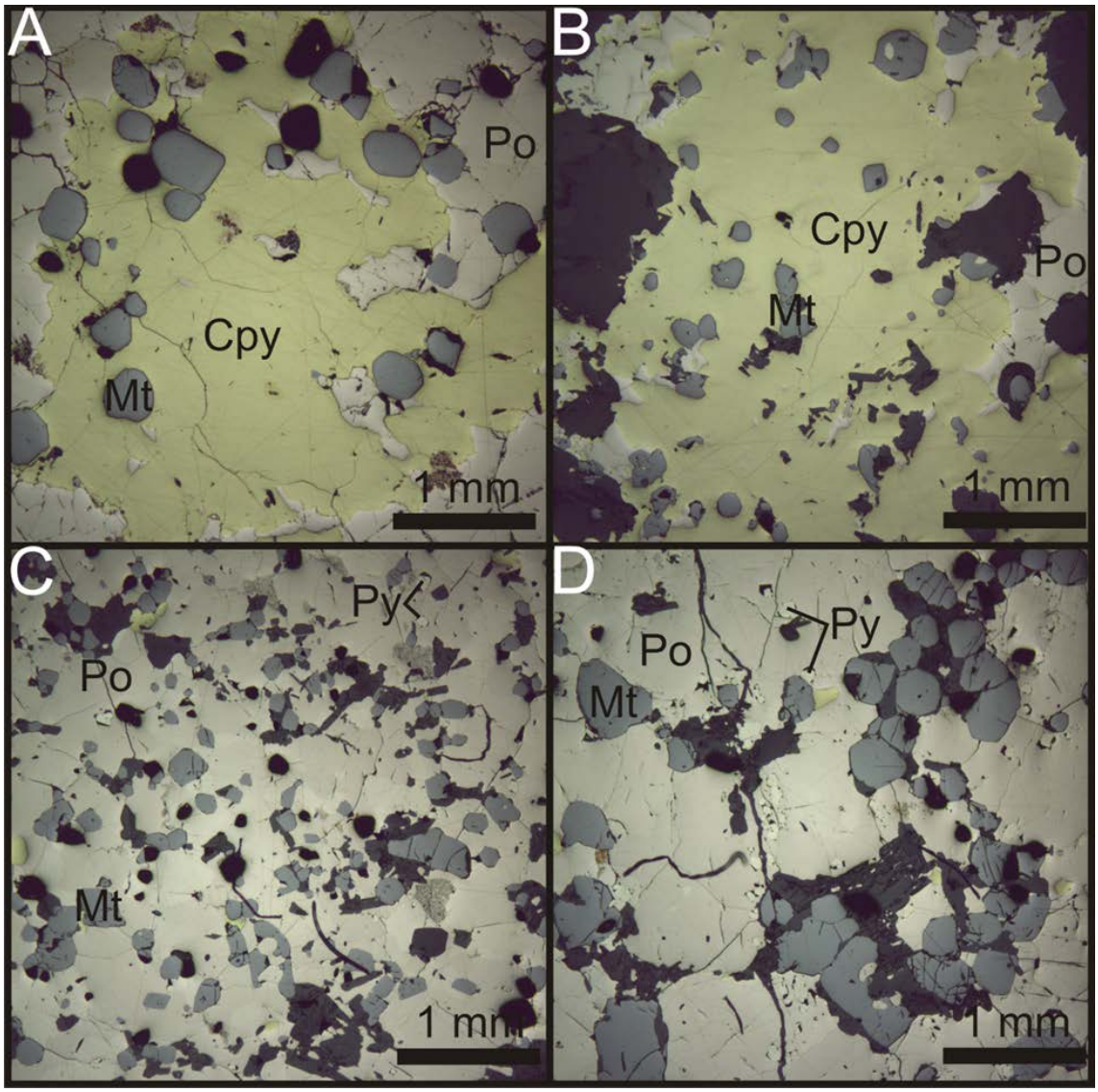

Figure 3.4. Petrographic characteristics of McConnell magnetite. (A,B) Chalcopyrite (Cpy) bearing samples often show magnetite (Mt) hosted entirely within, as well as along, grain boundaries of chalcopyrite. Magnetite grains hosted within chalcopyrite show smooth, rounded edges, and typically have fewer fractures than those hosted within pyrrhotite (Po). (C,D) Magnetite hosted within massive pyrrhotite samples are typically fractured, and associated with trace amounts of silicate gangue. The grain size of pyrrhotite often influences the grain size of boundary-hosted magnetite grains.

(Figure 3.4B) samples typically show magnetite hosted entirely within large (few mm – cm scale) grains of chalcopyrite as smooth, rounded, single inclusions (Figure 3.4D).

3.3.2 Exsolution products

The very fine exsolution blebs (1 - 10 μm) and lamellae (2 x 10 – 20 μm) within magnetite grains were analyzed by SEM-EDS to determine the composition and estimate the mineralogy of the exsolved phases. Lamellae oriented along the crystal faces of magnetites (Figures 3.5, 3.6B-C) are rich in Ti (Figure 3.7) and contain Mn and Cr, though Cr is often no different from magnetite host compositions (0.3 – 2 wt%). These lamellae are most probably the exsolution of ilmenite, or ulvospinel, which can often be misidentified and misinterpreted due to its extremely fine-grained size (Krasnova and Krezer, 1995). Exsolution blebs (Figure 3.6A) have elevated Al (Figure 3.7), Mg, and in some cases, Zn. Blebs may represent the formation of extremely small Al-spinel or gahnite inclusions. Spinels blebs contain trace Si as well, and thin rims of silicates are often found around magnetite grains.

Both exsolution products (lamellae and blebs) occur within the same magnetite grains, although exsolution lamellae are more abundant when magnetite is associated with chalcopyrite (shared grain boundaries). Exsolution blebs are orders of magnitude more common than exsolution lamellae within magnetite grains hosted only by pyrrhotite (Figure 3.6A), and do not show the zoned hatch pattern of ilmenite that some cpy-bounded magnetites contain. Magnetite grains often show a thin exsolution-free rim which surrounds the ilm-spn exsolution within the cores, which is especially apparent in grains with distinctive ilmenite exsolution (Figures 3.5, 3.6, 3.7).

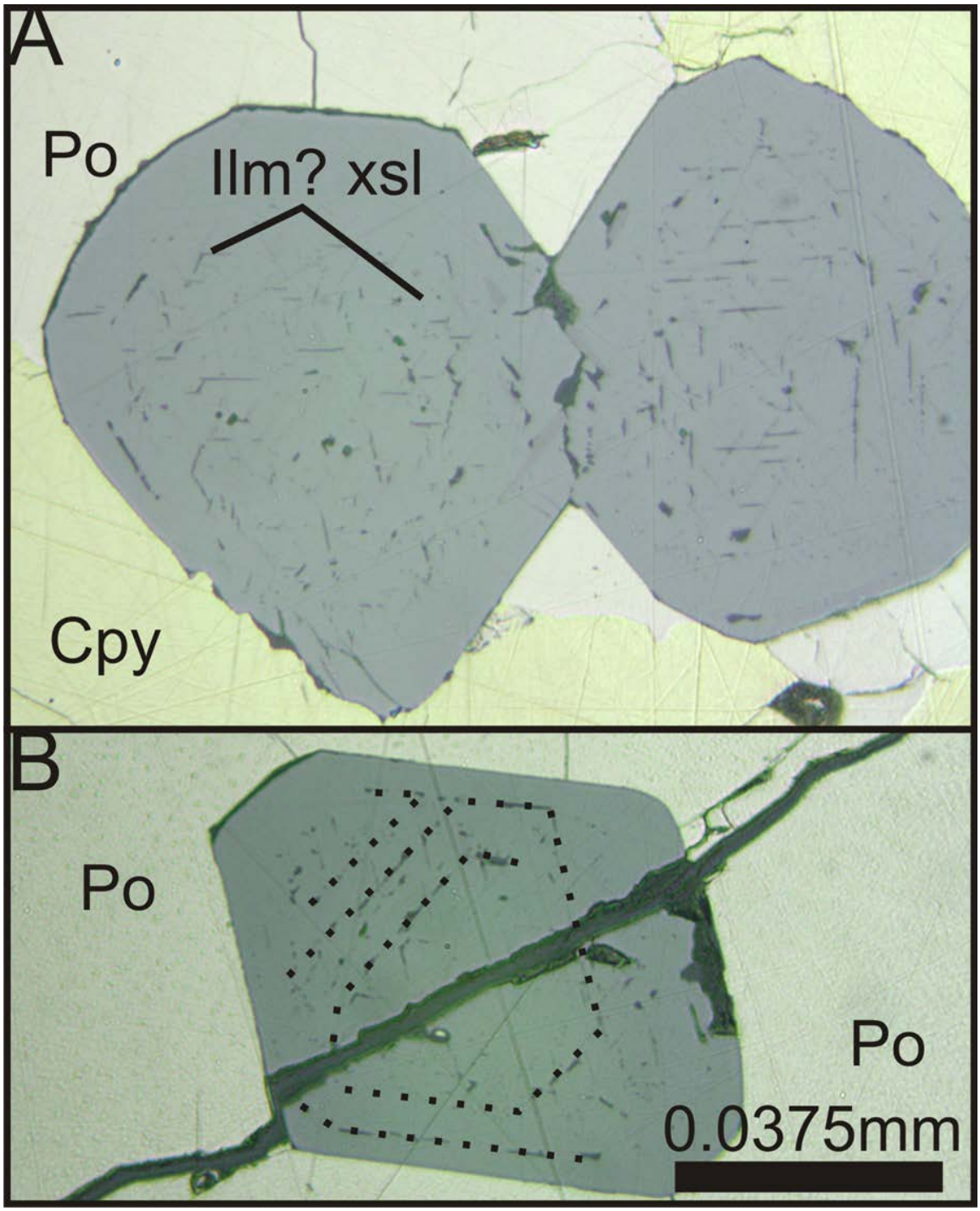

Figure 3.5. Magnetite exsolution products in reflected light. (A) Two magnetite grains hosted along chalcopyrite (Cpy) and pyrrhotite (Po) boundaries which appear to display some exsolution of an unidentified phase. Exsolution lamellae are straight or angular, appearing along cleavage planes. Magnetite-chalcopyrite boundaries appear jagged and perturbed. (B) A magnetite grain hosted entirely within a single fractured pyrrhotite grain, showing a smooth 6-faced crystal with apparent exsolution along growth zones. Fracture is likely the result of sample preparation.

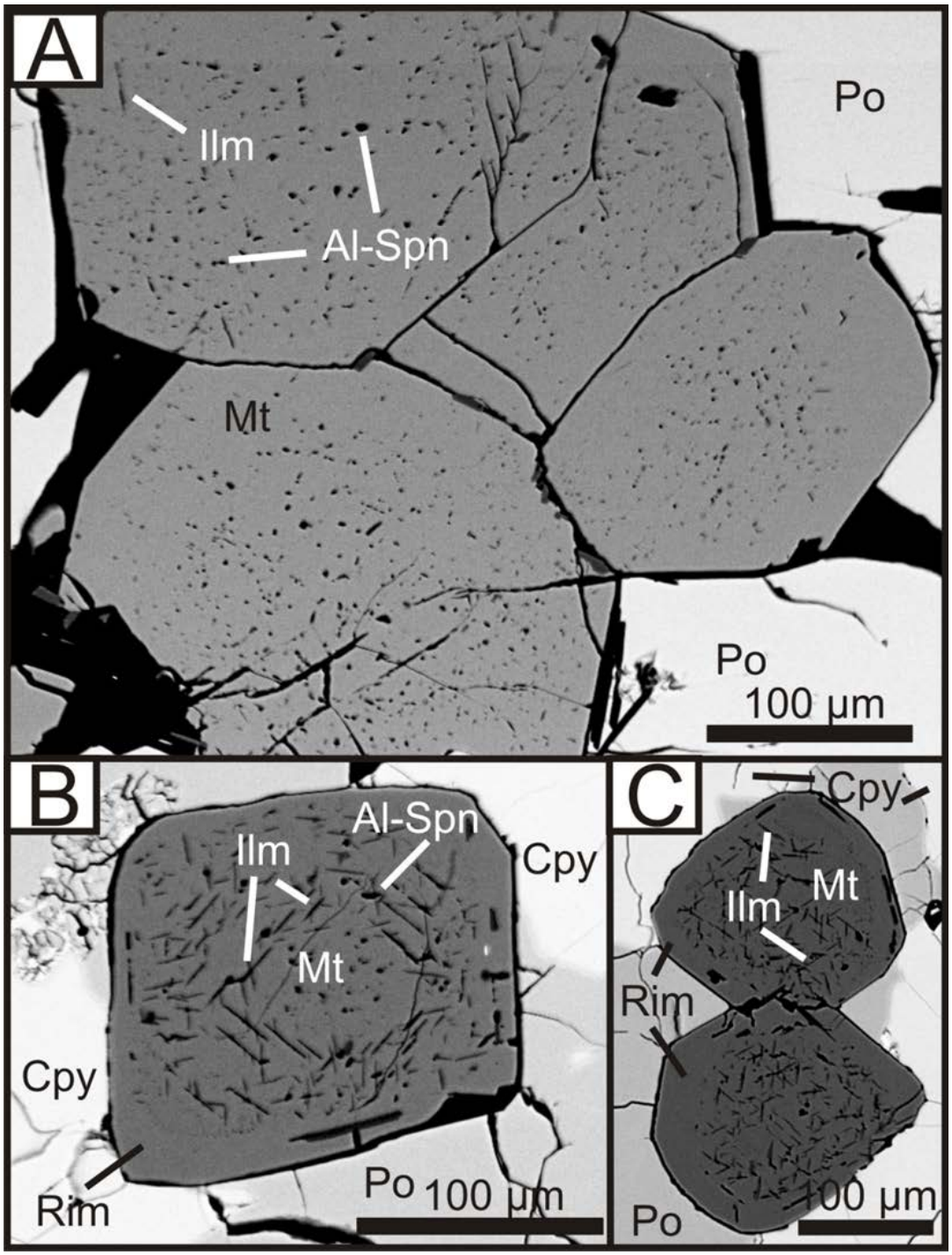

Figure 3.6. SEM images of magnetite (Mt) and exsolution products Ilm (ilmenite) and Al-Spn (Al-spinel). A) Large grains of magnetite form a small crystal aggregate hosted between massive pyrrhotite grains, magnetite is covered by Al-spinel exsolution distributed in a fairly heterogeneous "buckshot" pattern. B) Exsolution of both ilmenite and Al-spinel appear to be zoned within magnetite, an exsolution-free rim exists in most magnetite observed with this exsolution texture. C) A similar zoned ilmenite exsolution texture where exsolution occurs only within the core of the grain, grains are hosted along boundaries of chalcopyrite and pyrrhotite.

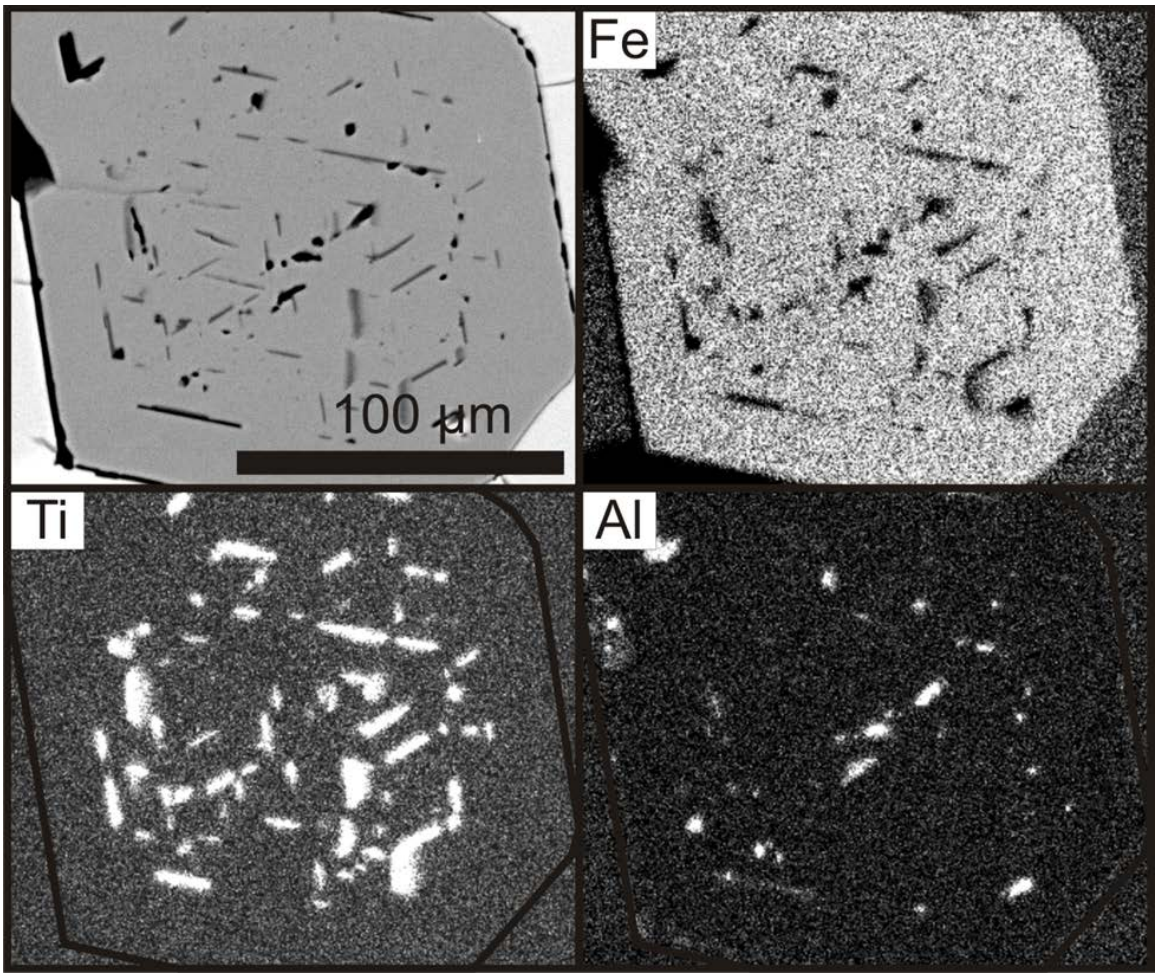

Figure 3.7. SEM element distribution maps of Ti, Fe, and Al within a magnetite grain hosted in massive pyrrhotite. Maps show exsolution lamellae are rich in Ti and relatively depleted in Fe, indicating the exsolved phase may be ilmenite. Exsolution blebs contain high Al and are interpreted to be the exsolution of small bits of Al-rich spinel (or ulvospinel).

3.3.3 Magnetite chemistry

Major element compositions of magnetite grains from SEM analyses show typical Fe_3O_4 chemistry with variable Cr concentrations (0.3 – 2 wt% Cr). Zoning of major elements in magnetite grains is not apparent due to the nature of the exsolution products within magnetite. Thin rims of SiO_2 often surround magnetite grains and infill fractures between magnetite and sulfides. Magnetite grains from 9 representative sulfide samples of McConnell ore were analyzed by LA-ICP-MS for the trace element concentrations of magnetite, accumulating 36 analyses. As small sulfide inclusions are common within magnetite grains, any analyses that showed anomalous sulfur peaks were discarded and a new magnetite grain was chosen for ablation. Exsolution products are included in analyses and represent initial homogenous composition of magnetite grains. Table 3.2 lists ranges of magnetite composition from each sample for the elements V, Cr, Co, Ni, Zn, Sr, Y, Zr, Sn, Sb, Pb, and Bi. As is common in the Sudbury area, the PGE and IPGE (Ru, Rh, Pd, Re, Ir, Pt) concentrations of most magnetite grains were below their respective detection limits, as were the elements Te, Cd, Tl, and the precious metals (Ag, Au) (Li et al., 1993; Dare et al., 2012). Cr, Sr, Zr, Zn, and Bi all show a wide range of concentrations within magnetite grains from various levels within the McConnell, while V, Sn, Co, Ni, and Y show a much closer, tightly packed cluster of compositions (Figures 3.8, 3.9, 3.10). Vanadium (413.88 – 2120.26 ppm) and tin (0.34 – 3.65 ppm) concentrations in McConnell magnetite grains form a defined field on a V-Sn plot (Figure 3.8B), and show a loose trend between sulfide mineralogy and relative concentration (Figure 3.8E-F). The most compatible lithophile elements (Cr, V, Ti) partition readily into early forming magnetite and are thus relatively depleted in later-forming grains.

Table 2. LA-ICP-MS analyses of magnetite grains hosted within McConnell ores

Sample	V	Cr	Co	Ni	Zn	Sr	Y	Zr	Sn	Sb	Pb	Bi
Mt-360-24	(ppm)	(ppm)	(ppm)	(ppm)	(ppm)	(ppm)	(ppm)	(ppm)	(ppm)	(ppm)	(ppm)	(ppm)
avg	456	199	13.7	337	17.1	0.54	0.39	9.81	0.56	0.05	0.66	0.04
stdev	29.6	166	6.27	257	10.2	0.22	0.14	13.8	0.19	0.02	0.23	0.03
max	495	472	23.7	691	34.7	0.93	0.58	33.7	0.85	0.08	0.85	0.08
min	414	58.1	8.17	89.6	10.0	0.38	0.25	1.49	0.34	0.02	0.28	0.01
Mt-360-26												
avg	1230	6680	10.7	100	380	0.04	0.07	0.13	0.95	0.06	0.14	0.01
stdev	41.0	2120	0.72	7.85	211	0.04	0.03	0.10	0.12	0.01	0.09	0.00
max	1280	9850	11.8	108	595	0.10	0.11	0.27	1.12	0.07	0.30	0.01
min	1170	4430	9.85	88.8	29.3	0.00	0.03	0.03	0.78	0.05	0.07	0.00
Mt-360-31												
avg	1910	10430	13.9	87.2	3340	0.12	0.12	0.32	1.29	0.17	0.92	0.02
stdev	69.2	4700	3.24	16.0	2970	0.12	0.06	0.44	0.41	0.14	0.57	0.01
max	2030	17200	18.3	107	7090	0.31	0.19	1.07	1.78	0.35	1.53	0.04
min	1860	5092	9.86	62.1	351	0.02	0.03	0.03	0.78	0.02	0.33	0.00
Mt-360-32												
avg	1450	5970	8.65	110	610	0.28	0.38	0.10	1.75	0.08	0.71	0.11
stdev	41.8	5910	3.74	4.20	1020	0.28	0.42	0.09	1.14	0.04	0.45	0.07
max	1500	14900	11.5	115	2380	0.65	1.05	0.26	3.65	0.15	1.45	0.21
min	1390	348	2.34	106	12.4	0.02	0.02	0.03	0.82	0.04	0.26	0.01
Mt-360-1												
avg	1820	5960	9.79	96.2	36.9	0.14	0.10	0.08	0.71	0.07	0.63	0.03
stdev	181	3290	0.68	11.5	28.1	0.09	0.07	0.03	0.05	0.02	0.19	0.02
max	2120	11100	10.6	114	84.9	0.25	0.19	0.12	0.75	0.11	0.94	0.06
min	1660	2150	8.98	83.4	15.3	0.04	0.03	0.04	0.63	0.04	0.45	0.01
Mt-360-2												
avg	1750	10700	14.8	114	2320	0.03	0.08	0.36	1.79	0.14	0.37	0.02
stdev	28.6	8200	4.44	15.3	1720	0.03	0.04	0.18	0.46	0.02	0.11	0.00
max	1770	24500	22.0	133	5200	0.07	0.14	0.65	2.38	0.17	0.50	0.02
min	1670	3750	10.3	94.7	712	0.01	0.04	0.16	1.11	0.12	0.21	0.01
Mt-360-13												
avg	658	18.9	9.68	96.3	15.3	0.32	0.22	2.88	0.70	0.03	0.18	0.01
stdev	25.0	4.50	1.27	15.3	1.22	0.42	0.27	4.96	0.06	0.01	0.02	0.00
max	684	26.6	11.1	114	17.3	1.05	0.69	11.5	0.79	0.05	0.20	0.01
min	630	15.2	8.39	80.4	14.2	0.04	0.04	0.01	0.64	0.02	0.15	0.01
Mt-360-18												
avg	774	73.4	8.43	93.2	149	1.03	1.10	0.03	0.92	0.02	0.35	0.03
stdev	34.2	52.6	0.22	12.0	134	1.71	1.79	0.04	0.39	0.01	0.27	0.02
max	829	158	8.65	113	306	3.99	4.21	0.09	1.59	0.03	0.80	0.05
min	736	26.2	8.09	82.1	15.3	0.02	0.02	0.01	0.61	0.01	0.14	0.00
Mt-360-19												
avg	1130	263	10.7	95.9	1600	0.04	0.07	0.45	1.32	0.16	0.42	0.01
stdev	127	174	1.81	12.6	1370	0.03	0.03	0.30	0.42	0.07	0.24	0.01
max	1240	476	12.5	116	3570	0.07	0.11	0.85	1.95	0.25	0.65	0.02
min	914	8.67	8.41	81.0	21.7	0.00	0.02	0.04	0.84	0.06	0.02	0.00

3.4 Discussion

3.4.1 Partitioning characteristics and comparison to other deposits

Nickel concentration of magnetite grains that exsolve from MSS is typically lower than grains that form from ISS (Dare et al., 2012; this study, Figure 3.8). Although Ni partitioning is strongly controlled by S content between MSS and sulfide liquid at higher temperatures, with $D^{mss/liq}$ ranging between 0.1 and 2 (Fleet and Pan, 1994; Li et al., 1996; Barnes et al., 1997), magnetite which crystallizes in early Fe-rich MSS would be depleted in Ni due to the incompatibility of Ni in MSS at high temperatures, favouring partitioning into residual sulfide liquid above temperatures of ~850° (Mungall et al., 2005; Mungall 2007). Diffusion and mobilization of Ni in the MSS, even at lower temperatures, is also something to consider. McConnell ores are relatively low-grade in Ni when compared to other Sudbury deposits (Hoffman et al., 1979; Huminicki et al., 2005; Barnes and Lightfoot 2005; Dare et al., 2010, Boucher, Chapter 2), having little pentlandite (<2vol% in most samples) and no millerite, with half of the bulk rock Ni concentration occuring in massive pyrrhotite. It is therefore reasonable to assume that magnetite formed from the initial sulfide melt, or exsolved from MSS or ISS in McConnell ores, would have less Ni concentration than more typical Sudbury deposits. Figure 3.8D shows a general depletion of Ni in magnetite from 3 sources; Coleman (North Range, Cu-rich ISS hosted magnetite), Creighton (South Range, primitive Fe-rich MSS hosted magnetite), and McConnell (primitive to evolved Fe-rich MSS hosted magnetite). McConnell magnetite generally carries ~100 ppm of Ni in solution, whereas Creighton magnetite shows several hundred to 1000 ppm, and Coleman magnetite averages several thousand to over 10,000 ppm Ni in solution. Although McConnell and Creighton magnetite are assumed to have a similar source (Fe-rich primitive MSS), the

sulfide melt at McConnell must have been depleted in Ni relative to Creighton. Coleman magnetite, which represents exsolution from a lower temperature ISS source similar to the adjacent McCreedy west environment (Dare et al., 2012), shows Ni concentrations an order of magnitude higher than Creighton and almost 2 orders of magnitude higher than McConnell. Ni and Co show little variation in samples (62.13 – 690.86 ppm and 2.34 – 23.66 ppm, respectively) with only a slight increase in concentrations with mineralogy (higher po+pn yields slightly higher concentrations of Ni and Co). Since Ni concentration of a melt has a direct influence on the O content and solubility of a given sulfide liquid (and therefore its position on a mss-magnetite binary in the Fe-O system), a melt depleted in Ni should crystallize magnetite at higher temperatures than a melt enriched in Ni (Naldrett, 1969; Fonseca et al., 2008). Therefore, magnetite from McConnell may have begun crystallization directly from the sulfide liquid in order to bring the system into the MSS stability field.

Chromium partitions favourably into magnetite from the primitive Fe-rich MSS component in both Creighton and McConnell samples, often at concentrations in the 1000 to 10000 ppm range, with some samples exceeding several wt% (Figure 3.9C). Most of these samples fall into the primitive MSS composition field (Figure 3.8A), but some also extend into the evolved portion of the V vs Cr and Sn vs Cr binaries as plotted by Dare et al. (2012), overlapping slightly with some Coleman samples. Chromium concentrations of Coleman magnetite extend to 70 – 80 ppm in the highest concentrated samples, but on average fall below 10 ppm concentration, several orders of magnitude lower than most Creighton and McConnell samples. Chromium concentrations within McConnell ores typically show a depletion in Cr from the top of the drill hole to the

bottom in bulk rock assays. Strangely enough, an inverse relationship exists between bulk rock and magnetite Cr concentrations, in that magnetite becomes more enriched in Cr deeper down the column. Below 700 ft, however, bulk rock Cr decreases to <100 ppm and concentrations within magnetite fall orders of magnitude (10's to 100's of ppm vs 1000's and 10000's ppm in samples from higher up the column). Magnetite grains from samples which are locally associated with silicates (massive sulfide with silicate inclusions or intermediate massive sulfide) often show a lower concentration of Cr than magnetite grains from the center of massive sulfides. The silicates in these samples may have locally depleted the sulfide liquid/MSS in Cr and subsequently the magnetite which crystallized in the vicinity. Figure 3.3 shows time-elapsed laser ablation signals for 3 magnetite grains, with Cr from the intermediate-massive sulfide sample (13) at much lower concentrations than Cr from the massive sulfide samples (1, 31). Diffusion of Cr from the sulfide melt to the silicate melt may explain why some magnetite grains plot in the Cr-depleted evolved sulfide field rather than the Cr-rich primitive sulfide field. Magnetite grains hosted in the highest interval (670.1 ft) and within samples between 725 – 750 ft appear to be extremely depleted in Cr regardless of sulfide abundance or mineralogy. This might imply that the center or core of the sulfide body was more enriched in Cr than the edges, though bulk rock assays do not show conclusive evidence for this hypothesis. Chromium can also be repartitioned from the magnetite host to its exsolution products (Knecht et al., 1977), so the texture and abundance of exsolution products is strongly correlated to the Cr content of McConnell magnetite as well.

Vanadium is typically quite compatible in MSS and magnetite relative to Zr or Sn and therefore should show enrichment in magnetite grains which crystallize early relative to

magnetite grains which crystallize later. Experiments by Toplis and Corgne (2002) have shown that between an oxide and silicate melt, oxygen fugacities between NNO and NNO-1.5 yield the highest V concentrations in magnetite for a fixed liquid composition, and therefore, higher partition coefficients for these oxygen fugacities than those of higher or lower values. Vanadium concentrations in McConnell and Coleman magnetite seem to show a loose correlation with Cr in that both decrease during prolonged evolution of the system with early-forming magnetite (Fe-rich MSS) enriched in V and Cr and later-forming magnetite (Cu-rich ISS) depleted in these elements. The compositional trends from all 3 environments (McConnell, Creighton, Coleman) appear to agree with this line of reasoning. Although Cr may be locally depleted due to crystallization of silicates, V does not appear to decrease substantially in McConnell samples which are associated with silicate gangue (INMS). While Cr can differ by orders of magnitude in MASU vs INMS samples, V only varies by a few hundred ppm in most samples. Vanadium partitions into magnetite-ulvospinel solid solutions preferentially to stoichiometric magnetite, though its partition coefficient is more greatly influenced by valence state and oxygen content than oxide composition (Toplis and Corgne, 2002).

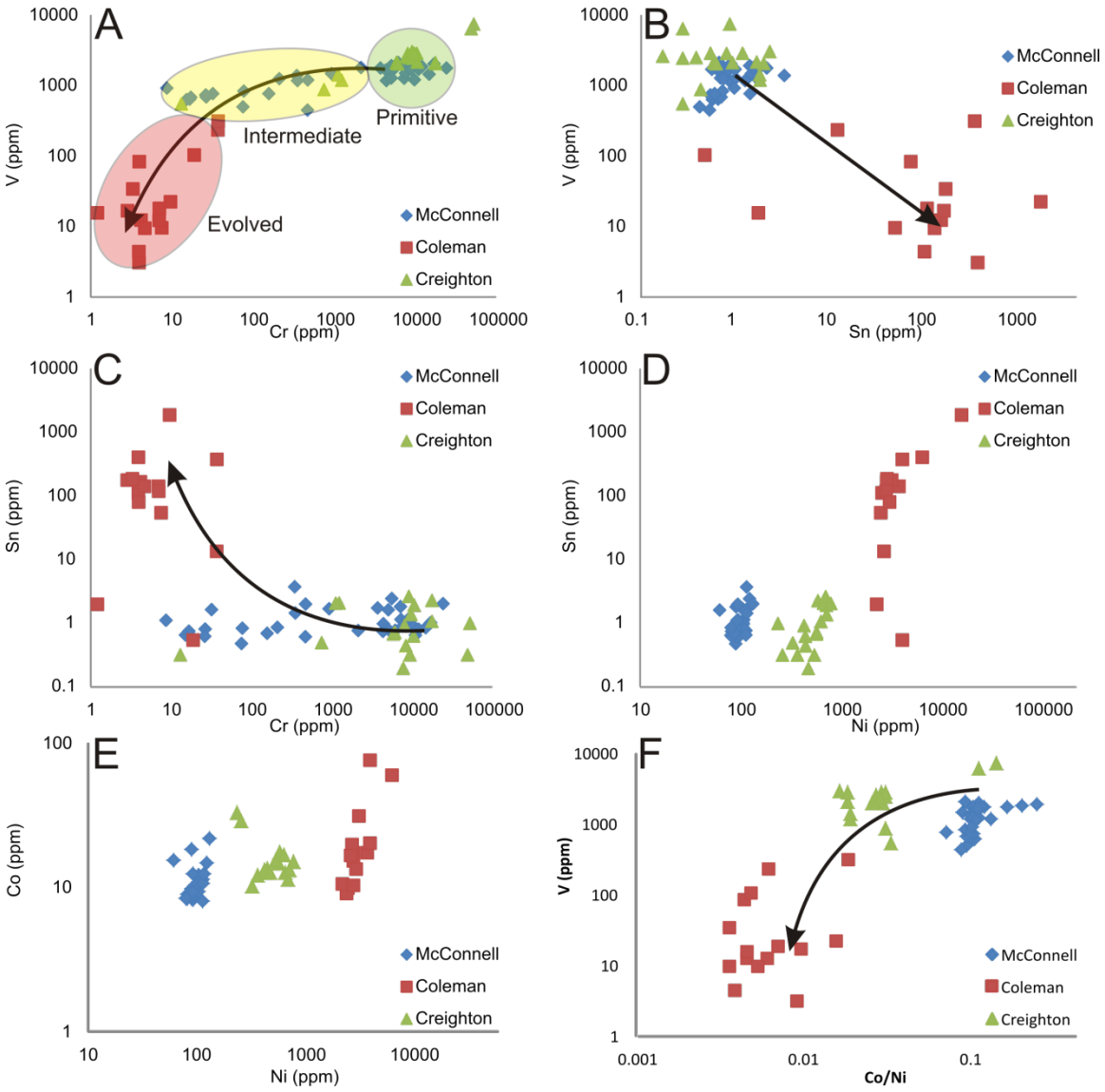

Figure 3.8. Scatter plots of laser ablation data for magnetite grains from Fe and Cu-rich sources. McConnell, Coleman (MacMillan 2014), and Creighton (Dare et al., 2012) showing trace element trends indicative of crystallization history. (A,B) Samples of McConnell and Creighton magnetite plot very similar V concentrations, while Coleman magnetite is relatively depleted in V. McConnell magnetite grains show decreasing Cr while V remains relatively constant. Arrows show the relative trend in V vs Cr and Sn that is expected between magnetite which crystallizes from MSS (McConnell, Creighton) and magnetite which crystallizes from ISS (Coleman). (C) Magnetite crystallized from ISS is enriched in Sn and depleted in Cr relative to magnetite which has crystallized from MSS. Arrow shows the expected trend between these two sources. (D) Ni concentrations relative to Sn in magnetite show fields between MSS and ISS sources, but McConnell is Ni depleted even for an MSS source. (E,F) Co concentrations in magnetite grains are comparable between all three deposits, but Ni varies. Co/Ni ratios are highest in McConnell magnetite and lowest in Coleman magnetite, showing a decreasing trend with time and source composition.

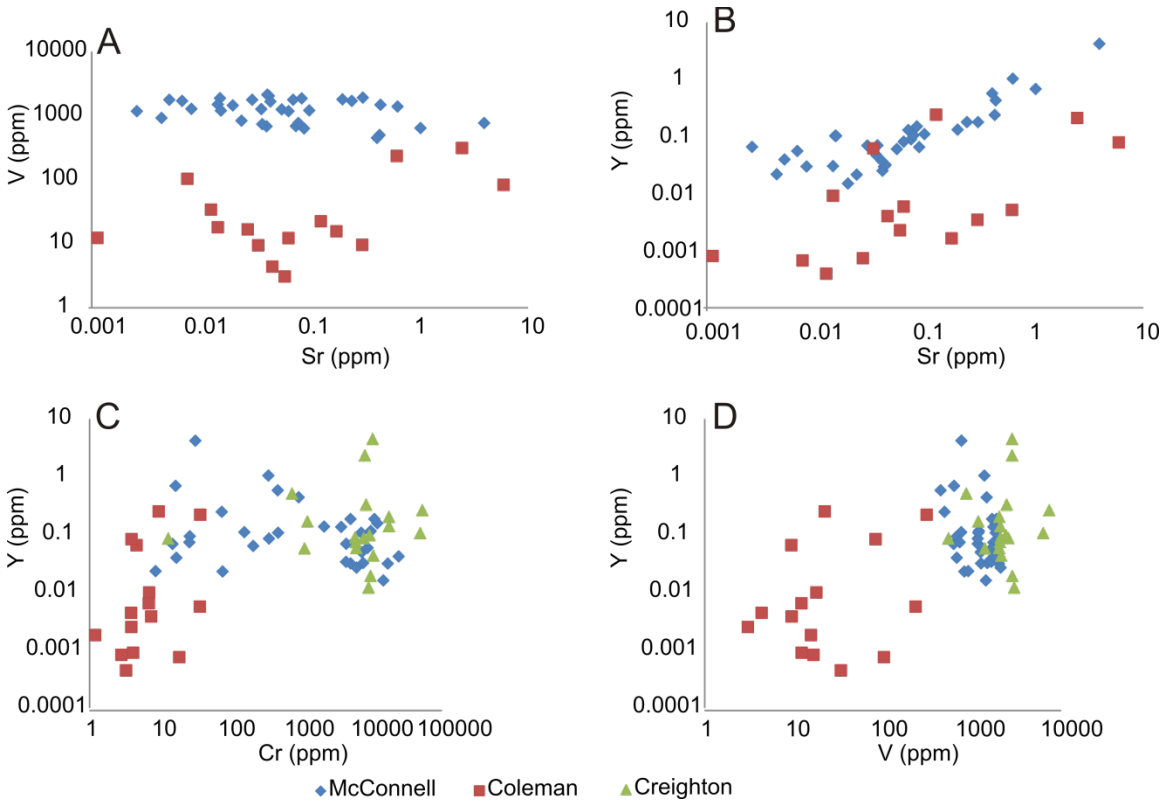

Figure 3.9. Lithophile element plots of magnetite from McConnell, Coleman, and Creighton ore bodies. (A,B) An overlap of Sr concentrations in McConnell and Coleman samples show two general fields between V and Sr, while Y seems to increase with Sr in both populations. (C,D) Populations of MSS and ISS sourced magnetite grains typically cluster together in binary plots of Y vs Cr and V, though some overlap does occur in Cr concentrations. Data from McConnell (This study), Coleman (MacMillan 2014), and Creighton (Dare et al., 2012)

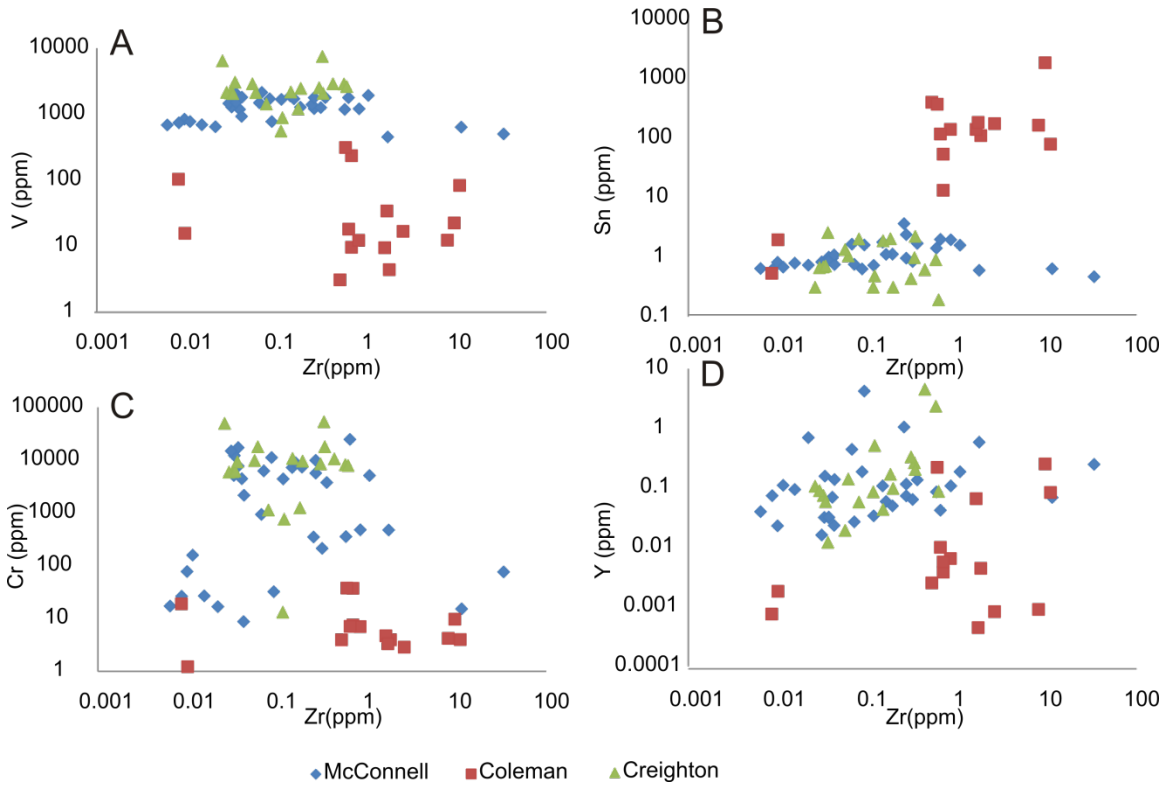

Figure 3.10. Compatible elements (V, Sn, Cr, Y) in magnetite vs Zr (extremely incompatible). Data from McConnell (This study), Coleman (MacMillan 2014), and Creighton (Dare et al., 2012)

In contrast to partitioning of V, magnetite composition is a major factor on the partition coefficients of Zr and other HFSE (Nielsen and Beard, 2000). Although Zr partitions preferentially into phases which crystallize from ISS (chalcopyrite, sphalerite), Zr within MSS tends to concentrate in magnetite rather than pyrrhotite (Englander 2005, this study). In regards to samples from McConnell and Coleman, Zr concentrations within magnetite overlap between MSS and ISS-sourced grains, and do not show any apparent trends vs other elements. The only element which appears elevated with increasing Zr concentration is V, though Y concentration increases with Zr in about half the samples from all 3 environments (Figure 3.10).

Minerals in the McConnell offset which exsolved from MSS formed from an Fe-rich sulfide melt (pyrrhotite, pentlandite, primary pyrite) represent the reservoir in which MSS-sourced magnetite would have formed. Magnetite from a primitive Fe-rich sulfide melt would form either before or at the onset of MSS crystallization (Naldrett, 1969) whereas magnetite from an evolved source would crystallize directly from the increasing oxygen content of the MSS as it crystallized at lower temperatures in an attempt to buffer the oxygen fugacity of the system (Fonseca et al., 2008). Using the trace elements of pyrrhotite and pentlandite compared to those within texturally-proximal magnetite can therefore help understand the partitioning behaviour between MSS and oxides, regardless of the oxide generation. Early-forming magnetite may also trap droplets of liquid sulfide as it cools (Figure 3.11). Figure 3.12 illustrates compositions of elements in magnetite compared to Fe-rich sulfides (pyrrhotite and pentlandite) as ratios (top) and absolute compositions (bottom). From these graphs, it can be seen that the major chalcophile elements within MSS (Ni, Co, Cu) concentrate selectively within sulfides, whereas

compatible lithophile elements (V, Cr, Zn) are more strongly concentrated within magnetite, as is expected from previous studies (e.g. Dare et al., 2012). The element Sr is more concentrated within pentlandite than magnetite, but is less concentrated within pyrrhotite than magnetite. Overall, however, Sr appears to favour sulfide phases over oxide phases. Zirconium, a fairly incompatible element, shows an almost even distribution between magnetite and pyrrhotite+pentlandite, choosing to partition into pentlandite over magnetite, and magnetite over pyrrhotite. Only Sn, which partitions preferably into Cu-rich sulfide over MSS and is incompatible in all phases, shows a tight cluster between compositions, evenly distributed between sulfides and magnetite. Tin appears to be slightly more compatible in magnetite than pyrrhotite, and is evenly distributed between magnetite and pentlandite.

3.4.2 Sulfide inclusions within magnetite

In most samples of massive and inclusion-rich massive sulfides, magnetite grains contain small inclusions of pyrrhotite-chalcopyrite blebs (Figure 3.11D). These inclusions are assumed to represent sulfide liquid which was trapped within the crystallizing magnetite grains (Figure 3.11). The sulfide liquid, once trapped, behaved like a small closed system within the magnetite grain, separating into Fe- and Cu-rich phases. Proportions of pyrrhotite and chalcopyrite within magnetite grains are very similar in most samples, with inclusions mimicking local sulfide mineralogy. In samples which display higher proportions of chalcopyrite in major phases, sulfide inclusions in texturally proximal magnetite often display increased chalcopyrite proportions as well. Although MSS also crystallizes small amounts of interstitial chalcopyrite while cooling, the band of massive chalcopyrite (Figure 3.2) that occurs near the base of the mineralization suggests

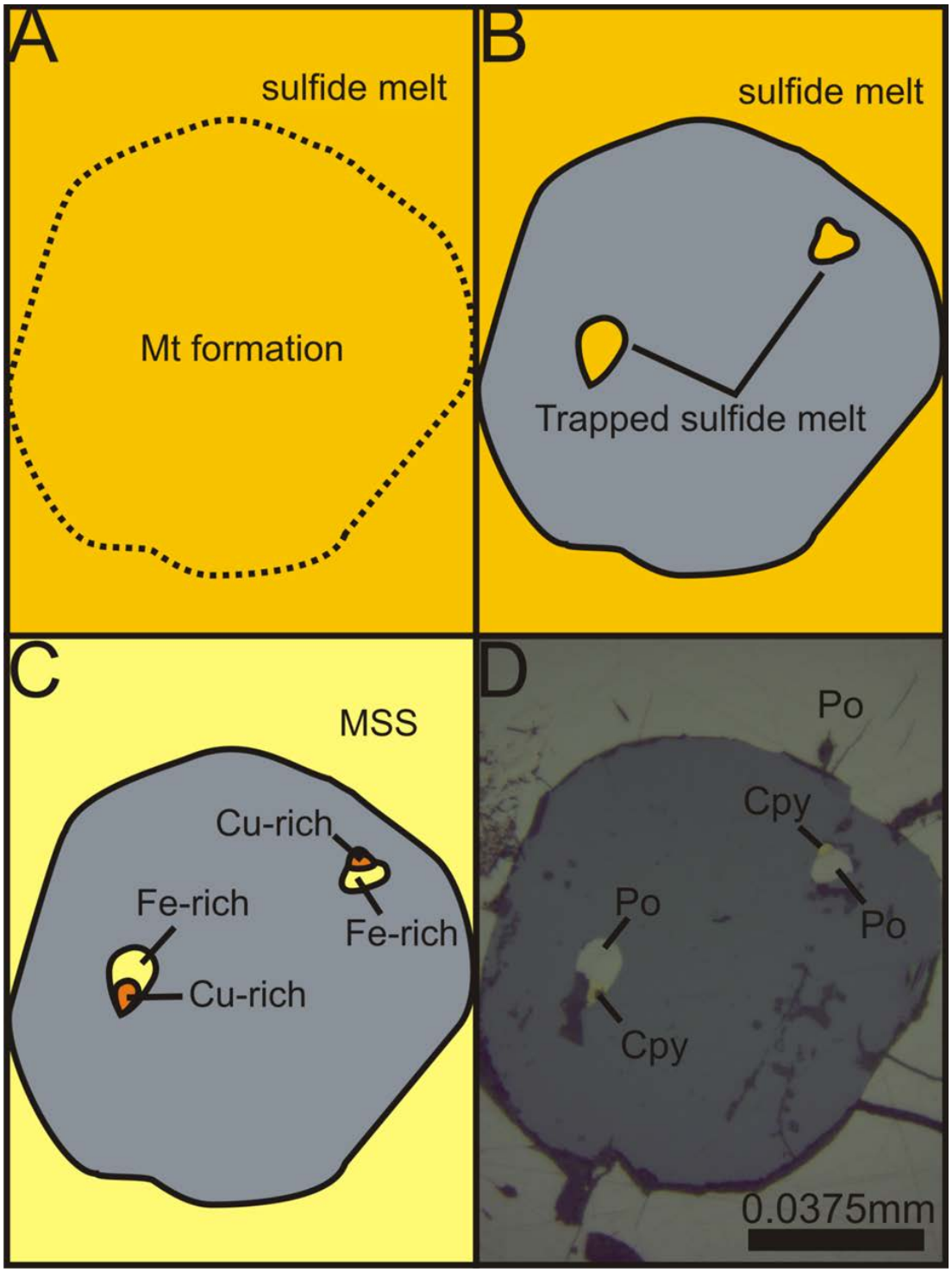

Figure 3.11. Cartoon illustrating initial magnetite crystallization which trapped sulfide droplets at high temperatures. Sulfide droplets indicate magnetite began crystallizing when sulfide liquid was either still undergoing fractionation or beginning to cool as an MSS phase. Chalcopyrite within trapped sulfide droplets is most likely the result of Cu segregation from cooling MSS.

that at least a small amount of a fractionated Cu-rich liquid existed during cooling. Likewise, in samples dominated by massive pyrrhotite with very little or no interstitial chalcopyrite, sulfide inclusions show very little or no chalcopyrite. Pentlandite is only rarely encountered in sulfide inclusions as miniscule rims between pyrrhotite and chalcopyrite, suggesting either the sulfide melt was insufficiently concentrated in nickel, or the small amount of nickel present in the inclusion diffused into the magnetite grain. These small pyrrhotite-rich sulfide assemblages indicate that the host magnetite grains must have formed before or during MSS crystallization while the Fe-rich liquid still had enough Cu in solid solution to differentiate and crystallize chalcopyrite. The walls of the magnetite grains would create an excellent buffer to oxygen and (most) chalcophile element exchange, meaning any chalcopyrite which formed within sulfide inclusions representing early (primitive) MSS or immiscible sulfide melt would be totally independent of the later-forming ISS of the McConnell system. On the other hand, magnetite grains which show inclusions that are enriched in chalcopyrite may have formed at lower temperatures during MSS-sulfide liquid fractionation or ISS crystallization, when Fe- and Cu-rich liquids were already differentiated. The mineralogy of the inclusions also suggest that magnetite grains which contain sulfide inclusions did not migrate or settle extensively during crystallization, and were formed very close or in-situ to where they currently exist. Magnetite grains which contain sulfide inclusions were not analyzed by LA-ICP-MS as the sulfides would contaminate the signal.

3.4.3 Exsolution products and mechanisms

Exsolution textures of McConnell magnetite are similar to those first described by Buddington and Lindsley (1964) and later by Haggerty (1991), showing “trellis-style”

ilmenite exsolution from magnetite along all directions of {111} parting planes and mimicking crystal growth zones and crystal faces (Figures 3.5-3.7). A second form of exsolution, also recognized by the previously mentioned authors, was that of Al-Cr-spinel from magnetite which showed a more random distribution within the oxide host. Chromium, Zn, and Al are not compatible with the ilmenite lattice (Mucke, 2003) and segregated into small amounts of Al-Cr-spinel in a buckshot or semi-zoned texture. The textures and chemical composition of phases which exsolved from the magnetite host are a complex function of several different parameters, such as temperature, composition of the original liquid and oxide phases during crystallization, oxygen content and sulfur fugacities, and cooling rates, which, among other things, affect whether or not oxides occur as separate phases or as a solid-solution above their solvus temperatures (Mucke 2003). It is widely accepted from the work of Buddington and Lindsley (1964) and Haggerty (1991) that trellis-style ilmenite exsolution texture is the result of oxidation-exsolution of a solid-solution oxide (magnetite-ulvite or magnetite-ulvospinel) which exists above temperatures of 600°C (Mucke, 2003). With progressive oxidation, subsolidus exsolution continues through progressive stages of exsolution textures (Haggerty, 1991). The effects of oxidation-exsolution in natural systems, however, are progressive from rim to core, while magnetite within the McConnell ores contains trellis-exsolution textures within the cores only, leaving a rim of exsolution-free magnetite in equilibrium with sulfides. Lattard (1995) showed that a redox reaction was not always required to achieve trellis textures, and noted that exsolution of ilmenite from a titaniferous spinel could be accomplished by vacancy relaxation in the spinel, and that vacancy concentrations were inversely correlated with the fO_2 at 1300°C. Chromium

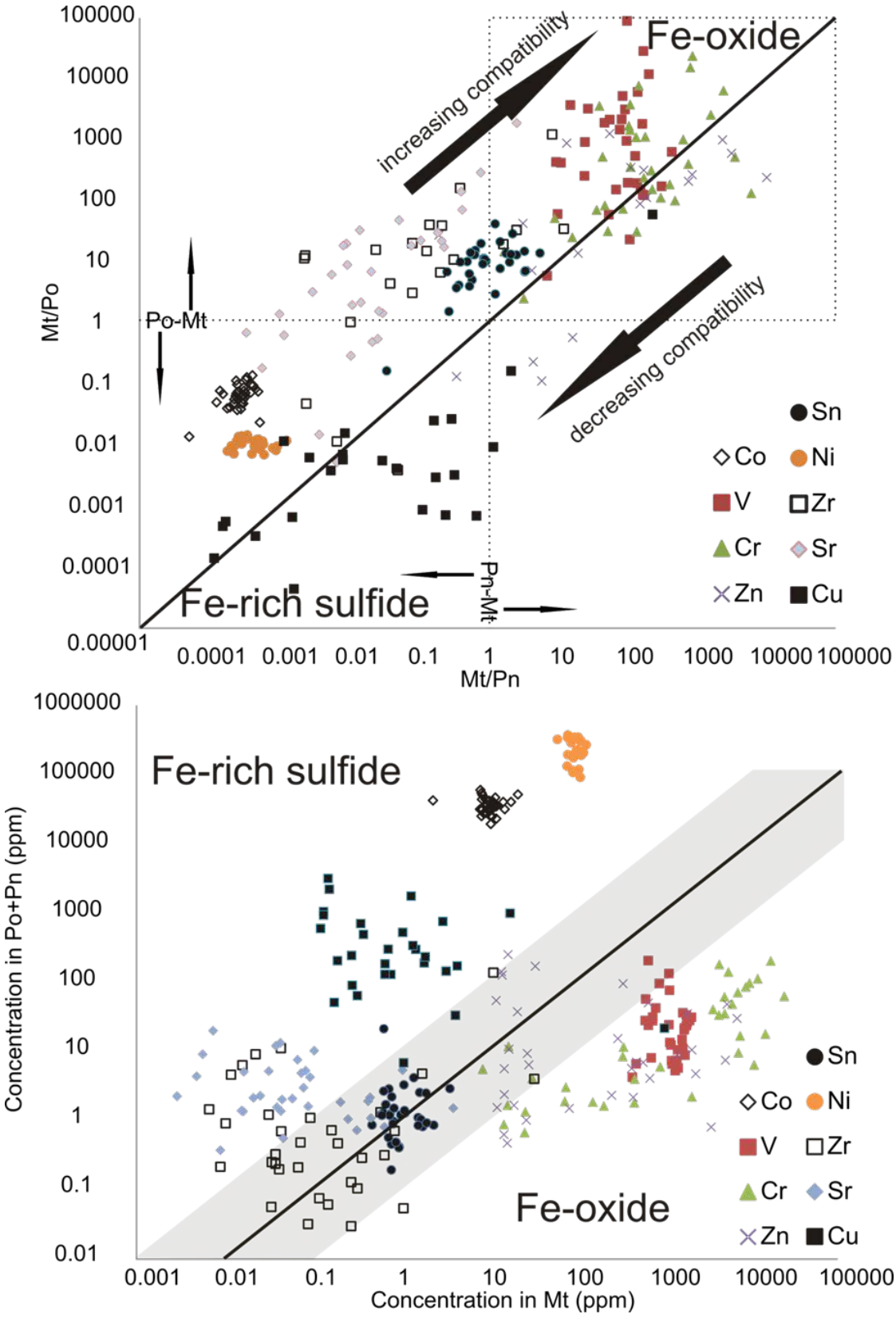
Fe-oxide
increasing compatibility
decreasing compatibility
Po-Mt
Pn-Mt
Fe-rich sulfide
Mt/Po
Mt/Pn
100000
10000
1000
100
10
1
0.1
0.01
0.001
0.0001
0.00001
0.0001
0.001
0.01
0.1
1
10
100
1000
10000
100000
Sn
Co
Ni
V
Zr
Cr
Sr
Zn
Cu
Fe-rich sulfide
Fe-oxide
Concentration in Po+Pn (ppm)
Concentration in Mt (ppm)
1000000
100000
10000
1000
100
10
1
0.1
0.01
0.001
0.01
0.1
1
10
100
1000
10000
100000

Figure 3.12. Compositions of magnetite+pyrrhotite+penltandite within McConnell ores, solid lines show even distribution, shaded areas depict concentrations an order of magnitude above and below even distribution lines. (Top) Ratios of magnetite over pyrrhotite (y-axis) and magnetite over pentlandite (x-axis) compositions. Pyrrhotite is more enriched in elements at values below 1 on the y-axis, while pentlandite is more enriched in values below 1 on the x-axis. (Bottom) Absolute concentrations of detectable chalcophile and lithophile elements within magnetite and its corresponding sulfide host(s). As concentrations move away from the solid into one field or another, elements are assumed to partition preferably into that phase (MSS for po+pn or oxide-SS for magnetite).

contents of the solid solution phases also affect vacancy concentrations (Knecht et al., 1977; Lattard, 1995). Electron exchange under partially reducing conditions from H_2 is another proposed method of trellis-exsolution (Krasnova and Krezer, 1995), though this particular model does not correspond to the McConnell (or other Sudbury deposits mentioned).

The explanation for exsolution textures of McConnell magnetite grains is quite complex. Magnetite grains contain exsolution blebs in the cores only (Figure 3.6), meaning the rims of magnetite may have formed at a different time and under different conditions than the cores of these grains. Magnetite within the McConnell ores does not appear to be zoned with respect to major elements, only exsolved phases. However, these elements may have existed in solid solution during the growth of magnetite rims, and were subsequently concentrated into exsolving phases. It may have also been that while MSS cooled, elements were partitioned from magnetite to MSS. Trace element zoning was not recorded in McConnell samples as the beam size of laser ablation was often only slightly smaller than the magnetite grains, increasing precision and lowering detection limits. As a result, the compositions of magnetite from LA-ICP-MS reflect the solid solution composition of the oxide phase (core and rim) before exsolution began (above ~600°C). This creates some problems if the core-rim compositions have different trace element concentrations. A suitable explanation for the formation of the rim may lie in the concentration of compatible lithophile elements (V, Ti, Cr) remaining in MSS as magnetite crystallizes (Dare et al., 2012). During crystallization, lithophile elements would partition into oxides preferentially over sulfides and locally deplete MSS. As a result, later-forming magnetite rims would show a depletion of compatible lithophile

elements, Ti sequestering in ilmenite exsolution within the core (Figure 3.7).

Two scenarios may be proposed for the observations made on the compositions and textures associated with McConnell magnetite: i) McConnell magnetite cores crystallized early from a primitive sulfide liquid (which had already undergone sulfide saturation and segregation from the silicate liquid) or exsolved from an early MSS source under similar conditions proposed for that of Creighton magnetite formation, though exsolution and core-rim textures are similar to that of McCreedy, possibly suggesting an evolved MSS source for the rims (Dare et al., 2012); ii) McConnell magnetite experienced fluctuations in O_2 or source composition, possibly crystallizing cores in a silicate melt (Fonseca et al., 2008) and settling into an immiscible sulfide liquid where later-forming rims were slowly formed, compatible lithophile elements (Ti, Cr) being concentrated in the solid-solutions within the cores of magnetite grains. As ilmenite does not exist as more than an exsolution phase in magnetite within McConnell samples, it could be assumed that the Ti contents of the silicate or sulfide melt (or both) were depleted compared to other Sudbury deposits. Likewise, no chromite grains were found in McConnell samples suggesting that Cr concentrations within the melt were not sufficient enough to segregate from the oxide-sulfide solid solutions to form discrete Cr-spinel grains.

3.5 Conclusions

Analyses of magnetite-sulfide assemblages from the McConnell ore body show distinct trends in partitioning behaviour of trace elements between MSS-oxide during crystallization. Although some uncertainty remains in the exact timing of magnetite crystallization within McConnell ores, the following conclusions were made based on composition and textural evidence: i) Magnetite began to form early in the crystallization

history of the system, either before or during primitive MSS crystallization, as the oxygen content of the melt would have been too high to form MSS first without magnetite; ii) Sulfide inclusions hosted within some magnetite grains would have been trapped as either a liquid or high-temperature solid-solution, indicating the magnetite formed before excessive fractionation of the sulfide phase; iii) Ni content, both within magnetite grains and McConnell ore, is lower than most other Sudbury deposits, indicating the melt that formed the McConnell was also depleted in Ni relative to other Sudbury deposits, lower Ni contents also raise oxygen solubility within sulfide melts leading to earlier-forming magnetite; iv) Exsolution textures of magnetite grains cannot be explained by oxidation-exsolution alone, and must represent some change in the system from core to rim growth.

Given the difficulty in understanding the evolution of the McConnell system (Chapter 2), it was expected that magnetite grains would also be difficult to interpret. Although most grains show an early primitive source, some grains cross the fields of MSS and ISS sources and may instead represent magnetite that crystallized directly from a sulfide liquid before MSS crystallization began. This scenario would agree with the hypothesis that O-rich sulfide liquids need to buffer oxygen by crystallizing oxides in order for MSS to stabilize, as set forward by Naldrett (1969). The low Ni tenors in McConnell ores are consistent with an O-rich sulfide liquid.

References

Ballhaus, C., Tredoux, M., and Spath, A., 2001, Phase relations in the Fe-Ni-Cu-PGE-S system at magmatic temperature and application to massive sulphide ores of the Sudbury Igneous Complex: Journal of Petrology, v. 42 (10), p. 1911-1926.

Barnes, S.-J., Makovicky, E., Karup-Moller, S., Makovicky, M., and Rose-Hanson, J., 1997, Partition coefficients for Ni, Cu, Pd, Pt, Rh and Ir between monosulfide solid solution and sulfide liquid and the implications for the formation of compositionally zoned Ni-Cu sulfide bodies by fractional crystallization of sulfide liquid: Canadian Journal of Earth Sciences, v. 34, p. 366–374.

Barnes, S-J., van Achterbergh, E., Makovicky, E., and Li, C., 2001, Proton microprobe results for the partitioning of platinum-group elements between monosulphide solid solution and sulphide liquid: South African Journal of Geology, v. 104, p. 275-286.

Barnes, S.-J., and Lightfoot, P.C., 2005, Formation of magmatic nickel-sulfide ore deposits and processses affecting their copper and platinum-group element contents: Economic Geology 100th anniversary volume, p. 179−213.

Barnes, S.J., and Roeder, P.L., 2001, The range of spinel compositions in terrestrial mafic and ultramafic rocks: Journal of Petrology, v. 42 (12), p. 2279-2302.

Buddington A. F. and Lindsley D. H. (1964) Iron–titanium oxide minerals and synthetic equivalents: Journal of Petrology, v. 5, p. 310–357.

Dare S. A. S., Barnes S.-J., Prichard H. and Fisher P. C., 2010, The timing and formation of platinum-groups minerals from the Creighton Ni–Cu–platinum-group element sulfide deposit, Sudbury, Canada: early crystallization of PGE-rich sulfarsenides: Economic Geology, v. 105, p. 1071–1096

Dare, S.A.S., Barnes, S-J., and Beaudoin, G., 2012, Variation in trace element content of magnetite crystallized from a fractionating sulfide liquid, Sudbury, Canada: Implications for provenance discrimination: Geochimica et Cosmochimica Acta, v. 88, p. 27-50.

Dasgupta, H.C., 1967, Intracrystalline element correlation in magnetite: Economic Geology, v. 62, p. 487-493.

Dupuis, C., and Beaudoin, G., 2011, Discriminant diagrams for iron oxide trace element fingerprinting of mineral deposit types: Mineral Deposita, v. 46, p. 319-335.

Fleet, M.E., Chryssoulis, S.L., Stone, W.E., and Weisener, C.G., 1993, Partitioning of platinum-group elements and Au in the Fe-Ni-Cu-S system: experiments on the fractional crystallization of sulfide melt: Contributions to Mineral Petrology, v.115, p. 36-44.

Fleet, M.E., and Pan,Y., 1994, Fractional crystallization of anhydrous sulfide liquid in the system Fe–Ni–Cu–S, with application to magmatic sulfide deposits: Geochimica et Cosmochimica Acta, v. 58, p. 3369–3377.

Fleet, M.E., Liu, M., and Crocket, J.H., 1999, Partitioning of trace amounts of highly siderophile elements in the Fe-Ni-S system and their fractionation in nature: Geohimica et Cosmochimica Acta, v. 63 (17), p. 2611-2622.

Fonseca, R.O.C, Campbell, I.H., O'Neill, H.S.C., and Fitzgerald, J.D., 2008, Oxygen solubility and speciation in sulphide-rich mattes: Geochimica et Cosmochimica Acta, v.72, p. 2619-2635.

Gasparrini, E., and Naldrett, A.J., 1972, Magnetite and ilmenite in the Sudbury nickel irruptive: Economic Geology, v. 67, p. 605-621.

Ghiorso, M.S., and Sack, R.O., 1991, Fe – Ti oxide geothermometry: thermodynamic formulation and the estimation of intensive variables in silicate magmas: Contributions to Mineral Petrology, v. 108, p. 485-510

Haggerty, S.E., 1991, Oxide textures. A mini atlas.: In: Lindsley, D.H., (eds) Oxide Minerals: petrologic and magnetic significance: Reviews in Mineralogy, Mineralogical Society of America, v. 25, p. 129-219.

Hill, R.L., and Sack., R.O., 1987, Thermodynamic properties of Fe-Mg titaniferous magnetite spinels: Canadian Mineralogist, v. 25, p. 443-464.

Horn, I., Foley, S.F., Jackson, S.E., and Jenner, G.A., 1994, Experimental determined partitioning of high field strength- and selected transition elements between spinel and basaltic melt: Chemical Geology, v. 117, p. 193-218.

Jana, D., and Walker, D., 1997, The influence of sulfur on partitioning of siderophile elements: Geochimica et Cosmochimica Acta, v. 61 (24), p. 5255-5277.

Klemm, D.D., Henckel, J., Dehm, R., and Von Gruenewaldt, G., 1985, The geochemistry of titanomagnetite in magnetite layers and their host rocks of the eastern Bushveld Complex: Economic Geology, v. 80, p. 1075–1088.

Knecht, B., Simons, B., Woermann, E., and EI Goresy, A., 1977, Phase relations in the system Fe-Cr- Ti-O and their application in lunar thermometry: Proceedings of the Eighth Lunar Science Conference: Geochimica et Cosmochimica Acta, Supplement 8, p. 2125-2135.

Krasnova, N.I., and Krezer, Y.L., 1995, New data on the nature of fine and ultrafine lamellae in titanomagnetite: European Journal of Mineralogy, v. 7, p. 1361-1372.

Lattard, D., 1995, Experimental evidence for the exsolution of ilmenite from titaniferous spinel: American Mineralogist, v.80, p. 968-981.

Lattard, D., Sauerzapf, U., Käsemann, 2005, New calibration data for the Fe-Ti oxide thermo-oxybarometers from experiments in the Fe-Ti-O system at 1 bar, 1000-1300°C and a large range of oxygen fugacities: Contributions to Mineral Petrology, v. 149, p. 735-754.

Li, C., Barnes, S-J., Makovicky, E., Rose-Hansen, J., and Makovicky, M., 1996, Partitioning of nickel, copper, iridium, rhenium, platinum, and palladium between monosulfide solid solution and sulfide liquid: Effects of composition and temperature: Ceochimica et Cosmochimica Acta, v. 60 (7), p. 1231-1238.

Mücke, A., 2003, Magnetite, ilmenite and ulvite in rocks and ore deposits: petrography, microprobe analyses and genetic implications: Mineralogy and Petrology, v. 77, p. 215-234.

Mungall, J.E., Andrews, D.R.A., Cabri, L.J., Sylvester, P.J., and Tubrett, M., 2005, Partitioning of Cu, Ni, Au, and platinum-group elements between monosulfide solid solution and sulfide melt under controlled oxygen and sulfur fugacities: Geochimica et Cosmochimica Acta, v. 69 (17), p. 4349-4360.

Naldrett, A.J., 1969, A portion of the system Fe-S-O between 900 and 1080°C and its application to sulfide ore magmas: Journal of Petrology, v.10, p. 171-201.

Naldrett, A.J., Singh, J., Krstic, S., Li, C., 2000, The mineralogy of the Voisey's Bay Ni-Cu-Co Deposit, Northern Labrador, Canada: Influence of oxidation state on textures and mineral compositions: Economic Geology, v. 95, p. 889-900

Nielsen, R.L., Forsythe, L.M., Gallahan, W.E., and Fisk, M.R., 1994, Major- and trace-element magnetite-melt equilibria: Chemical Geology, v. 117, p. 167-191

Nielsen, R.L., and Beard, J.S., 2000, Magnetite-melt HFSE partitioning: Chemical Geology, v. 164, p. 21-34.

Powell, R., and Powell, M., 1977, Geothermometry and oxygen barometry using coexisting iron-titanium oxides: a reappraisal: Mineralogical magazine, V. 41, P. 257-263.

Righter, K., Leeman, W.P., and Hervig, R.L., 2006, Partitioning of Ni, Co and V between spinel-structured oxides and silicate melts: Importance of spinel composition: Chemical Geology, v. 227, p. 1-25.

Sack, R.O., 1982, Spinels as petrogenetic indicators: Activity-composition relations at low pressures: Contributions to Mineral Petrology, v. 79, p. 169-186.

Sauerzapf, U., Lattard, D., Burchard, M., and Engelmann, R., 2008, The titanomagnetite-ilmenite equilibrium: New experimental data and thermo-oxybarometric application to the crystallization of basic to intermediate rocks: Journal of Petrology, v. 49 (6), p. 1161-1185.

Toplis, M.J., and Carroll, M.R., 1995, An experimental study of the influence of oxygen fugacity on Fe–Ti oxide stability, phase relations, and mineral-melt equilibria in ferro-basaltic systems: Journal of Petrology, v. 36, p. 1137–1170.

Toplis, M.J., and Corgne, A., 2002, An experimental study of element partitioning between magnetite, clinopyroxene and iron-bearing silicate liquids with particular emphasis on vanadium: Contributions to Mineral Petrology, v. 144, p. 22-37

Von Gruenewaldt, G., Klemm, D.D., Henckel, J., and Dehm, R.M., 1985, Exsolution features in titanomagnetites from massive magnetite layers and their host rocks of the upper zone, eastern Bushveld Complex: Economic Geology, v. 80, p. 1049-1061

Wechsler, B.A., Lindsley, D.H., Prewitt, C.T., 1984, Crystal structure and cation distribution in titanomagnetites ($Fe_{3-x}Ti_xO_4$): American Mineralogist, v. 69, p. 754-770.

Zhou, M.-F., Lightfoot, P.C., Keays, R.R., Moore, M.L., and Morrison, G.G., 1997, Petrogenetic significance of chromian spinels from the Sudbury Igneous Complex, Ontario,Canada: Canadian Journal of Earth Sciences, v. 34, p. 1405–1419.

Chapter 4: Concluding statements about the McConnell offset deposit

Findings from chapters 2 and 3 are summarized in this section. The mineralogical study paired with the magnetite geochemistry study shows that;

(i) The melt which created the McConnell offset was able to achieve sulfide saturation but did not sequester the same proportions of metals as other larger offsets. A limited silicate reservoir may be responsible for this. Further, the smaller McConnell system did not incorporate large quantities of arsenic and therefore did not crystallize abundant arsenides and sulfarsenides like other South Range deposits. As a result, cobalt and palladium sequestered primarily into MSS.

(ii) Pentlandite within McConnell ores is often altered and oxidizes quickly due to its contamination and variable metal/S ratios. Pentlandite often contributes to 50% of the lead in samples and contains appreciable palladium contents. Due to the cobalt in pentlandite and the contribution of pyrrhotite to the overall nickel budget due to low abundances of Ni-sulfides, bulk rock cobalt positively correlates with the amount of pentlandite in each sample and is a better indication of pentlandite concentration than bulk nickel. Due to contamination and possible problems with flotation and benefaction, nickel is not considered to be an economic resource in the McConnell.

(iii) Chalcopyrite is primarily dispersed through massive Fe-rich sulfides as small blebs and flames, but also occurs in larger quantities in silicate-rich intervals and one chalcopyrite-rich sheet. The small blebs intermittent through massive pyrrhotite is most likely attributed to the Cu-rich portions of MSS sequestering to form chalcopyrite, while the large sheet and Cu-rich disseminated and intermediate-massive intervals were most

likely the product of settling ISS. Chalcopyrite contains very low concentrations of deleterious metals, is not effected by hydrothermal alteration, and may be viably extracted without many problems.

(iv) Magnetite within McConnell ores can reach up to 20 vol%, indicating that the McConnell melt was sufficiently saturated in oxygen. Magnetite formed very early from cooling MSS, possibly crystallizing directly from the sulfide liquid before MSS began crystallizing, and can contain early cores and later-forming rims which reflect the evolution of the MSS.